POLITECNICO DI MILANO

Scuola di Ingegneria Industriale e dell'Informazione

Corso di Laurea Magistrale in Ingegneria Elettrica

Mode Conversion in Differential Lines with Cross-Section and Termination Imbalance

Relatore: Prof. Sergio A. Pignari

Correlatore: Dr. Flavia Grassi

Tesi di Laurea Magistrale di:
Xinglong Wu
Matr. 796122

Yuehong Yang
Matr. 796135

Anno Accademico 2014-2015

INDICE

INDICE DELLE FIGURE

INDICE DELLE TABELLE

ABSTRACT

Abstract in italiano

Al fine di trasmettere in modo efficiente segnali ad alta frequenza, è pratica comune ricorrere a linee di tipo differenziale, in quanto esse risultano idealmente immuni da interferenze esterne. Tuttavia, nella pratica, il possible sbilanciamento della linea stessa (principalmente dovute ad asimmetrie dei conduttori nella sezione trasversale) e delle sue reti terminali può dare origine a un indesiderato fenomeno di conversione da modo differenziale (segnale trasmesso) in modo comune (teoricamente non eccitato dalla sorgente di segnale) e viceversa con conseguenti problemi di integrità di segnale e compatibilità elettromagnetica.

In questo lavoro di tesi, il fenomeno di conversione modale in linee di trasmissione differenziali (linee twistate o tracce su PCB) affette da sbilanciamento è studiato in dettaglio, al fine di stabilire una stretta correlazione tra sbilanciamento e suscettibilità e emissioni radiate. A tale scopo, il formalismo delle linee di trasmissione multi-conduttore è stato combinato con l'ipotesi semplificativa di *weak imbalance* (debole sbilanciamento), il cui ruolo fondamentale nella comprensione del fenomeno è messo in evidenza ricorrendo all'analisi modale e al concetto di modo dominante. L'analisi qui presentata è prevalentemente focalizzata sulla conversione di modo differenziale in modo comune, fenomeno alla base delle emissioni radiate, e ha consentito la messa a punto di un modello predittivo semplificato, in cui lo sbilanciamento è rappresentato/interpretato circuitalmenete a mezzo di generatori controllati. Il modello è stato poi esteso per dualità al fenomeno di conversione da modo comune in differenziale, fenomeno alla base della suscettibilità radiata. L'accuratezza predittiva dei modelli proposti è stata preliminarmenete validata mediante simulazioni (basate sulla soluzione esatta della linea multi-conduttore originaria) e, in seguito, mediante misure sperimentali.

Oltre al modello deterministico precedentemente descritto, un modello probabilistitico rappresentativo del fenomeno di sbilanciamento è stato elaborato al fine di rappresentare correttamente l'aleatorietà dei parametri geometrici/elettrici alla base della conversione

modale. Sulla base dei modelli proposti, è stato possibile confrontare i contributi dovuti a sbilanciamento della linea e sezioni terminali separatamente. Infine, è stato sviluppato un modello SPICE finalizzato a stime di *worst-case* (caso peggiore) dell'entità dei disturbi indotti alle terminazioni della linea per effetto dello sbilanciamento.

Questa tesi documenta il lavoro svolto negli scorsi due anni in collaborazione con il Prof. Sergio A. Pignari e la Dott.ssa Flavia Grassi. L'attività è stata sviluppata in parte durante il nostro periodo di studio presso il Politecnico di Milano e in parte in Cina e ha portato alla pubblicazione di due articoli su rivista internazionale e due pubblicazioni in atti di conferenze internazionale, come riportato più in dettaglio in Appendice A. In quanto studenti coinvolti nel progetto di Doppia Laurea Magistrale attualmente in essere tra Politecnico di Milano e Xi'An Jiaotong University (Xi'an, Shaanxi, P. R. China), abbiamo anche separatamente sviluppato una seconda tesi sotto la guida di supervisori cinesi. Le attività svolte in tale contesto non sono state documentate in questo lavoro di tesi, ma solo brevemente riassunte in Appendice B.

Abstract in inglese

Effective transmission of high-frequency signals is usually achieved by the use of differential signaling through differential interconnections, which do not theoretically radiate and are ideally immune to external interfering fields. However, in actual differential-line realizations the possible imbalance affecting wiring structure and/or the line terminal networks is as the basis of undesired conversion of differential mode (DM) into common mode (CM) and vice versa with detrimental consequences in terms of signal integrity and electromagnetic compatibility (EMC).

In this thesis, the undesired imbalance and mode conversion as the basis of radiated emissions (RE) and susceptibility (RS) of differential-line circuits affected by either not-perfectly balanced loads or asymmetries in the line cross-section are investigated. To this end, multi-conductor transmission line (MTL) theory is combined with the assumption of weak imbalance, whose fundamental role is evidenced by resorting to modal analysis and to the concept of the dominant mode. The analysis mainly focuses on DM-to-CM conversion as the basis of RE issues, and leads to approximate equivalent circuit models for CM-voltage/current prediction where effects due to line and termination imbalance are

(separately) included by the use of controlled voltage and/or current sources. By duality, similar models for CM-to-DM conversion responsible for RS are also introduced. Prediction accuracy of the proposed approximate models is preliminarily assessed versus exact solution of MTL equations, and then validated by measurement carried out on different micro-strip lines.

Furthermore, to account for parameter uncertainty, a probabilistic model for line imbalance is developed, validated, and compared versus the contribution due to termination imbalance. Superposition of line and termination imbalance is therefore discussed based on the proposed modeling approach. Based on the above results, a SPICE model is eventually developed aimed at worst-case prediction of undesired modal voltages induced at line terminals by mode conversion due to line and termination imbalance.

This thesis summarizes a research work carried out within the last two years in collaboration with Prof. Pignari and Dr. Grassi. The activity was developed partially during our stay in Politecnico di Milano and partially in Xi'an Jiaotong University, and led to the publication of two journal papers and two conference papers, whose references are reported in APPENDIX A. As students involved in the Double Master Degree Program between Politecnico di Milano and Xi'an Jiaotong University (Xi'an, Shaanxi, P. R. China), we also developed a thesis under the supervision of our Chinese tutors. However, for the sake of brevity, the results obtained in the framework of these research activities are not discussed here in details. Abstracts of these works are reported in APPENDIX B.

.

1 INTRODUCTION

1.1 Differential signaling

Traditionally, for transmitting electrical signals through lines, the most common and simple method is single-ended signaling, which uses one wire to carry voltage signal and the other wire (usually ground) to work as reference voltage. With the development of electrical and electronic technologies, the working frequency of signals is becoming higher. Although single-ended signaling is less expensive, its lack of ability to reject electromagnetic interference (EMI) makes it scarcely used for fast-speed applications. On the contrary, transmission technologies based on differential signaling are key-ingredients of high-speed data links assuring satisfactory performance in terms of electromagnetic compatibility (EMC) and signal integrity (SI). Differential signaling is a method for electrically transmitting information using two complementary signals. The technique foresees to send the same electrical signal as a differential pair of signals, each in its own conductor, which means lines transmit information as the difference between the voltages on a pair of wires [1]. These lines are usually referred to as differential lines (DLs), and can be implemented as wiring structures or traces on a Printed Circuit Board (PCB).

Since the receiver only detects the difference between the signals carried by the two wires, differential signaling is more robust to electromagnetic noises than single-ended interconnections. One typical working schematic diagram is shown in Figure 1-1. From this figure, it’s easy to find out that the noise cancels out when the receiver recognizes the information as the difference of complementary signals. Due to this advantage, this method is used in both analog and digital signaling, such as RS-422, USB, HDMI and so on.

1.2 EMC problems due to imbalance of differential-line systems

One typical schematic diagram of DL systems is shown in Figure 1-2, where the two lines are for the signals and the other one is for the reference. The voltages and currents at each port of transmission lines are shown in Figure 1-2.

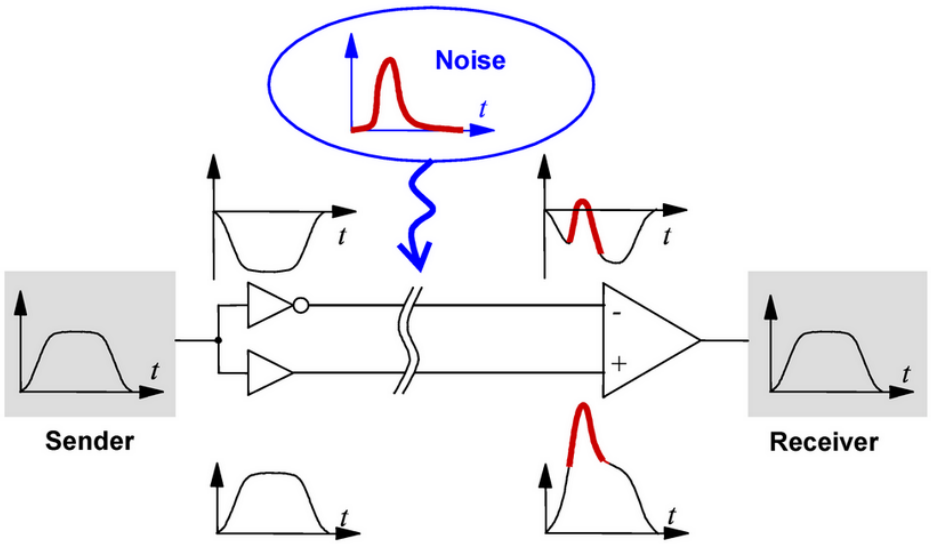

Figure 1-1 Working principle of differential signaling [1]

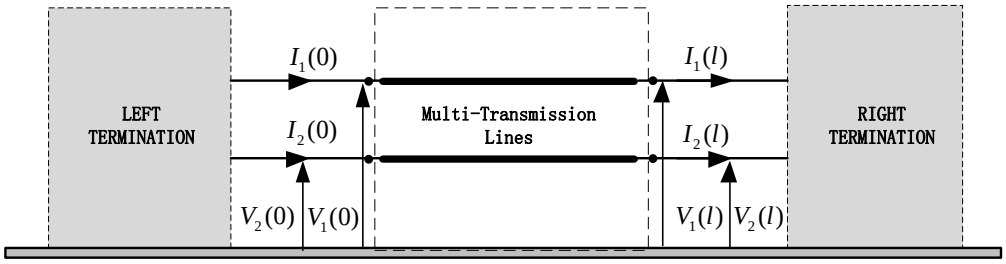

Figure 1-2 Typical schematic diagram of a DL system

In general, voltages and currents in three-conductor systems can be decomposed into common-mode (CM) and differential-mode (DM) components. Among the several definitions of modal quantities available in the literature,[2][3] as the following will be exploited in this work. Firstly, the signal information is included in the difference of voltages of two upper wires, excluding the reference line. Thus, DM voltage is defined as:

$$V_{dm} = V_1 - V_2 \tag{1.1}$$

Secondly, since CM voltage is the average value of the voltages at each port, it can be defined as:

$$V_{cm} = \frac{V_1 + V_2}{2} \tag{1.2}$$

Thirdly, DM current is expected to flow into left (right) terminal of one line and flow out from the same terminal of the other line. Therefore, the DM current should be defined as:

$$I_{dm} = \frac{I_1 - I_2}{2} \tag{1.3}$$

Fourthly, CM current can be recognized as the total current which flows in or out one port. Hence, it can be defined as:

$$I_{cm} = I_1 + I_2 \tag{1.4}$$

Concerning the above definition and the characteristics of differential signaling, it's easy to find out that for perfect differential signaling, $I_{cm} = 0$. This means that DM signaling has the ability to ideally reduce to zero radiated emission (RE) from the line, which is mainly related to CM current. At the same time, the external radiated electromagnetic noise is coupled into all wires and couldn't affect the DM values. In a word, since data transmission resorts to differential mode (DM) signaling, 1) no common mode (CM) currents and, therefore, RE are theoretically expected and 2) the noise pickup (Radiated Susceptibility, RS) should ideally cancel out at line terminations. Hence, differential line circuit should be theoretically immune to RE and RS issues.

However, for the sake of the effectiveness for differential signaling, the physical layer, including wiring harnesses and terminal networks, should meet stringent requirements in terms of balancing. Indeed, undesired asymmetries affecting the wiring structure or the terminal networks may give rise to unexpected conversion of DM into CM, and vice versa [3][4][5], with detrimental effects in terms of: (a) near- and far-field radiated emissions (ideally null) [6][7]; (b) degradation of CM-rejection properties and consequent susceptibility to the electromagnetic fields generated by nearby devices (RS), [6], and to ground-bounce noise (conducted susceptibility, CS), [8][9]. Additionally, balancing plays a crucial role in crosstalk mitigation [10]. In order for the detrimental effects due to mode conversion to be limited below precautionary levels, the International Telecommunication Union (ITU) Standard [11] foresees the use of an *ad hoc* probe to characterize the degree of imbalance of interconnections and telecommunication cables in terms of Longitudinal (LCL and LCTL) and Transverse (TCL and TCTL) Conversion (Transmission) Loss, which represent a measure of system ability to convert the CM into DM and vice-versa

Additionally, corresponding test setups [12] and measurement instruments [13] are also discussed. Hence, the interest, also from the prescriptive viewpoint [11], in characterizing, both theoretically and experimentally, the degree of imbalance of cables and interconnections for high-speed communications, so to trouble-shoot and possibly fix the ensuing EMC and SI problems.

1.3 The per unit length parameters for MTL

All the structural information about the line such as type of conductor, wire radii, and wire separation that distinguish one line from another are contained in the per-unit-length parameters of capacitance C (F/m) and inductance L (h/m)[10]. In order to study the mode conversion due to imbalance, the multi-conductor transmission line (MTL) equations should be used and discussed. But it is useless to solve the MTL equations if the p.u.l. parameters cannot be determined for the particular line cross-sectional configuration. Thus, this section focuses on the calculation of p.u.l. parameters. Two typical cross sections of MTL are shown in Figure 1-3.

The configurations of cross sections can be divided into two groups: lines immersed in a homogeneous medium (an example is shown in Figure 1-3a) and in an inhomogeneous medium (an example is shown in Figure 1-3b). For homogeneous media with permittivity ε and permeability μ (free-space values are: $\varepsilon=\varepsilon_0= 8.85\times10^{-12}$ F/m and $\mu=\mu_0= 4\pi\times10^{-7}$H/m), the following identity for p.u.l. parameters (inductance **L** and capacitance **C**) holds [14]:

$$\mathbf{LC} = \mathbf{CL} = \mu\varepsilon\mathbf{1}_2 \tag{1.5}$$

where $\mathbf{1}_2$ is the 2×2 identity matrix:

$$\mathbf{1}_2 = \begin{bmatrix} 1 & 0 \\ 0 & 1 \end{bmatrix} \tag{1.6}$$

Therefore, if one of these parameters is known, the other can be found according to (1.5).

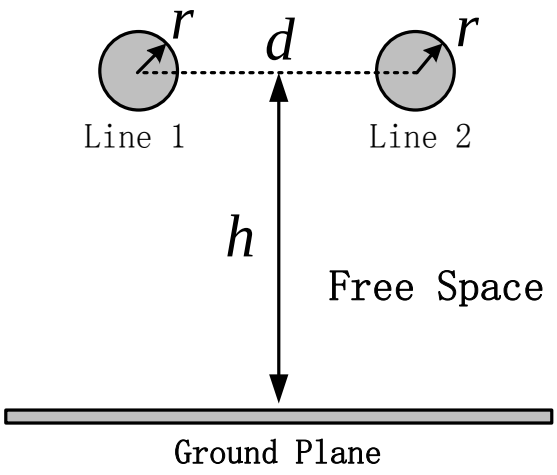

(a)

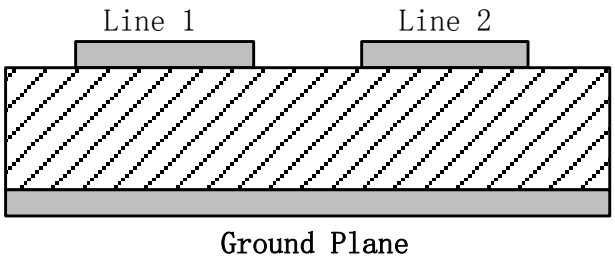

(b)

Figure 1-3 Two typical MTL cross sections

For lines in an inhomogeneous medium, their p.u.l. parameter can't be obtained from simply calculation. Numerical methods (i.e., such as the FEM-based numerical code Maxwell) must be used.

1.3.1 Calculation of per unit length parameters for lines in a homogeneous medium [10]

In order to derive the p.u.l. parameters for wire-type lines in Figure 1-3(a), it is important to concern the flux due to a current-carrying wire that penetrates a surface of unit length along the wire and whose edges are at radial distances R_1 and R_2 from the wire where R_2 is bigger than R_1, as shown in Figure 1-4.

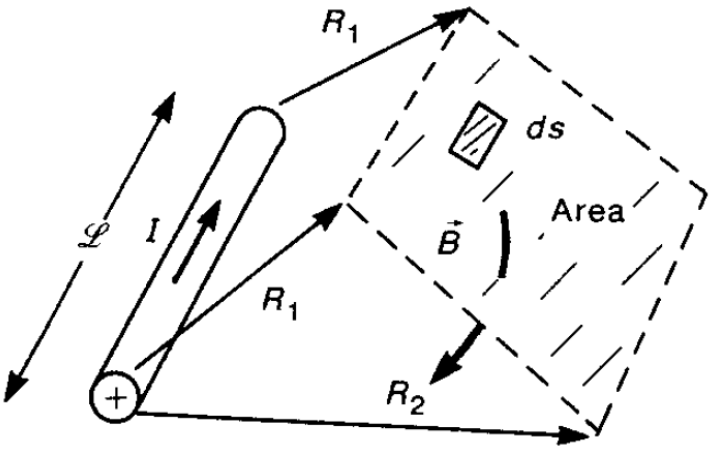

Figure 1-4 Magnetic flux calculation of a current-carrying wire through a surface [10]

According to Ampere's law, the magnetic induction strength B in free space in Figure 1-4 follows the following equations:

$$2\pi rB = \mu_0 I \tag{1.7}$$

where B is the magnetic induction flux with radius r and I is the current flow through the wire in Figure 1-4.

And according to magnetic flux definition ψ takes the expression as:

$$\psi = \int_S \vec{B} \bullet d\vec{s} \tag{1.8}$$

where s is the unit surface shown in Figure 1-4.

From (1.7) and(1.8), the magnetic flux in Figure 1-4 can be obtained as following:

$$\psi = \frac{\mu_0 I}{2\pi} \ln(\frac{R_2}{R_1}) \tag{1.9}$$

Under the assumption that the wires are sufficiently separated so that the charge and current distributions around the peripheries of the wires can be considered as uniform, the magnetic flux due to the current of a single wire can be calculated by(1.9). Then, the p.u.l. inductance can be obtained by (1.10) and the p.u.l. capacitance can be obtained by(1.5):

$$L = \frac{\psi}{I} \tag{1.10}$$

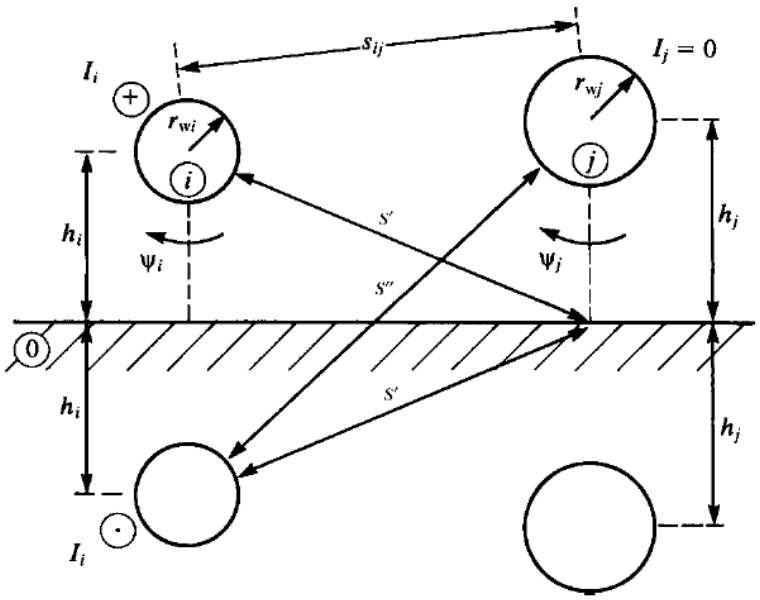

Figure 1-5 Illustration of the calculation of p.u.l. inductances

Therefore, considering typical MTLs in a homogeneous media, the calculation can be done according to (1.9) and(1.10). A typical MTL cross section is composed of two wires above an infinite ground plane, like Figure 1-5[10], which is used in the following chapters.

By replacing the ground plane with the wire images as shown in Figure 1-5, the self-inductance L_{ii} and mutual inductance L_{ij} (i,j=1,2 in this case) of this structure can be obtained as:

$$l_{ii} = \frac{\mu_0}{2\pi} \ln(\frac{2h_i}{r_{wi}}) \tag{1.11}$$

$$l_{ij} = \frac{u_0}{4\pi} \ln(1+\frac{4h_i h_j}{s_{ij}^2}) \tag{1.12}$$

Then, the p.u.l. capacitance can be obtained by(1.5).

1.3.2 Calculation of p.u.l. parameters for lines in an inhomogeneous medium

In order to derive the p.u.l. parameters for wire-type lines in Figure 1-3(b), some numerical methods could be used. In this work, the p.u.l. capacitance and inductance are obtained by using the electrostatic simulation in Maxwell software.

On one hand, since the dielectric materials in Figure 1-3(b) don't have the influence of magnetic properties, the p.u.l. inductance can be calculated by $\mathbf{L} = \mu\varepsilon \mathbf{1}_2 \mathbf{C}^{-1}$ in free space, where the capacitance matrix $\mathbf{C}$ is achieved by the Maxwell simulation with the structures in free space (without any dielectrics). On the other hand, the p.u.l. capacitance can be obtained directly by the Maxwell simulation with the dielectrics.

1.4 Three-conductor MTL theory and equations

According to the discussion about per-unit-parameters in the previous sub-section, simple transmission line can be modeled as a distributed parameter circuit. In particular, if the line is lossy, an elemental line-cell can be modeled as in Figure 1-6.

In many cases, when power losses are negligible, transmission lines can be considered as lossless transmission lines, as shown in Figure 1-7.

In this work, all models and simulations assume the transmission lines are lossless. The accuracy of this assumption is experimentally proved in Chapter 6. In the following discussions, without loss of generality, all transmission lines are considered as lossless.

According to the structure in Figure 1-6, the following first order lossless transmission-line equations can be written:

$$\frac{\partial V(z,t)}{\partial z} = -l\frac{\partial I(z,t)}{\partial t} \tag{1.13}$$

$$\frac{\partial I(z,t)}{\partial z} = -c\frac{\partial V(z,t)}{\partial t} \tag{1.14}$$

where z the longitudinal coordinate along the line, and t represents the time.

The above equations can be uncoupled by differentiating with respect to z or t and then substituting gives second order uncoupled transmission-line equations:

$$\frac{\partial^2 V(z,t)}{\partial z^2} = lc\frac{\partial^2 V(z,t)}{\partial t^2} \tag{1.15}$$

$$\frac{\partial^2 I(z,t)}{\partial z^2} = lc\frac{\partial^2 I(z,t)}{\partial t^2} \tag{1.16}$$

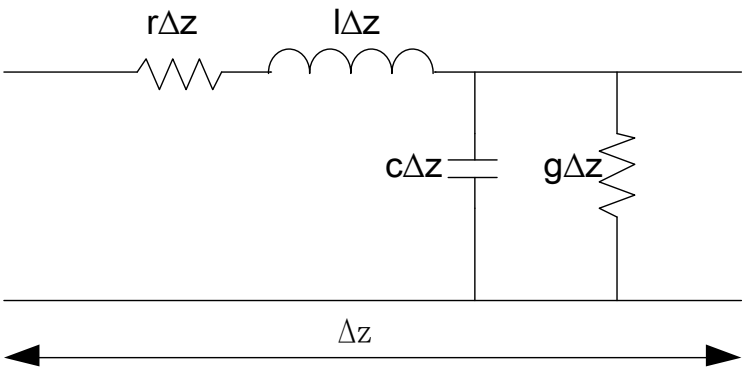

Figure 1-6 Elemental line cell of lossy transmission line

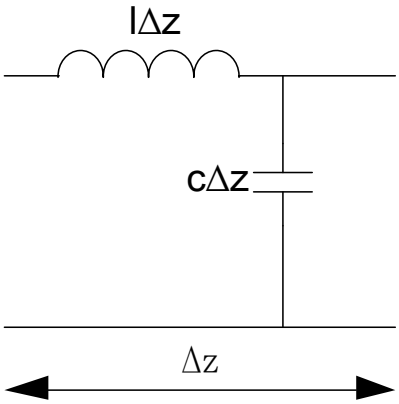

Figure 1-7 Elemental line cell of lossless transmission line

In the case of sinusoidal excitation, which means only single frequency signal is imposed, the above equations can be re-written in frequency domain:

First-order equations:

$$\frac{\partial \hat{V}(z)}{\partial z} = -j\omega l \hat{I}(z) \tag{1.17}$$

$$\frac{\partial \hat{I}(z)}{\partial z} = -j\omega c \hat{V}(z) \tag{1.18}$$

Second-order equations:

$$\frac{\partial^2 \hat{V}(z)}{\partial z^2} + \omega^2 lc \hat{V}(z) = 0 \tag{1.19}$$

$$\frac{\partial^2 \hat{I}(z)}{\partial z^2} + \omega^2 lc\, \hat{I}(z) = 0 \tag{1.20}$$

According to these lossless transmission-line equations, the output voltage and current can be got from the input voltage and current by using chain parameter matrix:

$$\begin{bmatrix} V(L) \\ I(L) \end{bmatrix} = \Phi \cdot \begin{bmatrix} V(0) \\ I(0) \end{bmatrix} \tag{1.21}$$

where

$$\Phi = \begin{bmatrix} \cos(\beta L) & -jvl\sin(\beta L) \\ -jvc\sin(\beta L) & \cos(\beta L) \end{bmatrix} \tag{1.22}$$

where v is the propagation velocity and β is the propagation constant (rad/m), taking the expressions $v = 1/\sqrt{lc}$ and $\beta = 2\pi/\lambda$, respectively .

Similarly, lossless 3-conductor MTL equations in frequency domain can be deduced as:

$$\frac{\partial \mathbf{V}(z)}{\partial z} = -\mathbf{Z}\,\mathbf{I}(z) \tag{1.23}$$

$$\frac{\partial \mathbf{I}(z)}{\partial z} = -\mathbf{Y}\,\mathbf{V}(z) \tag{1.24}$$

where

$$\mathbf{V} = \begin{bmatrix} V_1 \\ V_2 \end{bmatrix}; \mathbf{I} = \begin{bmatrix} I_1 \\ I_2 \end{bmatrix} \tag{1.25}$$

$$\mathbf{Z} = j\omega\mathbf{L} = j\omega\begin{bmatrix} \ell_1 & \ell_m \\ \ell_m & \ell_2 \end{bmatrix}, \quad \mathbf{Y} = j\omega\mathbf{C} = j\omega\begin{bmatrix} c_1 & c_m \\ c_m & c_2 \end{bmatrix}, \tag{1.26}$$

The second order equations are:

$$\frac{\partial^2 \mathbf{V}(z)}{\partial z^2} = \mathbf{Z}\,\mathbf{Y}\,\mathbf{V}(z) \tag{1.27}$$

$$\frac{\partial^2 \mathbf{I}(z)}{\partial z^2} = \mathbf{Y}\,\mathbf{Z}\,\mathbf{I}(z) \tag{1.28}$$

Generally, the above two second order equations are still coupled together because **ZY** and **YZ** are full matrices(**ZY≠YZ**).

The following matrix similarity transformation is used to decoupling the MTL Equations. Voltages and currents can be transformed to mode quantities as following:

$$\mathbf{V}_m(\mathrm{z}) = \mathbf{T}_V^{-1}\mathbf{V}(\mathrm{z}) \tag{1.29}$$

$$\mathbf{I}_m(\mathrm{z}) = \mathbf{T}_I^{-1}\mathbf{I}(\mathrm{z}) \tag{1.30}$$

Where $\mathbf{T}_V$ and $\mathbf{T}_I$ are suitable non-singular matrixes. Then, equation (1.27) and (1.28) can be re-written as:

$$\frac{\partial^2 \mathbf{V}_m(z)}{\partial z^2} = \mathbf{T}_V^{-1}\,\mathbf{Z}\,\mathbf{Y}\,\mathbf{T}_V\,\mathbf{V}_m(z) = \gamma^2\,\mathbf{V}_m(z) \tag{1.31}$$

$$\frac{\partial^2 \mathbf{I}_m(z)}{\partial z^2} = \mathbf{T}_I^{-1}\mathbf{Y}\mathbf{Z}\mathbf{T}_I\,\mathbf{I}_m(z) = \gamma^2\,\mathbf{I}_m(z) \tag{1.32}$$

Where γ^2 is a 2x2 diagonal matrix:

$$\gamma^2 = \begin{bmatrix} \gamma_1^{\,2} & 0 \\ 0 & \gamma_2^{\,2} \end{bmatrix} \tag{1.33}$$

Hence, equation (1.31) and (1.32) are decoupled in the modal domain.

Similarly, after some algebra, voltages and currents at the terminations of the MTL can be written as

$$\begin{bmatrix} \mathbf{V}(L) \\ \mathbf{I}(L) \end{bmatrix} = \Phi \cdot \begin{bmatrix} \mathbf{V}(0) \\ \mathbf{I}(0) \end{bmatrix} \tag{1.34}$$

Where the chain-parameter matrix Φ takes the expression:

$$\Phi = \begin{bmatrix} 0.5\mathbf{Z}\mathbf{T}_I(\mathrm{e}^{\gamma L}+\mathrm{e}^{-\gamma L})\mathbf{T}_I^{-1}\mathbf{Y} & -0.5\mathbf{Z}\mathbf{T}_I(\mathrm{e}^{\gamma L}-\mathrm{e}^{-\gamma L})\mathbf{T}_I^{-1} \\ -0.5\mathbf{T}_I(\mathrm{e}^{\gamma L}-\mathrm{e}^{-\gamma L})\mathbf{T}_I^{-1}\mathbf{Y} & 0.5\mathbf{T}_I(\mathrm{e}^{\gamma L}+\mathrm{e}^{-\gamma L})\mathbf{T}_I^{-1} \end{bmatrix} \tag{1.35}$$

After using of the chain parameter equations to get the voltages and currents at specific points with equations (1.34) and (1.35), values of voltages and currents can be converted into CM and DM domain by (1.1)-(1.4). This is an exact accurate way to calculate the CM and DM values, which is called ‘exact solution of MTL equations’ in the following chapters. But it can’t show the physical and internal meaning of CM, DM and corresponding conversions.

1.5 Research contents and main objectives

This work investigates the effects due to termination and line imbalance on the EMC characteristics of differential-line circuits, with the objective of giving a circuit interpretation (so called *prediction model* in the text) of the mode conversion mechanism at the basis of radiated emissions (RE) and radiated susceptibility (RS). DM-to-CM conversion is at the basis of unwanted RE, whereas RS mainly originates from the conversion of the CM noise picked-up from external electromagnetic sources into DM disturbance at the ports of the drivers/receivers connected at the line ends.

Originated from the imbalance mechanisms, this work mainly concentrates on the line and termination imbalance. The research aspects lie in:

1) The differential-line circuit under analysis is described, and modeled in the modal domain in detail by resorting to the MTL theory and model analysis in chapter 2. The concept of weak imbalance is introduced and validated for the decoupling of the DM and CM circuits.
2) The phenomenon of mode conversion of differential-line circuits with not-perfectly balanced loads/transmission lines is theoretically investigated in chapter 2 and 3, respectively, which leads to simple equivalent circuits in which DM-to-CM mode conversion is represented by dependent lumped sources. The equivalent circuits representative for mode conversion are validated versus exact solution of MTL equations. Conversely, the CM-to-DM conversion is developed and validated under the same strategy too.

3) Since imbalance is mainly due to the manufacture process or uncontrollable parameters in cable harness, i.e., they are deviations of some geometrical/electrical parameters from their nominal values, in chapter 4 the statistical characterization of mode conversion where the imbalances are treated as perturbations relating to some random variables is proposed. The comparison between the line imbalance and termination imbalance is carried out by Monte Carlo numerical simulations. After the comparison, the superposition of line and termination imbalances is also discussed.
4) Similarly, following the same strategy of model decoupling in the homogeneous media, the models for the TLs in inhomogeneous media are developed by recognizing a strict analogy with crosstalk. In this case, the dependent sources in the CM circuit are distributed along the TL, so the equivalent closed-form expressions for the coupling source in the secondary circuit are derived, as well as the CM current distribution along the line. Model accuracy is proved versus exact solution of MTL equations.
5) SPICE model representative for the mode conversion occurring in differential lines affected by imbalance either of the line cross-section (in homogeneous and inhomogeneous media) and the terminal networks is developed, and used for worst-case prediction of undesired modal voltages induced at line terminals.
6) The proposed prediction model is eventually validated by measurement carried out on different PCB samples.

2 MODELING STRATEGY FOR MODE CONVERSION

In this chapter, the differential line structure with perfect and unbalanced terminations and lines is described in detail. The weak imbalance assumption, neglecting the back interaction of the secondary circuit, is introduced.

2.1 Differential line structure under analysis

2.1.1 Description of the differential line structure under analysis

In order to investigate the mechanism of mode conversion due to imbalance, the differential line is modeled as a uniform and lossless multi-conductor transmission line terminated as in Figure 2-1. In this circuit, the line is driven from the left termination by a pair of voltage sources V_{S1}, V_{S2}, whose values can be conveniently selected in order to emulate DM or CM line excitation, for instance, if V_{S1}= -V_{S2}, the circuit is DM line excitation; while when V_{S1}=V_{S2}, the circuit is CM line excitation.

The networks at the left (X=L) and right (X=R) terminations are modeled by T-lumped parameter circuits with ground impedances Z_{GL}, Z_{GR} and series impedances Z_{1X}, Z_{2X}. In the ideal condition of perfect balance, the series impedances should equal to each other, i.e., $Z_{1X} = Z_{2X}$. However, it is usually difficult to achieve comparable levels of balance for line terminations due to several factors, e.g., tolerances and non-ideal behavior of the involved circuit components in the desired frequency range. So considering the imbalance condition, the assumption that the series impedances differ each other by $\Delta Z_X \in [0, Z_D/2]$ can be formulated as

$$Z_{1X,2X} = Z_D/2 \pm \Delta Z_X, \quad X = L, R, \tag{2.1}$$

where Z_D ideally equates the line DM impedance (matching condition), so to account for possible imbalance affecting line terminal networks.

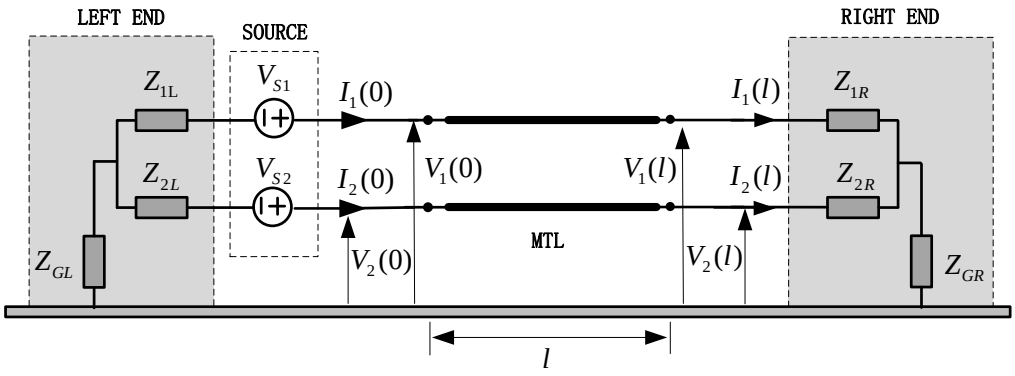

Figure 2-1 Principle drawing of the differential-line (DL) circuit under analysis

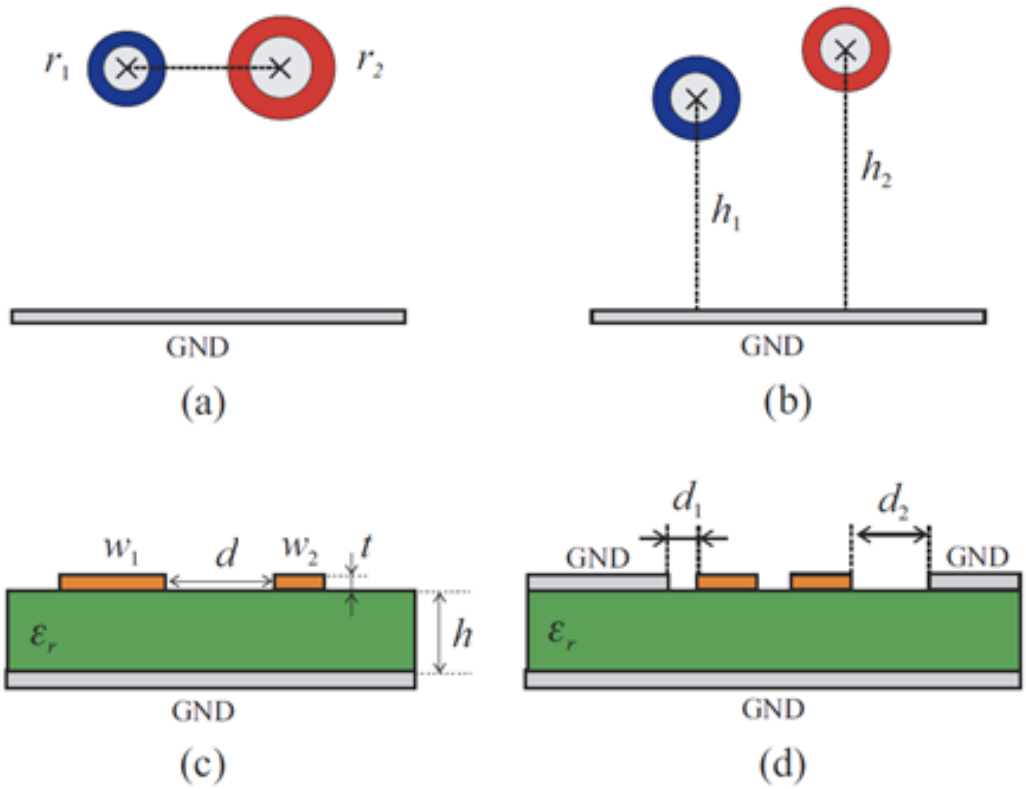

Figure 2-2 Examples of line cross-sections affected by geometrical imbalance.

At the same time, differential-line imbalance may arise not only due to line terminal sections but also due to undesired asymmetries in the realization of the wiring structure. More precisely, asymmetries in the line cross-section give rise to the so-called geometrical imbalance [15], [16]. In this case, some practical examples of differential lines with cross-sections affected by geometrical imbalance are sketched in Figure 2-2. In these lines, geometrical imbalance originates from the presence of signal lines (a) with different

radius/width [as in Figure 2-2(a) and Figure 2-2(c)], or (b) with different distance from the reference ground [as in Figure 2-2(b) and Figure 2-2(d)].

Since the effects of line parameters (such as: radius, height and so on) are similar, in the analysis, the possible imbalance affecting the line cross-section is accounted for by assuming that wire positioning may slightly differ from the reference cross-section as Figure 2-2(b).

The wire structures in Figure 2-2 are all in inhomogeneous media. However, in order to put in evidence the parameters that mainly play a role in mode conversion, the prediction model will be firstly developed assuming wiring structures in homogeneous media (e.g., in free space) and then extended to the inhomogeneous case.. An example of these simplified structures is shown in Figure 2-3(a), which is composed of two bare wires with equal radii r, separated by a distance d, and ideally running at the same height h above ground.

In this homogeneous TL, imbalance is assumed to be only due to the different height of wires above the ground, which is indicating in Figure 2-3(b) and in analogy to (2.1), the wire heights are assumed to differ from the height of the cable axis by $\Delta h \in [0, d]$, i.e.,

$$h_{1,2} = h \pm \Delta h / 2, \tag{2.2}$$

while wire separation, *d*, is kept constant.

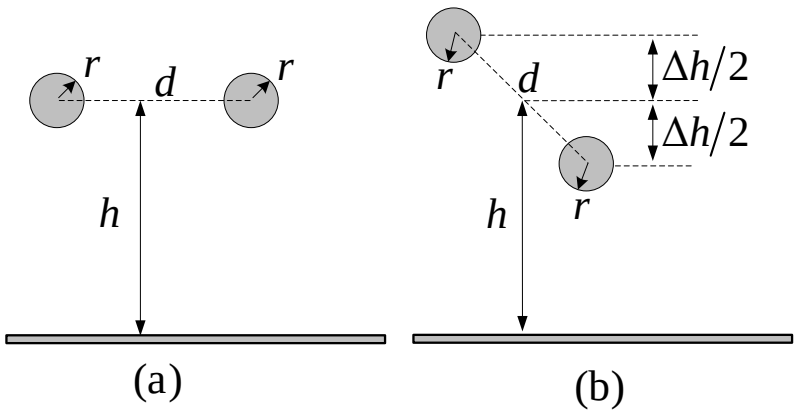

Figure 2-3 Line cross-section: (a) Perfectly balanced (reference structure); (b) slightly unbalanced.

2.1.2 MTL modeling and modal analysis

Propagation and conversion of modal quantities in the above-described differential line circuit are studied by combining MTL theory and modal analysis. Accordingly, CM and DM quantities are introduced starting from physical voltages and currents in Figure 2-1 by recourse to the transformation matrices as:

$$\mathbf{V}_m = \begin{pmatrix} V_{cm} \\ V_{dm} \end{pmatrix} = \mathbf{T}_V^{-1} \cdot \begin{pmatrix} V_1 \\ V_2 \end{pmatrix}, \quad \mathbf{I}_m = \begin{pmatrix} I_{cm} \\ I_{dm} \end{pmatrix} = \mathbf{T}_I^{-1} \cdot \begin{pmatrix} I_1 \\ I_2 \end{pmatrix}. \tag{2.3}$$

where $\mathbf{T}_V$ and $\mathbf{T}_I$ indicate the similarity transformation matrices and take the expressions:

$$\mathbf{T}_V = \begin{bmatrix} 1 & 0.5 \\ 1 & -0.5 \end{bmatrix}, \quad \mathbf{T}_I = \begin{bmatrix} 0.5 & 1 \\ 0.5 & -1 \end{bmatrix}. \tag{2.4}$$

Introduction of (2.3), (2.4) allows rephrasing in the modal domain the MTL equations describing the terminal sections and wiring structure.

In this occasion, if the differential lines are driven by a pair of differential source, V_{S1}= -V_{S2}=$V_S/2$, transfer the exciting source in model domain by (2.4) is:

$$V_{S,m} = \begin{bmatrix} V_{S,cm} \\ V_{S,dm} \end{bmatrix} = T_V^{-1} \cdot \begin{bmatrix} V_{S1} \\ V_{S2} \end{bmatrix} = \begin{bmatrix} 0 \\ V_S \end{bmatrix} \tag{2.5}$$

Similarly, for the CM excitation lines, with source V_{S1}=V_{S2}=V_S, the CM independent source can be obtained in the same way.

For the termination imbalance, the impedance matrices $\mathbf{Z}_X$ (X =L, R) associated with the passive part of the terminal networks in Figure 2-1 can be written as,

$$\mathbf{Z}_X = \begin{bmatrix} Z_{GX} + Z_{1X} & Z_{GX} \\ Z_{GX} & Z_{GX} + Z_{2X} \end{bmatrix}. \tag{2.6}$$

By employing the similarity transformation matrices $\mathbf{T}_V$ and $\mathbf{T}_I$, we can convert it into modal domain and the following general expression is obtained,

$$\mathbf{Z}_{X,m} = \mathbf{T}_V^{-1} \cdot \mathbf{Z}_X \cdot \mathbf{T}_I = \begin{bmatrix} Z_{GX} + Z_D / 4 & \Delta Z_X \\ \Delta Z_X & Z_D \end{bmatrix} = \begin{bmatrix} Z_{CM} & \Delta Z_X \\ \Delta Z_X & Z_{DM} \end{bmatrix}. \tag{2.7}$$

where $\mathbf{Z}_{X,m}$ is the modal termination impedance matrices, Z_{CM} and Z_{DM} , with capital subscript CM and DM specially indicates common and differential mode terminal impedances, respectively.

Therefore, the port constrains for the termination in model domain of each end can be written as：

$$\begin{pmatrix} V_{cm}(0) \\ V_{dm}(0) \end{pmatrix} = \begin{pmatrix} 0 \\ V_S \end{pmatrix} - Z_{L,m} \bullet \begin{pmatrix} I_{cm}(0) \\ I_{dm}(0) \end{pmatrix} \tag{2.8}$$

$$\begin{pmatrix} V_{cm}(\ell) \\ V_{dm}(\ell) \end{pmatrix} = Z_{R,m} \bullet \begin{pmatrix} I_{cm}(\ell) \\ I_{dm}(\ell) \end{pmatrix} \tag{2.9}$$

As for transmission line, its wiring structure is modeled as a uniform and lossless three-conductor MTL in free-space, with p.u.l. inductance and capacitance matrices as following:

$$\mathbf{L} = \begin{bmatrix} \ell_1 & \ell_m \\ \ell_m & \ell_2 \end{bmatrix}, \quad \mathbf{C} = \begin{bmatrix} c_1 & c_m \\ c_m & c_2 \end{bmatrix} = \frac{1}{v_0^2} \mathbf{L}^{-1}, \tag{2.10}$$

where inequality of diagonal entries, i.e., $\ell_1 \neq \ell_2$, $c_1 \neq c_2$, is at the basis of geometrical imbalance, v_0 denotes the light velocity in free space.

In a similar fashion, inductance and capacitance matrices can be converted into modal domain, leading to the following expressions for the modal p.u.l. parameters matrices:

$$\mathbf{L}_m = \mathbf{T}_V^{-1} \cdot \mathbf{L} \cdot \mathbf{T}_I = \begin{bmatrix} \dfrac{\ell_1 + \ell_2 + 2\ell_m}{4} & \dfrac{\ell_1 - \ell_2}{2} \\ \dfrac{\ell_1 - \ell_2}{2} & \ell_1 + \ell_2 - 2\ell_m \end{bmatrix} = \begin{bmatrix} \ell_{CM} & \Delta\ell \\ \Delta\ell & \ell_{DM} \end{bmatrix}, \tag{2.11}$$

$$\mathbf{C}_m = \mathbf{T}_I^{-1} \cdot \mathbf{C} \cdot \mathbf{T}_V = \begin{bmatrix} c_1 + c_2 - 2c_m & \dfrac{c_1 - c_2}{2} \\ \dfrac{c_1 - c_2}{2} & \dfrac{c_1 + c_2 + 2c_m}{4} \end{bmatrix} = \begin{bmatrix} c_{CM} & \Delta c \\ \Delta c & c_{DM} \end{bmatrix}, \tag{2.12}$$

where out-diagonal entries $\Delta\ell$, Δc (ideally null in the case of well-balanced wiring structures) are responsible for distributed coupling (and mode conversion) between the DM and CM lines with p.u.l. parameters ℓ_{DM}, c_{DM} and ℓ_{CM}, c_{CM}, respectively.

Since in free-space the characteristic impedance matrix $\mathbf{Z}_C$ is proportional to the p.u.l. length inductance matrix in (2.10) as $\mathbf{Z}_C = v_0 \mathbf{L}$, modal characteristic impedance matrix $\mathbf{Z}_{C,m}$ takes the expression:

$$\mathbf{Z}_{C,m} = \mathbf{T}_V^{-1}\mathbf{Z}_C\mathbf{T}_I = \begin{bmatrix} Z_{cm} & \Delta Z_\ell \\ \Delta Z_\ell & Z_{dm} \end{bmatrix} = \frac{v_0}{2}\begin{bmatrix} \frac{\ell_1+\ell_2}{2}+\ell_m & \ell_1-\ell_2 \\ \ell_1-\ell_2 & 2(\ell_1+\ell_2-2\ell_m) \end{bmatrix}. \tag{2.13}$$

where Z_{cm} and Z_{dm} with lower-case subscripts *cm* and *dm* indicate common and differential mode characteristic impedances, respectively.

Hence, resorting to the chain-parameter representation, the relationships between modal voltages and currents at line terminals can be cast as:

$$\begin{pmatrix} \mathbf{V}_m(\ell) \\ \mathbf{I}_m(\ell) \end{pmatrix} = \begin{bmatrix} \cos(\beta\ell)\mathbf{1}_2 & -j\sin(\beta\ell)\mathbf{Z}_{C,m} \\ -j\sin(\beta\ell)\mathbf{Z}_{C,m}^{-1} & \cos(\beta\ell)\mathbf{1}_2 \end{bmatrix} \cdot \begin{pmatrix} \mathbf{V}_m(0) \\ \mathbf{I}_m(0) \end{pmatrix}, \tag{2.14}$$

where ℓ is the line length, $\beta = 2\pi f / v_0$ the CM and DM propagation constant (i.e., $\beta_{cm}=\beta_{dm}=\beta$, degenerate mode), $\mathbf{1}_2$ the 2×2 identity matrix.

Hence, the voltage and current in the model domain or at each end of the transmission lines can be easily worked out with referring eq. (2.8), (2.9) and (2.14) simultaneously.

Meanwhile, from the above matrices, the occurrence of mode conversion can be readily ascribed to the presence of the non-null out-diagonal entries ΔZ_ℓ, ΔZ_X. These parameters represent a measure of the different impedance seen by each of the two wires with respect to ground at the terminal sections (ΔZ_X) or at each position along the DL (ΔZ_ℓ). Accordingly, the former contribution (i.e., imbalance due to line terminations) is responsible for lumped mode conversion at the DL ends, whereas the latter (i.e., imbalance due to asymmetries in the line cross-section) gives rise to distributed mode conversion

along the differential line. Conversely, if the interconnection and its terminal networks were perfectly balanced, out-diagonal entries in (2.7), (2.13) would be null, i.e., $\Delta Z_\ell = \Delta Z_X = 0,$ and CM and DM quantities would propagate separately.

2.2 Modeling strategy

In well-balanced case, the separated terminal network can be derived into modal domain as following:

$$\mathbf{Z}_{X,m}^{bal} = \begin{bmatrix} Z_{GX} + Z_D / 4 & 0 \\ 0 & Z_D \end{bmatrix} = \begin{bmatrix} Z_{CM} & 0 \\ 0 & Z_{DM} \end{bmatrix}. \tag{2.15}$$

where $\mathbf{Z}_{X,m}^{bal}$ denotes the termination impedance matrices of the balanced structure.

If the termination is imbalance, after mode conversion, the out-diagonal elements will not be null anymore. The imbalanced terminal network can be derived as (2.7).

Therefore, when comparing (2.7) with (2.15), the unbalanced case can be interpreted as a perturbation of the corresponding balanced structure.

$$\mathbf{Z}_{X,m} = \mathbf{Z}_{X,m}^{bal} + \begin{bmatrix} 0 & \Delta Z_X \\ \Delta Z_X & 0 \end{bmatrix}, \tag{2.16}$$

Similarly, under the assumption that d is large enough to make the distribution of current in the conductors uniform, in well-balanced case Figure 2-3(a), the mode conversion will diagonalize the L and C matrices. The mode p.u.l can be derived as:

$$\mathbf{L}_m^{bal} = \begin{bmatrix} L_{cm}^{bal} & 0 \\ 0 & L_{dm}^{bal} \end{bmatrix},\ \mathbf{C}_m^{bal} = \begin{bmatrix} C_{cm}^{bal} & 0 \\ 0 & C_{dm}^{bal} \end{bmatrix} \tag{2.17}$$

where,

$$L_{cm}^{bal} = \frac{\mu_0}{\pi}\left[\frac{\ln(\frac{2h}{r})}{4} + \frac{\ln(1+4\frac{h^2}{d^2})}{8}\right] \tag{2.18}$$

$$L_{dm}^{bal} = \frac{\mu_0}{\pi}[\ln(\frac{2h}{r}) - \frac{\ln(1+4\frac{h^2}{d^2})}{2}] \tag{2.19}$$

$$C_{cm}^{bal} = \frac{16\ln(\frac{2\mathrm{h}}{r}) - 8\ln(1+\frac{4h^2}{d^2})}{c_0^2 \Delta L_{square}^{bal}} \tag{2.20}$$

$$C_{dm}^{bal} = \frac{4\ln(\frac{2\mathrm{h}}{r}) + 2\ln(1+\frac{4h^2}{d^2})}{c_0^2 \Delta L_{square}^{bal}} \tag{2.21}$$

where $\Delta L_{square}^{bal} = \frac{\mu_0}{\pi}\{4[\ln(\frac{2h}{r})]^2 - [\ln(1+\frac{4h^2}{s^2})]^2\}$.

Obviously, in most cases, the geometric parameters of lines couldn't be perfectly equal to each other (well balanced). Thus, in unbalanced case(Figure 2-2(b)), the modal p.u.l can be derived as,

$$\mathbf{L}_m^{unb} = \begin{bmatrix} L_{cm}^{unb} & \Delta L \\ \Delta L & L_{dm}^{unb} \end{bmatrix},\ \mathbf{C}_m^{unb} = \begin{bmatrix} C_{cm}^{unb} & \Delta C \\ \Delta C & C_{dm}^{unb} \end{bmatrix} \tag{2.22}$$

where,

$$L_{cm}^{unb} = \frac{\mu_0}{8\pi}[\ln(\frac{4(h^2-\Delta h^2)}{r^2}) + \ln(1+4\frac{h^2-\Delta h^2}{d^2})] \tag{2.23}$$

$$L_{dm}^{unb} = \frac{\mu_0}{2\pi}[\ln(\frac{4(h^2-\Delta h^2)}{r^2}) - \ln(1+4\frac{h^2-\Delta h^2}{d^2})] \tag{2.24}$$

$$C_{cm}^{unb} = 8\frac{\ln[\frac{4(h^2-\Delta h^2)}{r^2}] - \ln[1+\frac{4(h^2-\Delta h^2)}{d^2}]}{c_0^2 \Delta L_{square}^{unb}} \tag{2.25}$$

$$C_{dm}^{unb} = 2\frac{\ln[\frac{4(h^2-\Delta h^2)}{r^2}] + 2\ln[1+\frac{4(h^2-\Delta h^2)}{d^2}]}{c_0^2 \Delta L_{square}^{unb}} \tag{2.26}$$

where Δh is the imbalance factor, $\Delta h \in [0, d]$, and

$$\Delta L_{square}^{unb} = \frac{\mu_0}{\pi}\{4\ln[\frac{2(h-\Delta h)}{r}]\ln[\frac{2(h+\Delta h)}{r}]-[\ln(1+\frac{4(h^2-\Delta h^2)}{d^2})]^2\} \tag{2.27}$$

The anti-diagonal elements in (2.22) can be derived as:

$$\Delta L = \frac{\mu_0}{4\pi}\ln(\frac{h-\Delta h}{h+\Delta h}),\ \Delta C = \frac{4\ln(\frac{h+\Delta h}{h-\Delta h})}{c_0^2 \Delta L_{square}^{unb}} \tag{2.28}$$

If Δh is equal to d, a total (or maximum) unbalance case could be obtained. Since in most cases, $h>>d$. The following approximation can be found:

$$\begin{cases} h^2-\Delta h^2 \approx h^2 \\ \ln[\frac{2(h-\Delta h)}{r}]\ln[\frac{2(h+\Delta h)}{r}] \approx [\ln(\frac{2h}{r})]^2 \end{cases} \tag{2.29}$$

Thus, from (2.17)-(2.29), the following approximate relationships can be found:

$$\begin{cases} L_{cm}^{unb} \approx L_{cm}^{bal}, L_{dm}^{unb} \approx L_{dm}^{bal} \\ C_{cm}^{unb} \approx C_{cm}^{bal}, C_{dm}^{unb} \approx C_{dm}^{bal} \\ \Delta L_{square}^{unb} \approx \Delta L_{square}^{bal} \end{cases} \tag{2.30}$$

Previous relationships show that, even though line imbalance occurs, CM and DM p.u.l. parameters will be the same as the perfect balance case. The only difference is that in $\boldsymbol{L}$ and $\boldsymbol{C}$ the out-diagonal elements will not be null in case of imbalance, that is to say:

$$\mathbf{L}_m^{unb} \approx \mathbf{L}_m^{bal} + \begin{bmatrix} 0 & \Delta L \\ \Delta L & 0 \end{bmatrix} \tag{2.31}$$

$$\mathbf{C}_m^{unb} \approx \mathbf{C}_m^{bal} + \begin{bmatrix} 0 & \Delta C \\ \Delta C & 0 \end{bmatrix} \tag{2.32}$$

Since in free-space the characteristics impedance matrix takes the expression $\mathbf{Z}_C = v_0 \mathbf{L}$, the unbalanced DL can be interpreted as a perturbation of the corresponding balanced structure with characteristic impedance matrix:

$$\mathbf{Z}_{C,m} = \mathbf{Z}_{C,m}^{bal} + \begin{bmatrix} 0 & \Delta Z_\ell \\ \Delta Z_\ell & 0 \end{bmatrix}, \tag{2.33}$$

where $\mathbf{Z}_{C,m}^{bal}$ denotes the characteristic impedance of the balanced structure.

From the above approximation, the following results can be also obtained:

$$Z_{cm} = Z_{cm}^{bal} \cong 60 \ln\left(2h / \sqrt{r\, d}\right) \tag{2.34}$$

$$Z_{dm} = Z_{dm}^{bal} \cong 120 \ln(d / r), \tag{2.35}$$

and the imbalanced coefficient ΔZ_ℓ can be expressed as function of geometrical parameters as

$$\Delta Z_\ell = v_0 \frac{\ell_1 - \ell_2}{2} \cong 30 \ln\left(1 + \frac{\Delta h}{h}\right) \cong 30 \frac{\Delta h}{h}. \tag{2.36}$$

In a similar way, also $\mathbf{Z}_{C,m}^{-1}$ in (2.14) can be written as:

$$\mathbf{Z}_{C,m}^{-1} = \mathbf{T}_I^{-1}(v_0\mathbf{C})\mathbf{T}_V = \begin{bmatrix} Z_{cm}^{-1} & v_0 \frac{c_1 - c_2}{2} \\ v_0 \frac{c_1 - c_2}{2} & Z_{dm}^{-1} \end{bmatrix} = \left(\mathbf{Z}_{C,m}^{bal}\right)^{-1} + \frac{1}{Z_{cm} Z_{dm}} \begin{bmatrix} 0 & -\Delta Z_\ell \\ -\Delta Z_\ell & 0 \end{bmatrix} \tag{2.37}$$

on condition that $\Delta Z_\ell^2 / (Z_{cm} Z_{dm}) << 1$.

Writing modal matrices $\mathbf{Z}_{X,m}$, $\mathbf{Z}_{C,m}$ and $\mathbf{Z}_{C,m}^{-1}$ as in (2.16), (2.33) and (2.37) enables to study the effects due to line and termination imbalance separately, and to subsequently superimpose the two effects to predict the overall modal voltages and currents at line terminals.

Additionally, the modeling approach here adopted is based on the observation that imbalance either due to terminal networks and due to asymmetries in the line cross-section arise from imperfection or tolerance in the manufacture process. Therefore, in practical cases, the overall imbalance is weak. The back-interaction on the dominant mode of currents and voltages excited by mode conversion in the secondary mode is negligible. For

instance, if the DL is driven by a DM source (i.e., if $V_{S1} = -V_{S2} = \frac{1}{2}V_S$), the modal matrices in (2.16), (2.33) and (2.37) can be further approximated as:

$$\mathbf{Z}_{X,m} \cong \mathbf{Z}_{X,m}^{bal} + \begin{bmatrix} 0 & \Delta Z_X \\ 0 & 0 \end{bmatrix}, \tag{2.38}$$

$$\mathbf{Z}_{C,m} \cong \mathbf{Z}_{C,m}^{bal} + \begin{bmatrix} 0 & \Delta Z_\ell \\ 0 & 0 \end{bmatrix}, \qquad \mathbf{Z}_{C,m}^{-1} \cong \left(\mathbf{Z}_{C,m}^{bal}\right)^{-1} + \begin{bmatrix} 0 & -\dfrac{\Delta Z_\ell}{Z_{cm} Z_{dm}} \\ 0 & 0 \end{bmatrix}, \tag{2.39}$$

by virtue of the assumption of weak-imbalance. Hence, the system of equations in (2.14) for the DM (dominant mode) can be cast and solved as the first step as

$$\begin{pmatrix} V_{dm}(\ell) \\ I_{dm}(\ell) \end{pmatrix} \cong \begin{bmatrix} \cos(\beta\ell) & -j\sin(\beta\ell) Z_{dm} \\ -j\sin(\beta\ell) Z_{dm}^{-1} & \cos(\beta\ell) \end{bmatrix} \cdot \begin{pmatrix} V_{dm}(0) \\ I_{dm}(0) \end{pmatrix}, \tag{2.40}$$

$$V_{dm}(0) \cong V_S - Z_D I_{dm}(0)\,, \tag{2.41}$$

$$V_{dm}(\ell) \cong Z_D I_{dm}(\ell), \tag{2.42}$$

where all contributions due to the CM (secondary mode) are disregarded. Similar results, omitted for brevity, are obtained for CM quantities when the DL is driven by the CM source $V_{S1} = V_{S2} = V_S$. Therefore, under the assumption of weak imbalance, voltages and currents of the dominant mode can be computed as the wiring structure and its terminal networks were perfectly balanced, by solution of the equivalent modal circuits in Figure 2-4.

Accuracy of the prediction obtained by the approximate modal circuits in Figure 2-4 can be proven by comparison versus exact solution of MTL equations. As a specific example, a 1 m-long wiring structure composed of two bare wires with radius r = 0.5 mm, wire distance d =2.5mm, nominal height h =50 mm, and fed by a pure DM source $V_{S1} = -V_{S2}$ = 0.5 V is considered. The plots in Figure 2-5 represent DM voltages at the right DL-end for different degrees of line and termination imbalance and for ground impedances $Z_{GL} = Z_{GR}$= 0 Ω (worst-case condition for termination imbalance [6]). The comparison clearly shows that DM voltages are not influenced by possible imbalance affecting either the line cross-

section or the terminal networks even for uncertainties on the values of the series impedances in (2.1) on the order of 40% (in this case, the maximum differences observed in Figure 2-5 are on the order of 0.3 dB).

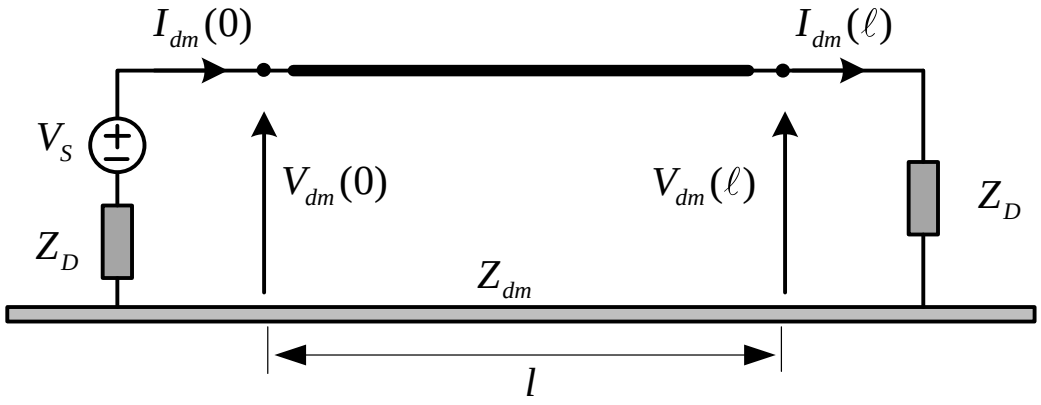

(a)

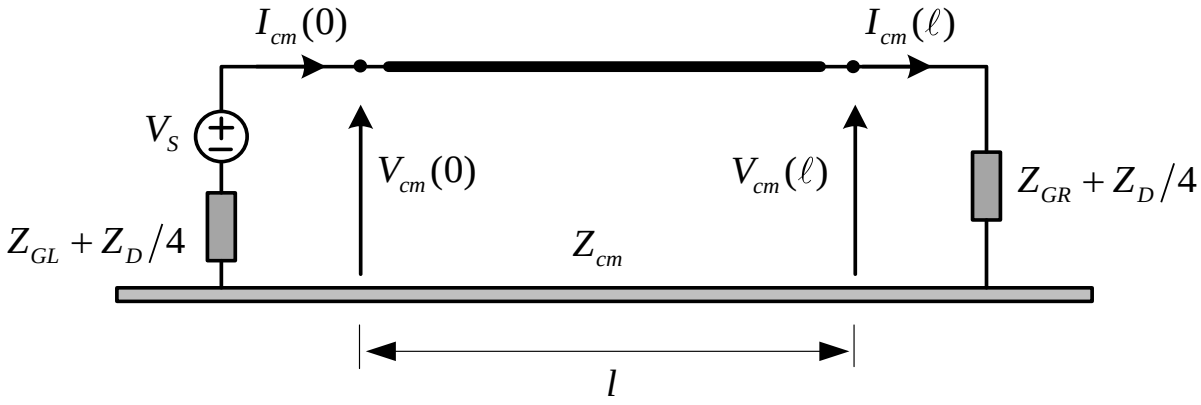

(b)

Figure 2-4 Approximate (a) DM and (b) CM circuits obtained under the assumption of weak unbalance for (a) DM and (b) CM excitation of the DL circuit in Figure 2-1.

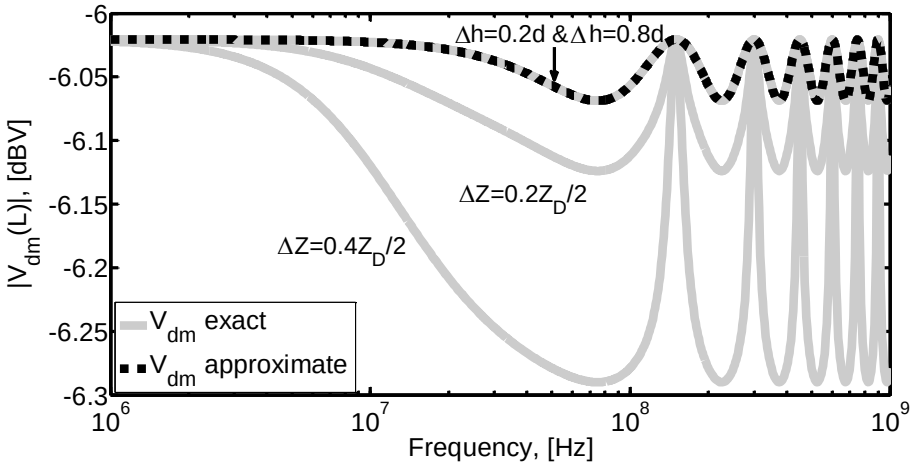

Figure 2-5 DM voltages at the right DL end (Z_D = 0.9 Z_{dm}, $Z_{GL(R)}$ = 0 Ω). Solid grey curves: exact solution of MTL equations. Dashed-black curve: DM circuit in Figure 2-4(a)

3 MODE CONVERSION DUE TO UNDESIRED TERMINATION IMBALANCE

In this Chapter, the phenomenon of mode conversion of differential-line circuits terminated with not-perfectly balanced loads is investigated. By resorting to the assumption of weak-imbalance, it can be modeled by simple equivalent circuits in which mode conversion is represented by dependent sources. The proposed approach has general value and the potential to readily explain and quantify the role of termination imbalance in systems involving differential lines.

3.1 Termination networks under analysis

To investigate the model conversion due to the termination imbalance of differential circuits, specific feeding conditions will be exploited in the following sections to drive the transmission line shown in Figure 2-1.

In this structure, the interconnection is assumed to be perfectly balanced (e.g., the simulation results shown in this work refer to two bare wires running at the same height above ground). The terminal networks (theoretically balanced and ideally matched to the line DM impedance) are assumed to be slightly unbalanced. Without loss of generality, they are modeled by lumped T-circuits, with ground impedances Z_{GL}, Z_{GR} and series impedances taking the general expression in (2.1). Here we introduce coefficients δ_X (i.e., $0<\delta_X<1$) indicating the degree of imbalance at the left ($X=L$) and right ($X=R$) termination, which takes the expression $\delta_X = \dfrac{\Delta Z_X}{Z_D/2}$. So that we can rewrite (2.1) as:

$$\begin{matrix} Z_{S1,X} \\ S2,X \end{matrix} = Z_D(1\pm\delta_X)/2, \quad X = L,R \tag{3.1}$$

For this structure, resorting to the modal decomposition in [2] proves that modal voltages and currents propagate separately along the line, and are related at line terminations by two uncoupled systems of equations—one for the CM (subscript *cm*) and the other for the DM (subscript *dm*)—in the equation(2.14). Mode mixing arises at the terminal networks, whose impedance matrixes $\mathbf{Z}_L$, $\mathbf{Z}_R$ can be written in the modal domain as

$$\mathbf{Z}_{X,m}=\begin{bmatrix} Z_{GX}+Z_D/4 & \delta_X Z_D/2 \\ \delta_X Z_D/2 & Z_D \end{bmatrix}=\begin{bmatrix} Z_{CM} & \Delta Z_X \\ \Delta Z_X & Z_{DM} \end{bmatrix}. \tag{3.2}$$

In (3.2), subscript $X = L, R$ denotes the left and right line-end, respectively, impedances Z_{CM} and Z_{DM} are the CM and DM impedances of each terminal network, respectively, and cross-impedances ΔZ_X account for mode conversion through the imbalance coefficient δ_X. It is worth noting here that the right-most expression in (3.2) is general, in fact it can be obtained by processing input impedance measurement data of any terminal network. Therefore, the results obtained in the following are not limited to the specific circuit model initially adopted in Figure 2-1, involving coefficients δ_X, with $0<\delta_X<1$.

3.2 DM-to-CM conversion due to termination imbalance

In the analysis, the TLs are assumed to be driven by a pure DM voltage source (dominant mode). So in Figure 3-1, a DM voltage source V_S (DM signaling) is connected with the left TL-end and the CM current distribution due to such a circuit excitation is evaluated. To this end, the uncoupled TL equations in (2.14) are combined with the coupled sets of port-constraints enforced by the terminal networks, i.e.,

$$V_{dm}(0)=V_S-Z_D I_{dm}(0)-\Delta Z_L I_{cm}(0), \tag{3.3}$$

$$V_{cm}(0)=-Z_{CM} I_{cm}(0)-\Delta Z_L I_{dm}(0), \tag{3.4}$$

$$V_{dm}(\ell)=Z_D I_{dm}(\ell)+\Delta Z_R I_{cm}(\ell), \tag{3.5}$$

$$V_{cm}(\ell)=Z_{CM} I_{cm}(\ell)+\Delta Z_R I_{dm}(\ell). \tag{3.6}$$

This leads to the equivalent modal circuit in Figure 3-1, where although the signal source VS directly acts on the DM only, modal quantities can still mix at the line-ends. In spite of this, if the terminal networks are weakly unbalanced, solution of such a circuit can be sequentially approached. As a matter of fact, as long as termination imbalance is weak, one can ignore the back-interaction of the induced CM currents on DM quantities (dominant mode). This allows re-writing (3.3), (3.5) as

$$V_{dm}(0)\approx V_S-Z_D I_{dm}(0) \qquad V_{dm}(\ell)\approx Z_D I_{dm}(\ell) \tag{3.7}$$

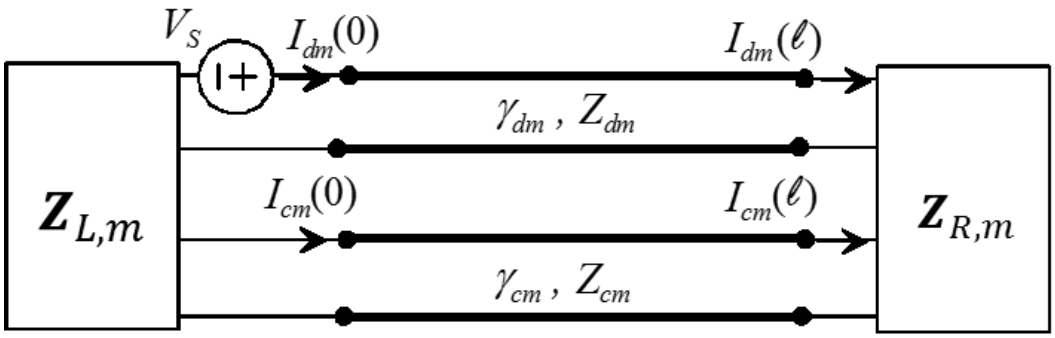

Figure 3-1 Differential circuit driven by a DM voltage source VS: Equivalent circuit model (exact model) in the modal domain.

and predict DM quantities as the first step by solution of the equivalent modal TL in Figure 3-2(a), which does not depend on termination imbalance. Afterwards, CM currents can be handled, by giving a circuit interpretation in terms of controlled voltage sources [Figure 3-2 (b)] to the DM-related terms in (3.4), (3.6). Closed-form expressions for the voltage sources driving the CM circuit in Fig. 3(b) can be obtained after some simple algebra involving the obtained DM currents. This yields:

$$\tilde{V}_L = -\Delta Z_L I_{dm}(0) = \frac{\Delta Z_L}{Z_D}\cdot\left[V_{dm}(0) - V_S\right] = \frac{-(\alpha_D \mathrm{sh}_{dm} + \mathrm{ch}_{dm})\Delta Z_L Z_{dm}^{-1}}{(1+\alpha_D^2)\mathrm{sh}_{dm} + 2\alpha_D \mathrm{ch}_{dm}} V_S \tag{3.8}$$

$$\tilde{V}_R = \Delta Z_R I_{dm}(\ell) = \frac{\Delta Z_R}{Z_D}\cdot V_{dm}(\ell) = \frac{\Delta Z_R Z_{dm}^{-1}}{(1+\alpha_D^2)\,\mathrm{sh}_{dm} + 2\alpha_D\,\mathrm{ch}_{dm}} V_S \tag{3.9}$$

where $\mathrm{sh}_{dm} = \sinh(\gamma_{dm}\ell)$, $\mathrm{ch}_{dm} = \cosh(\gamma_{dm}\ell)$, and $\alpha_D = Z_D / Z_{dm}$ accounts for mismatch at the terminations of the DM circuit. The CM-current distribution is then evaluated as a function of the line coordinate ξ as:

$$I_{cm}(\xi) = [\alpha_C \sinh(\gamma_{cm}\xi) + \cosh(\gamma_{cm}\xi)]\, I_{cm}(0) - Z_{cm}^{-1}\sinh(\gamma_{cm}\xi)\tilde{V}_L, \tag{3.10}$$

where $I_{cm}(0) = \dfrac{Z_{cm}^{-1}\{\tilde{V}_L\,[\alpha_C \sinh(\gamma_{cm}\ell) + \cosh(\gamma_{cm}\ell)] - \tilde{V}_R\}}{(1+\alpha_C{}^2)\sinh(\gamma_{cm}\ell) + 2\alpha_C \cosh(\gamma_{cm}\ell)}$ and coefficient α_C = Z_{CM} / Z_{cm} accounts for mismatch at each end of the CM circuit. Once the current-distribution in (3.10) is known, several models are available in the literature for RE prediction (e.g., in [10]).

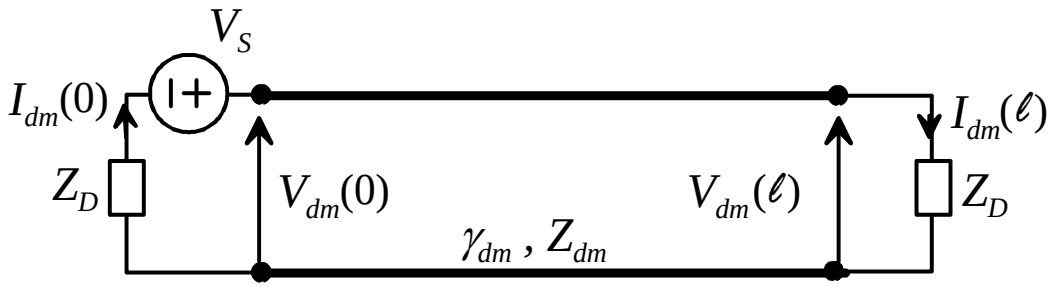

(a)

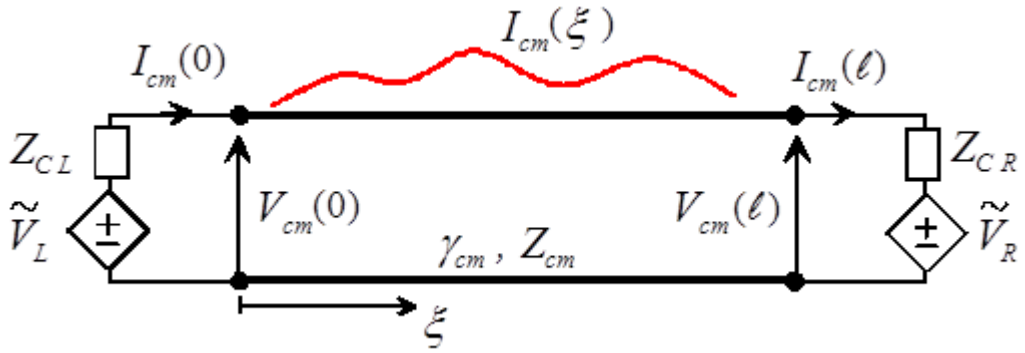

(b)

Figure 3-2 Predict model: Approximate (a) DM and (b) CM circuits obtained under the assumption of weak imbalance of line terminations.

3.3 Validation and comparative analysis

In Figure 3-2(b), DM-to-CM conversion is represented by two voltage sources proportional to (a) the DM voltages across the left-end (3.8) and right-end (3.9) impedances of the DM circuit, and (b) the degree of imbalance of each termination. Indeed, $\Delta Z_X / Z_D = \delta_X/2$, with $X=L, R$. Therefore, the larger δ, the larger the amount of DM converted into CM and, as a consequence, the weaker is the assumption at the basis of model derivation. However, limitations of the weak-imbalance assumption cannot be formulated in terms of δ only. Indeed, the CM impedance Z_{CM} also plays a role of paramount importance, as they determine the amount of CM currents re-converted (back interaction) into DM. Particularly, since CM currents are the largest for minimum value of Z_{CM}, the most stringent conditions on δ apply in this case. In passing, the influence of mismatch (α_D) shall be also accounted for. However, Z_D is usually almost matched to Z_{dm}; as a specific example, the results here shown were obtained for $\alpha_D = 0.8$.

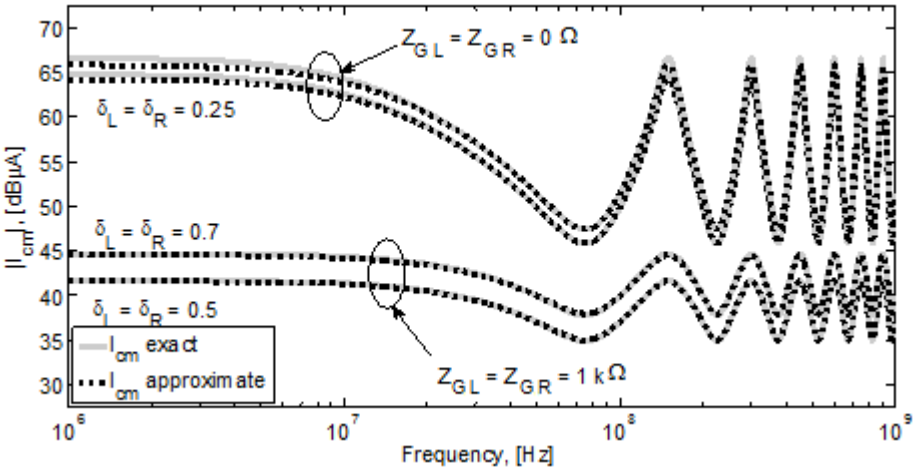

(a)

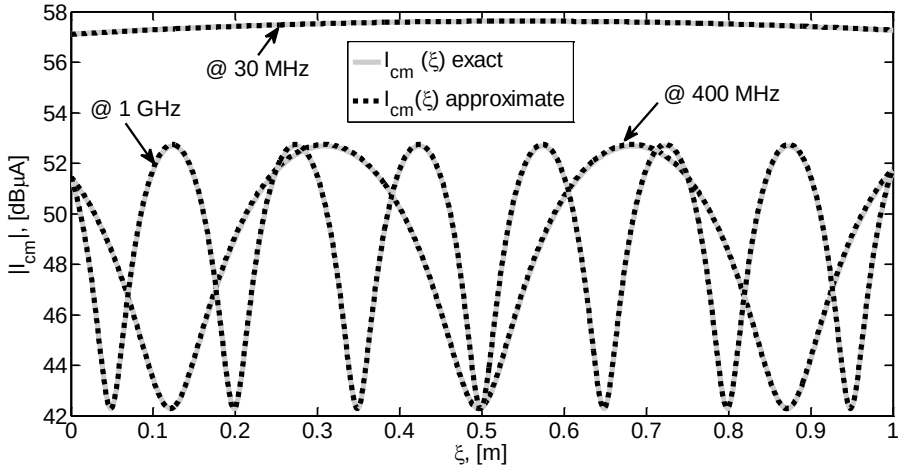

(b)

Figure 3-3 Exact v.s. approximate prediction model: (a) Frequency response of $I_{cm}(0)$; and (b) CM current distribution (Z_{GL}=Z_{GR} = 0 Ω; δ_R = δ_L = 0.3).

Specific examples of comparison between exact and approximate predictions in terms of (a) frequency response of CM currents at line terminations and (b) CM current distribution at specific frequencies are shown in Figure 3-3(a) and Figure 3-3(b), respectively. The comparison confirms model accuracy and sensitivity to CM impedances. Namely, while in the worst-case condition (i.e., Z_{GL} =Z_{GR}=0 Ω), imbalance coefficients on the order of δ = 0.25-0.3 may lead to maximum discrepancies (which occur for frequencies at which the line length is much shorter than the wavelength λ) on the order of 0.5-0.9 dB, the maximum discrepancies obtained for CM impedances much larger than Z_{cm} do not exceed

0.3 dB even for values of δ on the order of 0.7. Although not shown here for brevity, discrepancies on the same order of magnitude are observed also in DM current prediction.

3.4 CM-to-DM conversion

TL susceptibility to external electromagnetic (EM) fields has been exhaustively studied in the past, leading to equivalent circuit models of the victim TL where the interference (i.e., a plane wave field impinging the line) is represented by lumped and distributed voltage and/or current sources. Among these, we will refer to the Agrawal model [17], and since the target is evaluating CM and DM currents at line terminations, we will represent the interference via lumped voltage sources connected with the line ends. Additionally, since in typical cable bundles the wires are in close proximity to each other, the *filament bundle* approximation [18] can be exploited, which considers CM-to-DM conversion as the dominant contribution to DM interference. For the specific line under analysis, this leads to the circuit model in Figure 3-4, where each wire is driven by the voltage sources V_{SL}, V_{SR}. Expressions for these sources, omitted here for brevity, depend on the specific characteristics of the impinging EM wave and can be found in [18].

3.4.1 Approximate solution by the weak-imbalance assumption

Solution of the circuit in Figure 3-4 in the modal domain requires combining the uncoupled equations in (2.14) with the port constraints enforced by the terminal networks, i.e.,

$$V_{cm}(0) = -V_{SL} - Z_{CM} I_{cm}(0) - \Delta Z_L I_{dm}(0), \tag{3.11}$$

$$V_{dm}(0) = -Z_D I_{dm}(0) - \Delta Z_L I_{cm}(0), \tag{3.12}$$

$$V_{cm}(\ell) = -V_{SR} + Z_{CM} I_{cm}(\ell) + \Delta Z_R I_{dm}(\ell), \tag{3.13}$$

$$V_{dm}(\ell) = Z_D I_{dm}(\ell) + \Delta Z_R I_{cm}(\ell). \tag{3.14}$$

It is worth noting the presence of the source terms into the CM-voltage expressions only. This confirms that CM is the main effect involved in field-to-wire coupling, while the DM is a secondary effect, which results from CM-to-DM conversion due to termination imbalance. Under the assumption of weak imbalance, the back-interaction of the induced DM currents on CM quantities can be neglected, and CM voltages in (3.11), (3.13)can be re-written as,

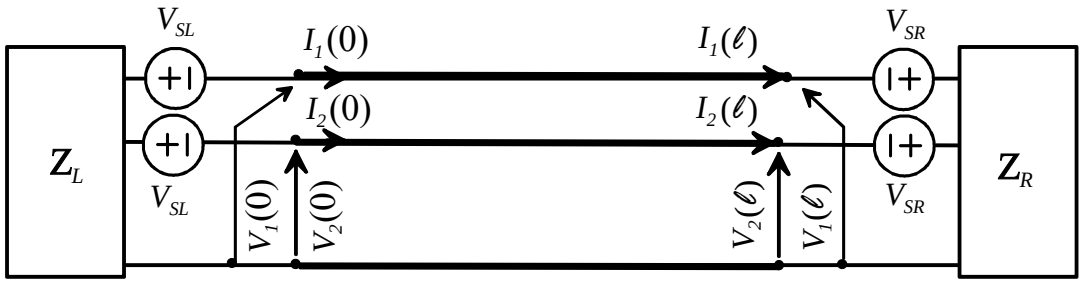

Figure 3-4 Equivalent circuit model of the differential line illuminated by an impinging EM field: Agrawal model [17].

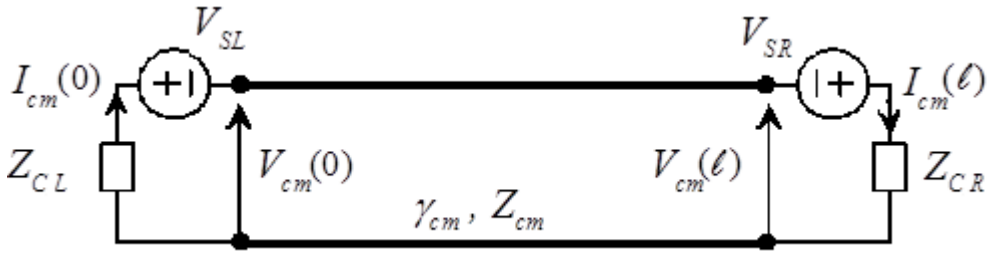

(a)

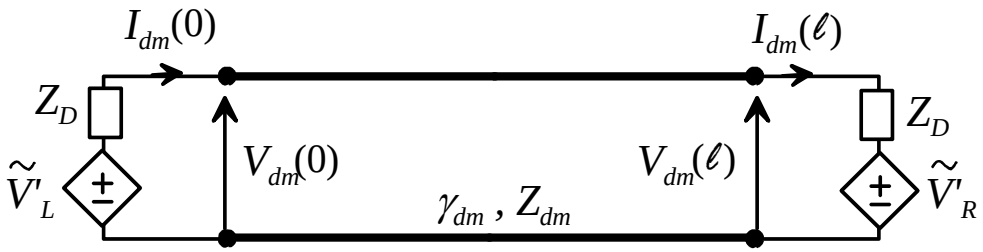

(b)

Figure 3-5 RS prediction model: Approximate (a) CM and (b) DM circuits obtained under the assumption of weak imbalance of line terminations.

$$V_{cm}(0) \approx -V_{SL} - Z_{CM} I_{cm}(0), \tag{3.15}$$

$$V_{cm}(\ell) \approx -V_{SR} + Z_{CM} I_{cm}(\ell). \tag{3.16}$$

This approximation leads to the equivalent CM circuit in Figure 3-5(a), which does not depend on the degree of imbalance of the terminal units and can be solved as the first step. The obtained CM currents, $I_{cm}(0), I_{cm}(\ell)$, become the source terms for the DM circuit in Figure 3-5(b). Indeed, according to(3.12)(3.14), this circuit is driven by two voltage sources proportional to CM currents through the impedances ΔZ_L, ΔZ_R, i.e., $\tilde{V}'_L = -\Delta Z_L I_{cm}(0)$,

$\tilde{V}'_R = \Delta Z_R I_{cm}(\ell)$. Preliminary solution of the CM circuit yields the following expressions for the voltage sources in Fig. 6(b):

$$\tilde{V}'_L = \frac{\Delta Z_L}{Z_{CM}} \cdot [V_{SL} + V_{cm}(0)] = \frac{\Delta Z_L Z_{cm}^{-1}[V_{SL}(\alpha_C \,\mathrm{sh}_{cm} + \mathrm{ch}_{cm}) - V_{SR}]}{(1+\alpha_C{}^2)\,\mathrm{sh}_{cm} + 2\alpha_C\,\mathrm{ch}_{cm}}, \tag{3.17}$$

$$\tilde{V}'_R = \frac{\Delta Z_R}{Z_{CM}} \cdot [V_{SR} - V_{cm}(\ell)] = \frac{\Delta Z_R Z_{cm}^{-1}[V_{SR}(\alpha_C \,\mathrm{sh}_{cm} + \mathrm{ch}_{cm}) - V_{SL}]}{(1+\alpha_C{}^2)\,\mathrm{sh}_{cm} + 2\alpha_C\,\mathrm{ch}_{cm}}, \tag{3.18}$$

where $\mathrm{sh}_{cm} = \sinh(\gamma_{cm}\ell)$, $\mathrm{ch}_{cm} = \cosh(\gamma_{cm}\ell)$, The DM noise currents are then readily evaluated by solution of the DM circuit in Figure 3-5(b).

3.4.2 Weak imbalance and CM-to-DM conversion

The sources driving the DM circuit in Figure 3-5(b) can be interpreted as the product of the voltage across termination CM impedances in Figure 3-5(a) by the CM-to-DM conversion factor $\Delta Z_X/Z_{CM}$ (with $X=L, R$). Such a coefficient characterizes termination's ability in converting the CM into DM, by weighing the degree of imbalance of a given termination by its CM impedance. Indeed, it is very similar to the well-known concept of common mode rejection ratio (CMRR), to which it can be easily related as $\Delta Z / Z_C$ = 2 / CMRR. For a given degree of imbalance, the CM-to-DM conversion factor shows that the smaller the CM impedance, the more efficient the conversion mechanism. Particularly, for minimum CM impedance values the DM currents are the largest and the most stringent conditions on the maximum degree of imbalance shall apply. Indeed, the back-interaction of the DM currents on the CM circuit can no longer be neglected, unless limiting δ_X. However, even in the worst-case condition Z_{GL} = Z_{GR} = 0 Ω (i.e., Z_{CM} = Z_D/4), no significant differences between exact and approximate predictions of both modal currents are observed for values of δ_X up to 0.4. For values of δ_X larger than 0.4, the observed discrepancies are also influenced by the specific incidence conditions of the incoming EM field. For end-wire and broadside excitation [10] with generic elevation angles and an electric-field vector in the vertical polarization, the approximate model mainly leads to underestimation of the peaks observed in the standing wave region. For generic incidence conditions, small discrepancies are also observed in the lower frequency range. Specific examples of comparison obtained for δ_L= δ_R= 0.5 are shown in Figure 3-6 and confirm model accuracy even in the presence of CM impedances with minimum value.

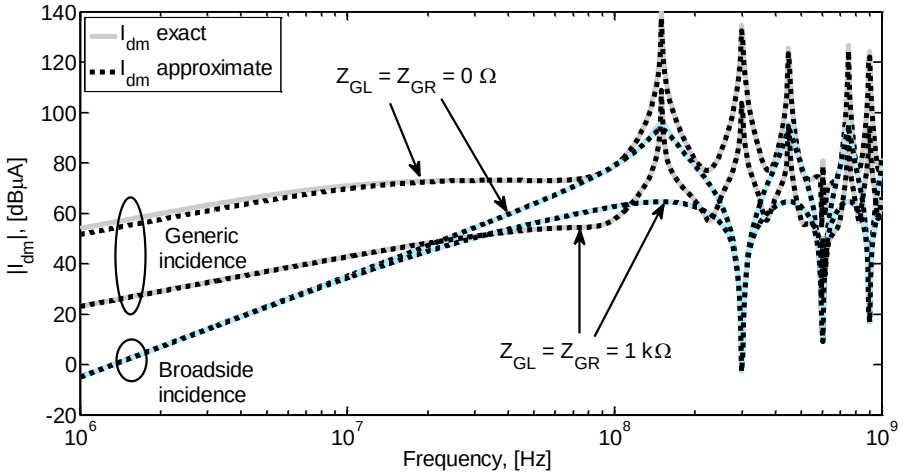

Figure 3-6 DM current $I_{dm}(\ell)$ predicted by the exact (solid curves) and approximate (dotted curves) circuit models in Figure 3-4 and Figure 3-5, respectively. The plots were evaluated by a plane wave with electric-field strength E_0 = 100 V/m and (a) generic incidence conditions, i.e., $\eta = 2\,\pi/5$, $\theta = \pi/5$, $\psi = \pi/6$ according to angles definition in Figure 2-1 of [18], and (b) broadside incidence, i.e., $\eta = 0$, $\theta = \pi/4$, $\psi = \pi/2$.

4 MODE CONVERSION DUE TO UNDESIRED LINE IMBALANCE

In this Chapter, a model representative for the mode conversion occurring in differential lines affected by imbalance of the line cross-section is developed. The model is based on the assumption of weak imbalance, and allows approximate prediction of modal quantities, through modeling of the contributions due to line imbalance by controlled sources with (possibly) frequency dependent gain. The numerical validation is also conducted upon the proposing of the decoupled DM/CM circuits. Accordingly, the reversed mechanism, CM-to-DM model conversion, is discussed.

4.1 Line geometrical structure and corresponding terminations under analysis

To analyze mode conversion due to geometrical imbalance, the differential line is modeled as the same as defined in Figure 2-1: a uniform and lossless MTL. The line is driven from the left end (i.e., $z = 0$) by two equal but opposite voltage sources, assuring DM signaling. The wiring structure analyzed hereunder is shown in Figure 2-3.

Additionally, line terminal sections are assumed to be well-balanced, and modeled by lumped T-circuits with series impedances $Z_D/2$, and ground impedances Z_{GL}, Z_{GR} (for Z_{GL} = Z_{GR} =0Ω, this setup reproduces the impedance conditions for Conversion-Loss parameter measurement recommended in [11][12]).

4.2 DM-TO-CM conversion due to line imbalance

According to (2.13), (2.37), the contribution due to line imbalance can be analyzed starting from the equations in (2.14). Hence, DM and CM voltages and currents at line ends can be predicted by the following system of equations:

$$\begin{pmatrix} V_{dm}(\ell) \\ I_{dm}(\ell) \end{pmatrix} \cong \begin{bmatrix} \cos(\beta\ell) & -j\sin(\beta\ell)Z_{dm} \\ -j\sin(\beta\ell)Z_{dm}^{-1} & \cos(\beta\ell) \end{bmatrix} \cdot \begin{pmatrix} V_{dm}(0) \\ I_{dm}(0) \end{pmatrix} \tag{4.1}$$

$$\begin{pmatrix} V_{cm}(\ell) \\ I_{cm}(\ell) \end{pmatrix} \cong \begin{bmatrix} \cos(\beta\ell) & -j\sin(\beta\ell)Z_{cm} \\ -j\sin(\beta\ell)Z_{cm}^{-1} & \cos(\beta\ell) \end{bmatrix} \cdot \begin{pmatrix} V_{cm}(0) \\ I_{cm}(0) \end{pmatrix} + \begin{pmatrix} V_{\Delta} \\ I_{\Delta} \end{pmatrix} \tag{4.2}$$

$$V_{cm}(0) = -Z_{CM} I_{cm}(0), \qquad V_{cm}(\ell) = Z_{CM} I_{cm}(\ell), \tag{4.3}$$

$$V_{dm}(0) = V_S - Z_{DM} I_{dm}(0), \qquad V_{dm}(\ell) = Z_{DM} I_{dm}(\ell), \tag{4.4}$$

where:

$$V_{\Delta} = -j\sin(\beta\ell)\Delta Z_{\ell} I_{dm}(0), \tag{4.5}$$

$$I_{\Delta} = j\sin(\beta\ell)\Delta Z_{\ell} (Z_{cm} Z_{dm})^{-1} V_{dm}(0). \tag{4.6}$$

A circuit interpretation of (4.1)-(4.6) is shown in Figure 4-1, where effects due to imbalance of the line cross-section are included into the CM circuit by the voltage and current sources V_{Δ}, I_{Δ} in Figure 4-1(b). Likewise those in termination imbalance, these sources are proportional to DM currents and voltages at the terminations of the DM circuit in Figure 4-1(a) and to the imbalance coefficient ΔZ_{ℓ}, which clearly put in evidence the anti-diagonal entries ΔL and ΔC contribute to the model conversion. However, they are actually representative of a distributed instead of a lumped mechanism of mode conversion, and can be lumped at one termination (here the right one) only as long as prediction of voltages and currents at line terminals is the target.

As a matter of fact, their amplitudes depend on the line length and operating frequency through the sinus term. More precisely, as long as the line length is sufficiently smaller than the wavelength $\lambda = v_0 / f$, it can be shown that V_{Δ}, I_{Δ} are proportional to the ratio ℓ / λ, and become null for frequency approaching zero. Conversely, the sources in (3.9), (3.10) are independent of frequency apart from the frequency dependence of the involved DM currents. Nevertheless, in this respect it's worth noting that in practical cases ΔZ_L, ΔZ_R (in Chapter 3) are inherently frequency dependent, since balance performance of terminal networks generally degrade at increasing frequency. For instance, frequency performance of typical center-tap RF transformers (baluns) can be considered [8].

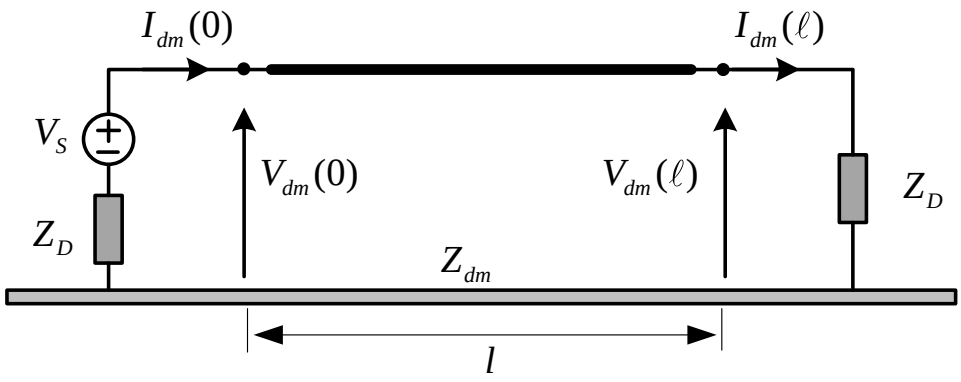

(a)

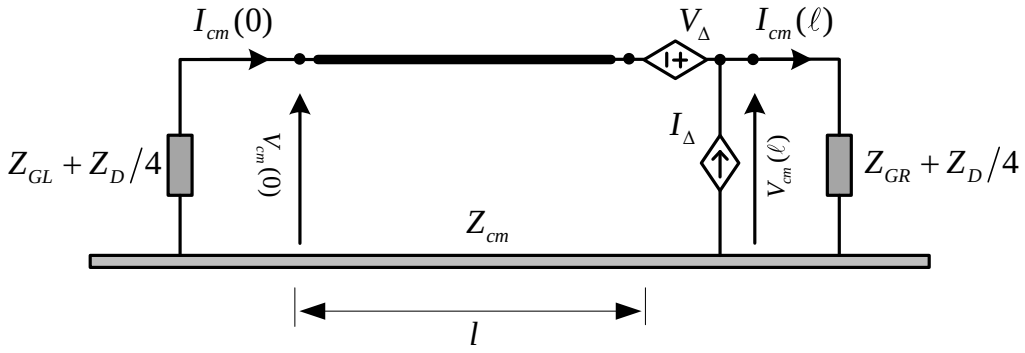

(b)

Figure 4-1 Approximate (a) DM and (b) CM circuits obtained under the assumption of weak imbalance of line imbalance

4.3 Validation and comparative analysis

In this subsection, model accuracy is validated versus exact solution of MTL equations. Specific examples are shown in Figure 4-2.

Concerning line imbalance, the plots in Figure 4-2 investigate the influence on CM voltages of the ground impedances [Figure 4-2 (a)] and of possible mismatching at the terminations of the DM circuit [Figure 4-2 (b)]. By the light of these results, the following differences with respect to termination imbalance can be stated. First, at low frequency CM voltages due to line imbalance always increase with +20 dB/dec frequency slope, due to the distributed nature of mode conversion. Second, maximum CM voltages are induced at line terminals for large (instead of minimum) values of the ground impedances Z_G [in Figure 4-2 (a) for $Z_G = Z_{GL} = Z_{GR} = 1$ kΩ]. Third, since amplitudes and relative signs of the

current and voltage sources V_Δ, I_Δ descend from geometrical properties of the line cross-section, it can be easily proven that contributions due to these sources always sum at the left termination (i.e., close to the signal source), and subtract at the right-end. Therefore, CM voltages at the left termination are larger or, at worst, equal to those at the right termination. As far as model accuracy is concerned, since Δh is very small with respect to h (i.e., $h >> d$), the weak imbalance assumption is always satisfied for $\Delta h \in [0, d]$. Namely, the plots in Figure 4-2 show that even for large degrees of imbalance [upper curves in Figure 4-2 (a)] and strong mismatching of the DM circuit [Figure 4-2 (b)] the differences between exact (grey-solid curves) and approximate (black-dotted curves) predictions is negligible for whatever values of Z_{GL}, Z_{GR}.

4.4 CM-TO-DM conversion due to line imbalance

Similarly, the proposed model can also be successfully extended to analyze the opposite mechanism of conversion from CM (excited by the CM source $V_{S1} = V_{S2} = V_S$) to DM. Indeed, as long as the weak imbalance assumption is satisfied, CM voltages and currents at line terminals can be predicted as the first step by the CM equivalent circuit in Figure 4-3(a), and subsequently exploited as source terms, i.e.,

$$V'_\Delta = -j \sin(\beta \ell) \Delta Z_\ell I_{cm}(0), \tag{4.7}$$

$$I'_\Delta = j \sin(\beta \ell) \Delta Z_\ell (Z_{cm} Z_{dm})^{-1} V_{cm}(0), \tag{4.8}$$

in the equivalent DM circuit in Figure 4-3 (b).

Similar simulation results can be used to prove the accuracy of such an approximate model even for relatively large degrees of imbalance affecting the wiring structure.

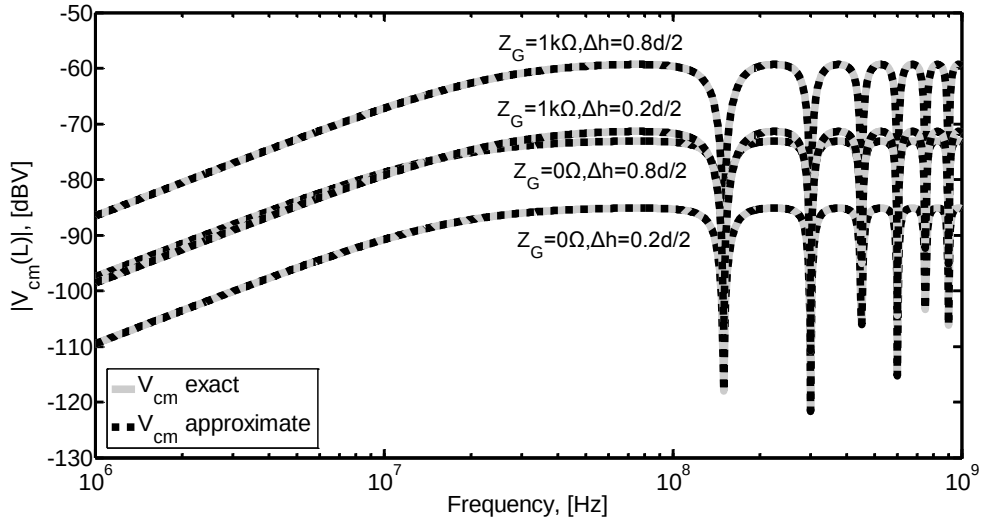

(a)

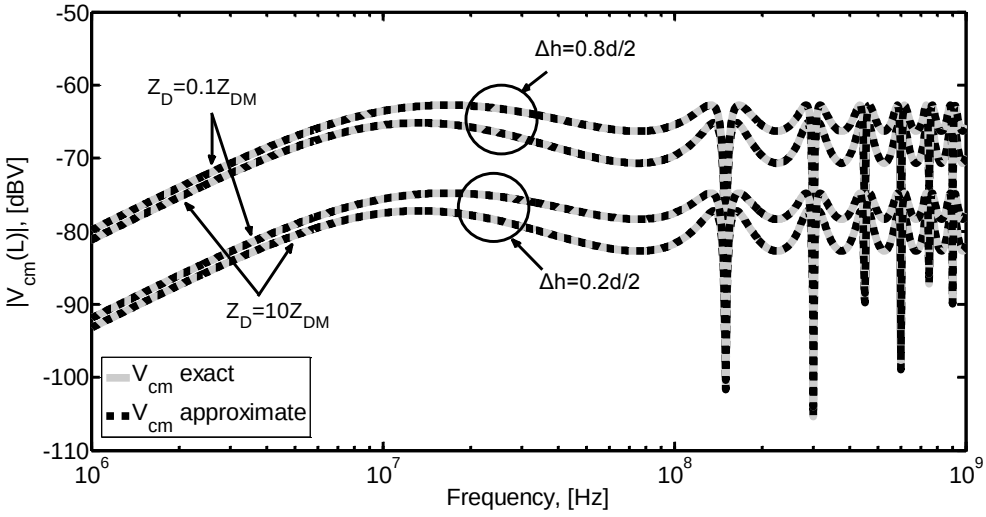

(b)

Figure 4-2 CM voltages due to line imbalance: Proposed model (dotted curves) vs exact MTL solution (grey-solid curves). Influence of (a) ground impedance Z_G = 0 Ω, 1 kΩ, and (b) mismatching (i.e., $Z_D \neq Z_{dm}$) of the DM circuit (Z_G = 1 kΩ).

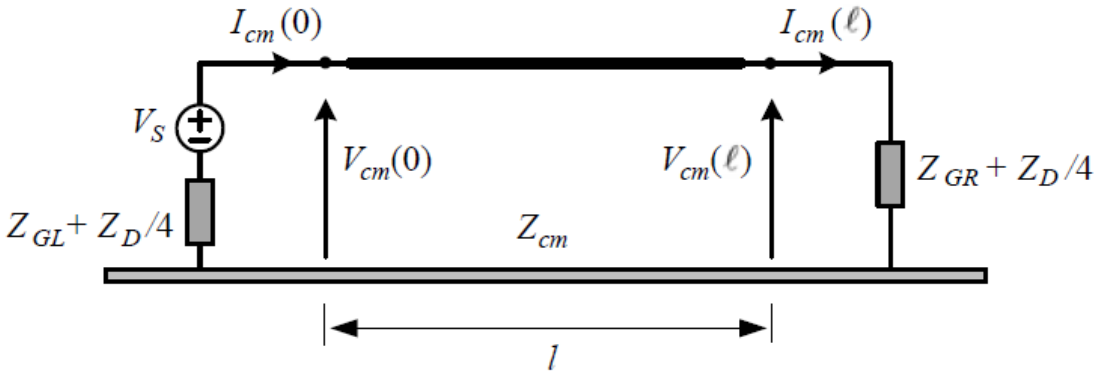

(a)

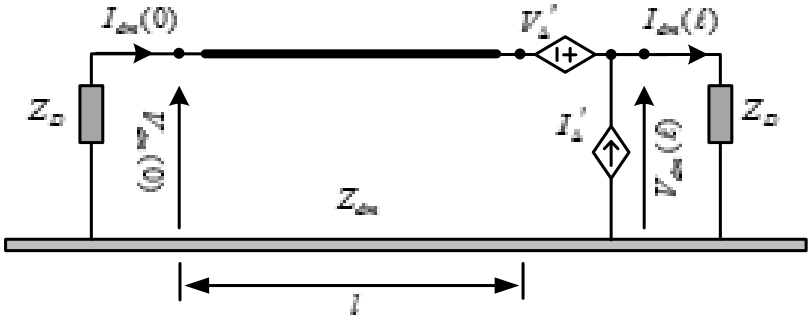

(b)

Figure 4-3 (a) CM circuit (b) DM circuit accounting for CM-to-DM conversion due to line and termination imbalance.

4.5 Upper-bounds to the near- and far-end conversion loss in unbalanced differential lines

As mentioned in Chapter 1, the degree of DM-to-CM conversion and CM-to-DM conversion, which is affected by the line geometrical parameters and should be limited below precautionary levels, can be estimated by measuring the conversion-loss parameters (TCL and LCL, respectively) recommended in ITU standard [11].

In order to derive upper bounds to the associated conversion-loss parameters as function of line geometrical parameters, starting from a measurement setup based on the use of a Network Analyzer (NA) and on the theory of the mixed-mode scattering parameters (SP), analytical expressions of the mixed-mode SPs responsible for mode conversion is cast in closed form resorting to an approximate approach to the solution of the associated TL

equations in the modal domain. Piece-wise linear upper bounds to the involved mixed-mode SPs are then derived, validated versus exact solution of TL equations, and used to investigate mode-conversion sensitivity to geometrical parameters of the DL cross-section.

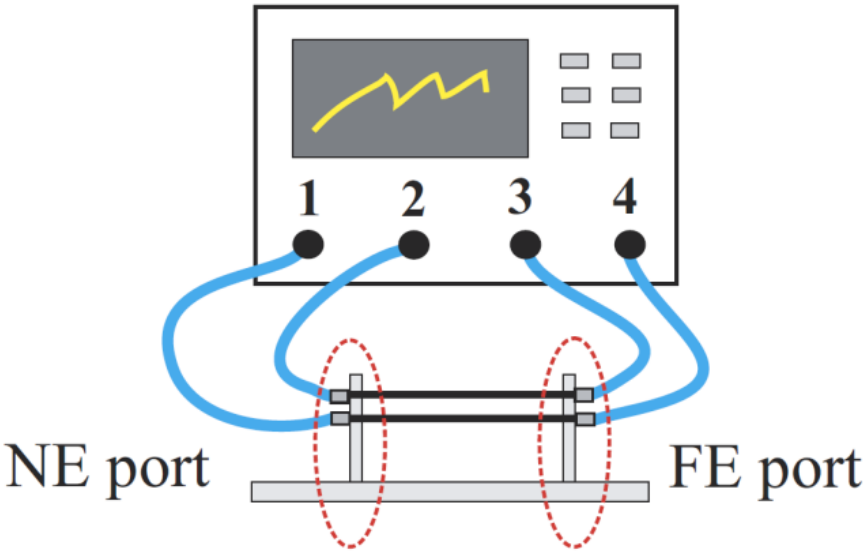

Figure 4-4 Experimental setup for the measurement of conversion loss parameters, [13]

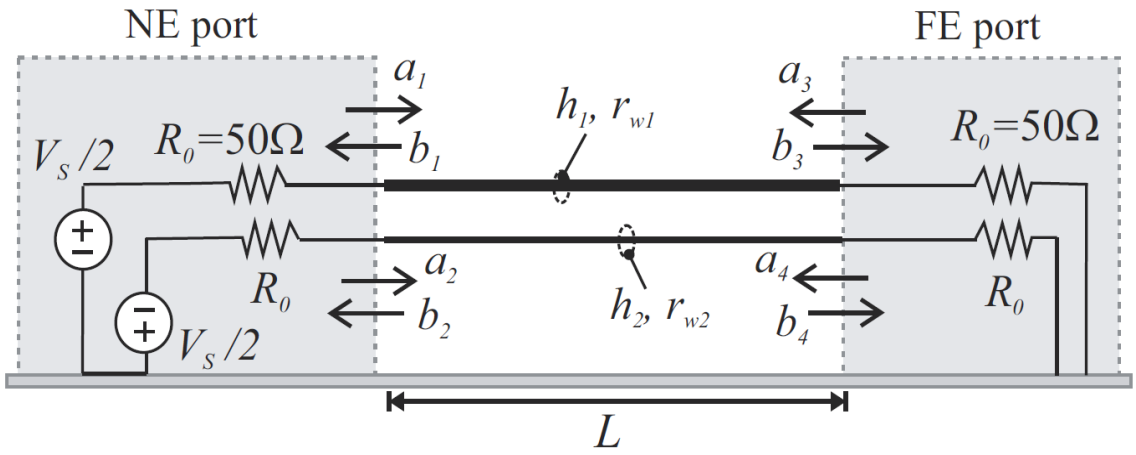

Figure 4-5 Circuit model of the test setup (Figure 4-4) used to measure NE and FE DM-to-CM conversion parameters $S_{cd,NN}$, $S_{cd,FN}$.

4.5.1 Measurement setup

Near-end (NE) and far-end (FE) conversion loss at the output ports of a DL above ground can be measured by exploiting a four-port NA (see Figure 4-4), and by introducing the mixed-mode SP to rephrase the measured SP matrix in terms of CM and DM power waves [2]. This leads to:

$$\begin{pmatrix} \mathbf{b}_{dm} \\ \mathbf{b}_{cm} \end{pmatrix} = \begin{bmatrix} \mathbf{S}_{dd} & \mathbf{S}_{dc} \\ \mathbf{S}_{cd} & \mathbf{S}_{cc} \end{bmatrix} \cdot \begin{pmatrix} \mathbf{a}_{dm} \\ \mathbf{a}_{cm} \end{pmatrix} \tag{4.9}$$

where $\mathbf{b}_{xm} = [b_{NE,xm}\ b_{FE,xm}]^T$, $\mathbf{a}_{xm} = [a_{NE,xm}\ a_{FE,xm}]^T$, $x=c,d$ are backward and forward power-wave vectors in the modal domain (related to the physical power-waves in Figure 4-5 by the similarity transformation in [2]). In (4.9), the mode conversion occurring along the DL is represented by the out-diagonal sub-matrices $\boldsymbol{S}_{cd}$, $\boldsymbol{S}_{dc}$, whose entries are ideally null for perfectly-balanced DLs. For the sake of brevity, we will hereinafter focus the attention on DM-into-CM conversion only, which is represented by matrix $\boldsymbol{S}_{cd}$. Namely, the entries of $\boldsymbol{S}_{cd}$ relate the DM forward waves at the NE and FE terminations of the DL with the resulting CM backward waves, as:

$$\begin{pmatrix} b_{NE,cm} \\ b_{FE,cm} \end{pmatrix} = \begin{bmatrix} S_{cd,NN} & S_{cd,NF} \\ S_{cd,FN} & S_{cd,FF} \end{bmatrix} \cdot \begin{pmatrix} a_{NE,dm} \\ a_{FE,dm} \end{pmatrix} \tag{4.10}$$

In (4.10), the mixed-mode SP $S_{cd,NN}$ (=$S_{cd,FF}$ in case of symmetry with respect to the modal ports) represents DM-to-CM conversion loss at the NE port and is proportional to the inverse of TCL, whereas $S_{cd,FN}$ (= $S_{cd,NF}$ in case of symmetry with respect to the modal ports) represents DM-to-CM conversion loss at the FE port and is proportional to the inverse of TCTL. Similar considerations are valid for the diagonal and out-diagonal entries of matrix $\boldsymbol{S}_{dc}$, which are associated with CM-to-DM conversion and proportional to the inverse of LCL and LCTL, respectively [13].

In order to derive analytical expressions for the SP $S_{cd,NN}$, $S_{cd,FN}$ at the terminations of an unbalanced differential line, the measurement setup in Figure 4-4 is modeled as shown in Figure 4-5, where (a) DM forward power waves take the value: $a_{NE,dm} = V_S / (2\sqrt{2R_0})$, $a_{FE,dm}$=0 (since the impedance at both DM ports is equal to the DM resistance 2 R_0 = 100 Ω involved in the definition of mixed-mode SPs), and (b) the conductors of the two-wire line

above ground are assumed to be bare and lossless, for the sake of simplicity. In such a wiring structure, a certain degree of imbalance may arise due to slightly-different heights above ground of the two conductors or due to different wire radii. As a matter of fact, in both cases, modeling the above structure as a uniform and lossless three-conductor transmission line (TL) in free space leads to asymmetries in the associated p.u.l. inductance and capacitance matrices that are at the basis of mode conversion. Namely, if CM and DM voltages and currents are introduced and used to convert in the modal domain the p.u.l. matrices in (2.10), the obtained matrices are full, with out-of-diagonal entries proportional to the difference between the self-inductances and capacitances. Due to these differences, transformation in the modal domain of the setup in Figure 4-5 yields DM and CM circuits, which are coupled each other as shown in Figure 4-6.

Hence, although the voltage source V_S is feeding the DM circuit only, non-null CM voltages $V_{NE,cm}$, $V_{FE,cm}$ are to be expected, whose relationship with the SP $S_{cd,NN}$, $S_{cd,FN}$ in (2) can be cast as:

$$S_{cd,NN} = 4V_{NE,cm}/V_S\,, \quad S_{cd,FN} = 4V_{FE,cm}/V_S. \tag{4.11}$$

To evaluate the CM voltages $V_{NE,cm}$, $V_{FE,cm}$ in (4.11) , like the prediction model in the previous prediction model in the previous chapters, an approximate solution approach is here adopted, which is based on the assumption of weak coupling between the modal circuits in Figure 4-6.

Under the assumption of matching of the DM circuit (i.e., $Z_{dm} = 2\ R_0 = 100\ \Omega$), piece-wise linear upper bounds to the NE and FE conversion-parameters $S_{cd,NN}$, $S_{cd,FN}$ can be easily derived from the obtained analytical expressions of the CM voltages $V_{NE,cm}$, $V_{FE,cm}$ as:

$$\left.\begin{matrix} S_{cd,NN} \\ cd,FN \end{matrix}\right|_{LF} \approx \frac{\pi}{2R_0} c_0(\ell_1 - \ell_2)\left(1 \pm \frac{R_0^2}{c_0^2 \det(\mathbf{L})}\right)\cdot\frac{L}{\lambda} \tag{4.12}$$

$$\left.\begin{matrix} S_{cd,NN} \\ cd,FN \end{matrix}\right|_{HF} \approx \frac{Z_{cm}}{R_0^2 + 4Z_{cm}^2} c_0(\ell_1 - \ell_2)\left(1 \pm \frac{R_0^2}{c_0^2 \det(\mathbf{L})}\right) \tag{4.13}$$

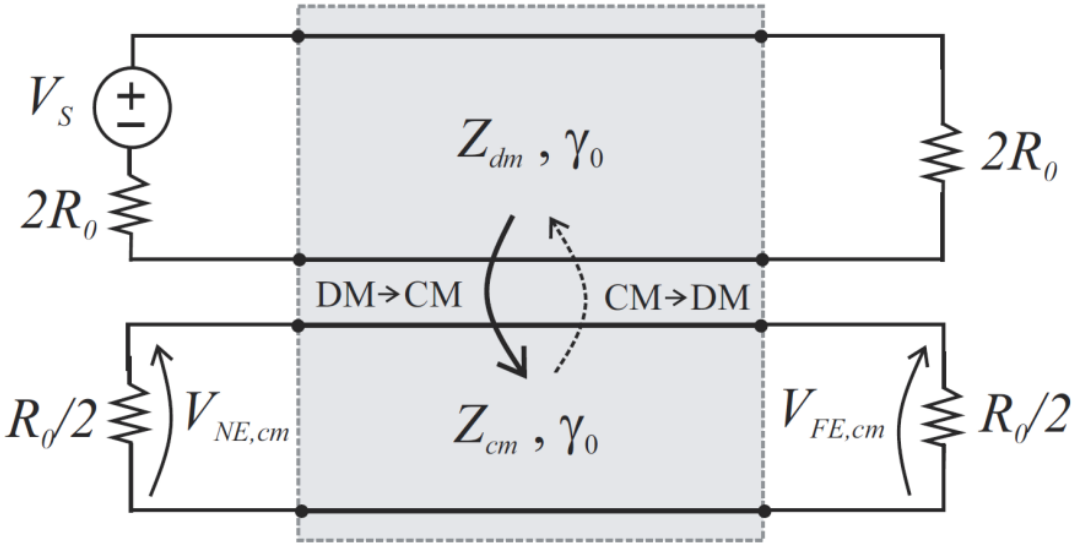

Figure 4-6 Equivalent modal circuit of the setup in Figure 4-5

where ℓ_1, ℓ_2 and det(**L**) are the p.u.l. self-inductances and the determinant of the p.u.l. inductance matrix in (2.10), Z_{cm} is the impedance of the CM circuit in Figure 4-6, $\lambda = f / c_0$ denotes the wavelength at frequency f, and c_0 is the speed of light in free-space. From (4.12), (4.13), it can be observed that: (a) mode conversion is proportional to the difference between the self-inductances ℓ_1, ℓ_2 (as long as wire distance is almost constant); (b) the FE parameter $S_{cd,FN}$ results to be smaller or at worst equal to $S_{cd,NN}$, due to the ± sign in (4.12), (4.13); (c) at low frequency (LF) DM-to-CM conversion is proportional to frequency, whereas at high frequency (HF), the frequency response of $S_{cd,NN}$ and $S_{cd,FN}$ is bounded by flat upper bounds. The above LF and HF intervals are separated by frequency.

$$f^* = \frac{c_0}{\pi L} \cdot \frac{Z_{cm}^{-1} R_0 / 2}{1 + (Z_{cm}^{-1} R_0 / 2)^2} \tag{4.14}$$

which strongly depends on the degree of mismatching, i.e., $(R_0/2)/Z_{cm}$, at the terminations of the CM circuit.

4.5.2 Numerical simulations

Accuracy of the upper-bounds in (4.12), (4.13) are proven in Figure 4-7 by comparison versus predictions of the SP $S_{cd,NN}$ obtained by exact solution of TL equations. These results were evaluated by setting parameters in Figure 4-5 to: r_{w1}=r_{w2}=0.3mm; L=1m, and

$h_{1(2)} = \bar{h} \pm \delta_h / 2$, where $\bar{h} = (h_1 + h_2)/2$ denotes the height of the DL axis, and $\delta_h = h_1 - h_2$. For numerical simulation, the distance between the wire centers was kept constant to the value s=2.75 r_{w1}, so that the DM impedance is almost equal to 100 Ω (condition of matching at the terminations of the DM circuit). In the first plot [Figure 4-7(a)], accuracy of (4.12)-(4.14) is proven for different values of $\bar{h}$ and δ_h. Particularly, the pair of curves in the middle was obtained for $\bar{h} = 10\,\text{mm}$, and $\delta_h = s$, and kept as reference to investigate the sensitivity of DM-to-CM conversion to possible variations of $\bar{h}$ and δ_h. Namely, the second and third configuration were obtained starting from such a reference configuration by doubling the value of δ_h and $\bar{h}$, respectively. This yielded the upper and lower pairs of curves in Figure 4-7(a), that–besides proving accuracy of the proposed upper bounds–show that mode conversion is almost proportional to δ_h and to $1/\bar{h}$, respectively (note the shift of ± 6 dB with respect to the curves in the middle). In the second plot [Figure 4-7(b)], the two wires are let to slightly move with respect to the nominal position $h_{1(2)} = \bar{h}$ so to keep $\bar{h}$ constant to the average value $\bar{h} = 10\,\text{mm}$. Assuming variations in wire positioning anyway limited within the interval $|\delta_h|/s = 1$, repeated run simulations obtained for 1000 values of δ_h normally distributed around the mean value δ_h=0 yielded the exact predictions of $S_{cd,NN}$ plotted in Figure 4-7(b) by thin colored curves. For simplicity, upper bounds to these curves were evaluated by (4.12)-(4.14), and plotted (black lines) for the worst-case only, i.e., $|\delta_h|/s = 1$.

The significant spread of results (~100 dB even for relatively small values of δ_h) in Figure 4-7(b) in combination with the fact that geometrical asymmetries responsible for mode conversion are inherently unknown/uncontrolled quantities suggests to conveniently exploit the proposed upper bounds for the development of computationally-efficient stochastic models, where geometrical parameters that are relevant in mode conversion are treated as random variables.

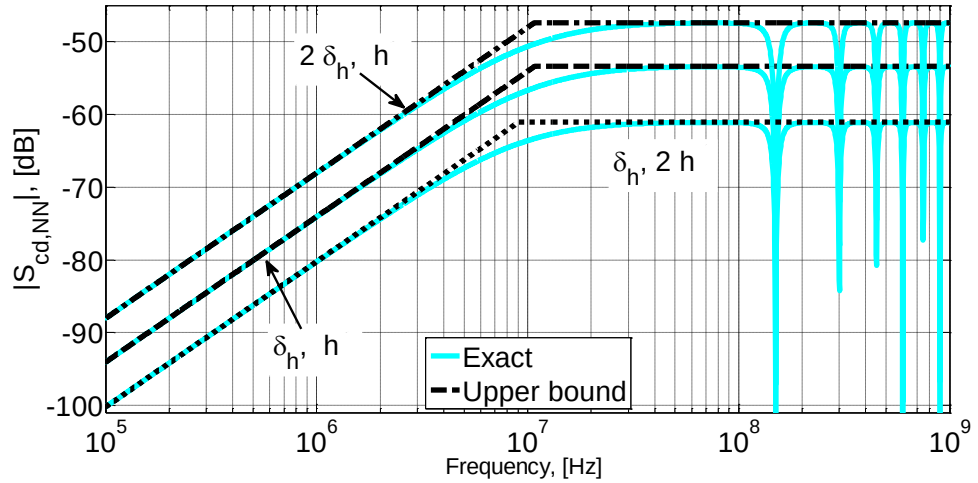

(a)

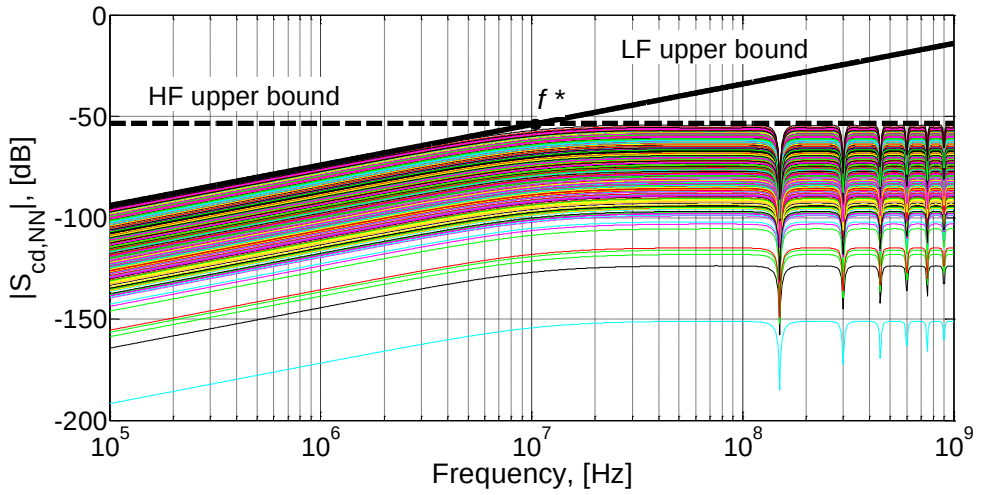

(b)

Figure 4-7 Validation of the upper bounds in (4.12)-(4.14) vs $S_{cd,NN}$ prediction obtained by exact solution of TL equations.

5 LINE AND TERMINATION IMBALANCE: COMPARISON AND SUPERPOSITION

In the previous chapters, conversion models due to line imbalance and terminations imbalance were established. Hereinafter, the two imbalance mechanisms in homogeneous media are compared based on the statistical analysis with selected random variables, with the aim of evaluating the significance of the line imbalance and termination imbalance. In section 5.2, line and termination imbalance are further combined together by the superposition principle, and the equivalent DM-to-CM and CM-to-DM conversion model, including line and termination imbalance are both developed.

5.1 Statistic comparison between line imbalance and termination imbalance

In this section, effects due to possible imbalance affecting the wiring structure are investigated by statistical analysis, with the objective to identify the parameters that play a significant role on mode conversion. Particularly, since line imbalance stems from uncertainties in cable manufacture, that is deviation of some geometrical/electrical parameters from their nominal values, the main quantities responsible for mode conversion result to be inherently unknown and uncontrolled. And similar case will happen for terminations in practice.

Hence, in order to make the comparison more clear, instead of a deterministic model, the model here proposed provides a statistical characterization of mode conversion, where (a) the unbalanced line is treated as a perturbation of the corresponding balanced line; (b) uncontrolled/unknown geometric parameters are treated as random variables, and (c) the terminal networks are not perfectly balanced.

5.1.1 Statistical analysis: description of the wiring structure

In order to evidence the effect of imbalance, a canonical differential-line structure with characteristics as those in Figure 2-1 is considered. It's composed of two identical bare wires of radius *r* ideally running at the same height *h* above an ideal ground plane. To include possible line imbalance due to uncertainties in wires' positioning, we will let the two wires move with respect to the nominal position, so that the actual wire height above

ground (i.e., h_1, h_2) may slightly differ from h. Particularly, in order to keep wire separation, d, constant (as, for example, in an appliance cord), we will hereinafter constrain the wires to rotate along a circle with diameter d as shown in Figure 5-1. In line with this assumption, their actual heights h_1, h_2 can be expressed as function of the rotation angle α as:

$$h_1(\alpha) = h + \sin(\alpha) d/2; \tag{5.1}$$

$$h_2(\alpha) = h - \sin(\alpha) d/2. \tag{5.2}$$

For statistical analysis, the rotation angle α is treated as a random variable (RV), with normal distribution $N(\mu_\alpha;\sigma_\alpha^2)$ around the nominal value $\alpha = 0$ (i.e., $\mu_\alpha = 0$).

Similarly, concerning the terminal networks, in this section, the series impedances in Figure 2-1 are let to slightly differ from their nominal value by the imbalance coefficients δ_L, δ_R as defined in (3.1) :

$$\begin{matrix} Z_{1L} \\ 2L \end{matrix} = Z_D(1 \pm \delta_L)/2 \tag{5.3}$$

$$\begin{matrix} Z_{1R} \\ 2R \end{matrix} = Z_D(1 \pm \delta_R)/2 \tag{5.4}$$

where δ_L and δ_R obey normal distributions:

$$\delta_R \sim N(0;\sigma_{\delta R}^2), \quad \delta_L \sim N(0;\sigma_{\delta L}^2). \tag{5.5}$$

5.1.2 Statistical analysis

The above described wiring structure is modeled as a uniform and lossless three-conductor transmission line, characterized by 2×2 p.u.l. inductance, $\mathbf{L}$, and capacitance, $\mathbf{C} = c_0^{-2}\mathbf{L}^{-1}$ (c_0 being the speed of light in free space), matrices with entries evaluated by the analytical expressions in chapter 2 under the simplifying assumption $d \geq 5r$, which is used to insure the charge and current distributions around the peripheries of the wires are essentially uniform. When the whole structure is transformed in the modal domain, it yields the circuit model in Figure 5-2, which clearly puts in evidence that although the voltage source V_S

excites the DM only, non-null voltages can be measured across the terminations of the CM circuit due to mode conversion and mixing along the wires.

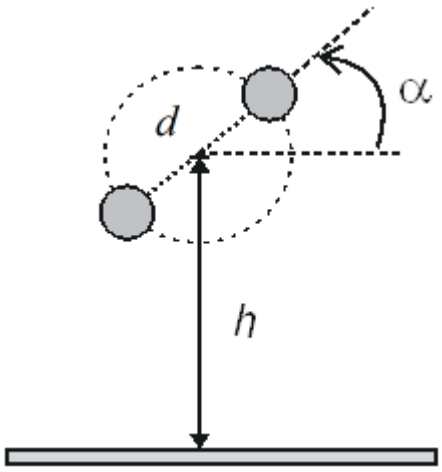

Figure 5-1 Cross-section view of the wiring structure for Statistical analysis

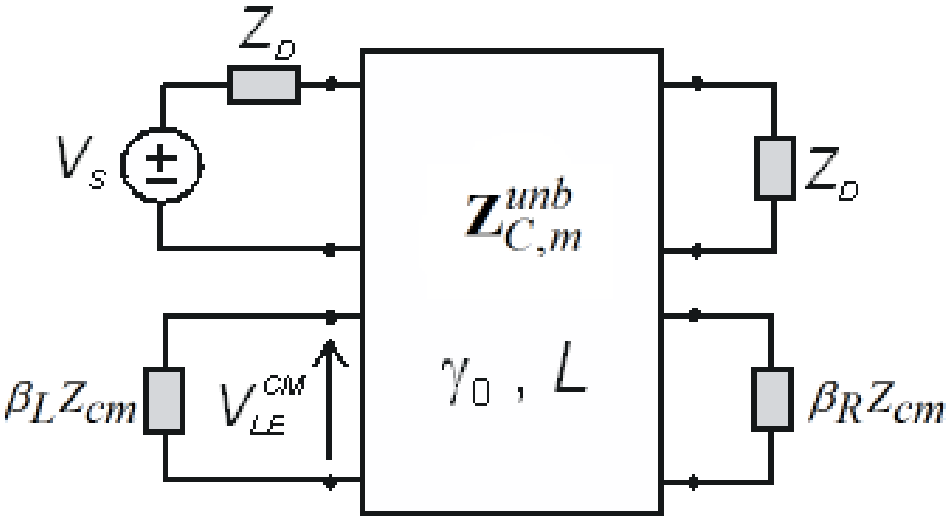

Figure 5-2 Equivalent circuit model in the modal domain (upper: DM; lower: CM).

Particularly, as long as the condition $h >> d$ is satisfied (as in typical EMC test setups, where $h \cong 50\,\text{mm}$), the modal characteristic impedance matrix $\mathbf{Z}_{C,m}^{unb}$ of the unbalanced structure in Figure 5-1 can be interpreted as a perturbation of the modal characteristic impedance matrix $\mathbf{Z}_{C,m}^{bal}$ of the corresponding balanced structure related to the random variable α (i.e., the reference TL with $h_1 = h_2 = h$). Indeed, it can be written as

$$\mathbf{Z}_{C,m}^{unb} \cong \mathbf{Z}_{C,m}^{bal} + \mathbf{Z}(\alpha) = \begin{bmatrix} Z_{cm} & 0 \\ 0 & Z_{dm} \end{bmatrix} + \begin{bmatrix} 0 & Z_{CD}(\alpha) \\ Z_{DC}(\alpha) & 0 \end{bmatrix} \tag{5.6}$$

where: $Z_{dm} \cong c_0 \mu_0 \pi^{-1} \ln(d/r)$, $Z_{cm} \cong c_0 \mu_0 (2\pi)^{-1} \ln\left[2h/\left(r\sqrt{d/r}\right)\right]$ denote DM and CM characteristic impedances, respectively, [8], whereas impedances $Z_{DC}(\alpha)$, $Z_{CD}(\alpha)$ account for mode conversion. These results are the rationale for the choice to keep wire separation constant. Namely, under such a condition, CM and DM line impedances are not affected by line imbalance, and coincide with those of the reference (i.e., balanced) configuration. Hence, line imbalance does not affect the matching of the DM circuit, which can be anyway enforced by $Z_D = Z_{dm}$. Furthermore, coefficients β_L, β_R in Figure 5-2 can be readily defined as $\beta_X = (Z_{GX} + Z_D/4)/ Z_{cm}$, $X = L, R$.

As target variable, the voltage transfer ratio F_{LE} of the CM voltage V_{LE}^{cm} induced at the left termination of the modal circuit in Figure 5-2 over the voltage source V_S is considered, since this quantity can be easily correlated to Transverse Conversion Loss as long as $Z_{GL} = Z_{GR} = 0$. Additionally, the transfer function F_{LE} is written as the product of the following two functions:

$$F_{LE} = \left|V_{LE}^{cm}/V_S\right| = \left|M_{LE}(\gamma_0 L, \beta_L, \beta_R)\right| \cdot \left|G_{LE}(\beta_R, Z_{dm}, Z_{cm}, h, d, r, \alpha)\right|. \tag{5.7}$$

The transfer function M_{LE} retains the frequency dependence of F_{LE} , and takes the expression:

$$M_{LE}(\gamma_0 l, \beta_L, \beta_R) = \frac{\beta_L c_0 \sinh(\gamma_0 l)}{2\left[\sinh(\gamma_0 l)(1+\beta_L\beta_R) + \cosh(\gamma_0 l)(\beta_L + \beta_R)\right]}; \tag{5.8}$$

Where l denotes the line length and $\gamma_0 = j\omega/c_0$ is the common propagation constant of DM and CM quantities (degenerate mode). Conversely, effects due to line imbalance are accounted for by the transfer function G_{LE}. The exact analytical expression of G_{LE} is quite complex as it involves the difference between the p.u.l. self-inductance and self-capacitance parameters in [10]. As explicative examples, the solid curves in Figure 5-3(a) show the dependence of G_{LE} as a function of the rotation angle α for a differential line with h= 50 mm, r = 0.5 mm, d= 2.5 mm, and for two different values of the ground impedances Z_{GL}, Z_{GR}. The observed almost-linear behavior of G_{LE} around α = 0 suggests to

approximate the exact analytical expression by resorting to a Taylor series expansion in a suitably-small interval around $\alpha = 0$. This leads to the approximate expression [see dashed lines in Figure 5-3(a)], which just considers the first two parts (the constant part is zero) of the Taylor expansion:

$$G_{LE}(\beta_R, Z_{dm}, Z_{cm}, h, d, r, \alpha) \cong K_{LE} \cdot \alpha, \tag{5.9}$$

$$K_{LE} = \frac{d\mu_0}{4\pi h Z_{dm}}\left[1 - \frac{4Z_{dm}Z_{cm}\pi^2\beta_R\varepsilon_0\mu_0^{-1}}{\ln(h/d)\ln(4h/d) - \ln(h/r)\ln(4h/r)}\right], \tag{5.10}$$

The analytical expressions in (5.7)-(5.10) can be readily used to evaluate the probability density function (pdf) of F_{LE} in (5.7), by recalling that if α follows a normal distribution $N(0;\sigma_\alpha^2)$, the pdf of its magnitude, $|\alpha|$, is an half-normal distribution [19], with $\mu_{|\alpha|} = \sigma_\alpha\sqrt{2/\pi}$, and $\sigma_{|\alpha|}^2 = \sigma_\alpha^2(1-2/\pi)$. Hence, also F_{LE} in (5.7) is half-normally distributed, with:

$$\mu_{F_{LE}} = \sigma_\alpha\sqrt{2/\pi}\cdot|M_{LE}|\cdot|K_{LE}| \tag{5.11}$$

$$\sigma_{F_{LE}}^2 = \sigma_\alpha^2(1-2/\pi)\cdot M_{LE}^2\cdot K_{LE}^2. \tag{5.12}$$

To validate these analytical results, a repeated-run analysis is applied to a specific differential line with geometrical parameters: h= 50 mm, r= 0.5 mm, d = 2.5 mm, l = 1 m. At each step, the solution process requires (a) to evaluate the line p.u.l. parameters, (b) to find suitable transformation matrices which allow to decouple the multi-conductor TL equations, (c) to solve the system equations with respect to the physical voltages V_1, V_2, and (d) evaluate CM voltages as $V_{CM} = (V_{S1} + V_{S2})/2$. As a specific example, the simulation results obtained for 1000 randomly selected values of the RV $\alpha \sim N(0;\sigma_\alpha^2)$, with $\sigma_\alpha = \pi/18$, and ground impedances Z_{GL}=Z_{GR}=1kΩ [worst case in Figure 5-3(a)], are here considered, that exhibit a spread in F_{LE} levels larger than 60 dB. The good agreement (the maximum discrepancies are less than 1 dB) between the mean value and standard deviation of F_{LE} predicted by the analytic model (solid line) and obtained by post-processing numerical results (dashed lines) is shown in Figure 5-3 (b), and proves the accuracy of the statistical estimates in (5.11) and (5.12).

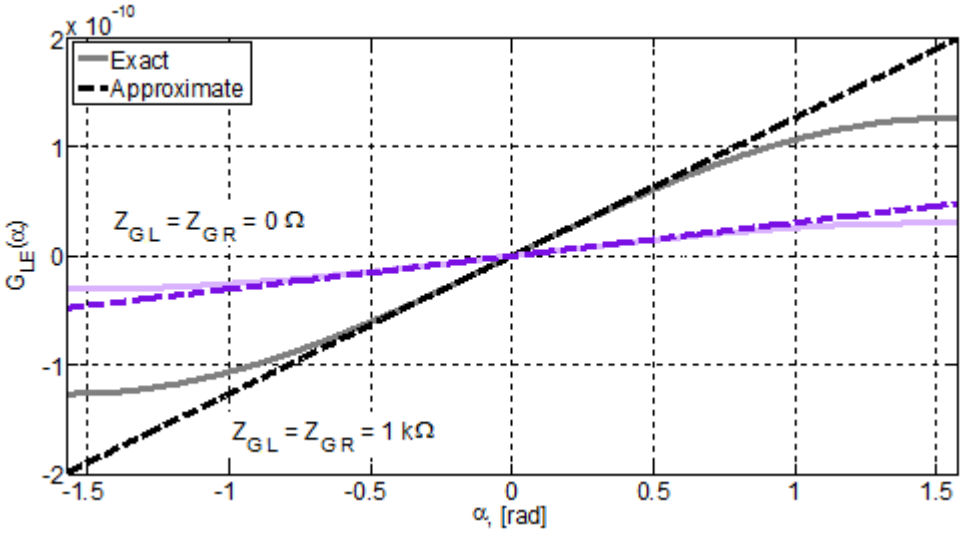

(a)

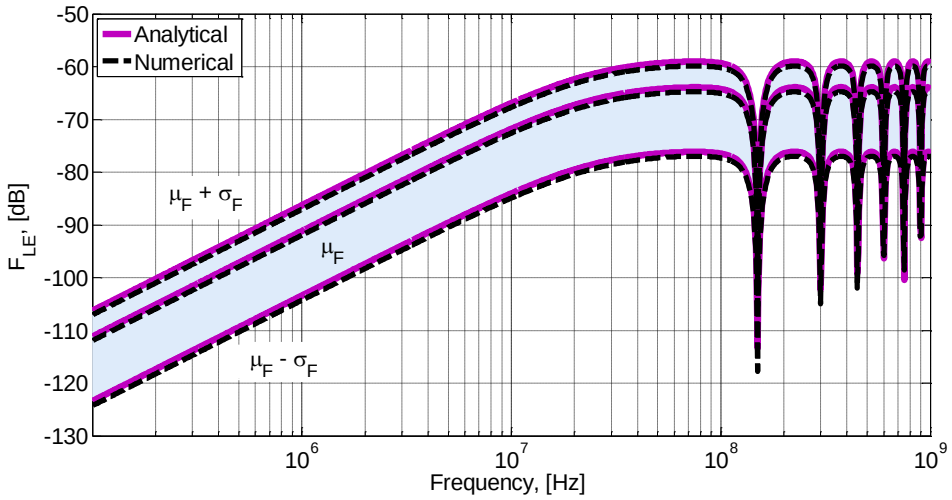

(b)

Figure 5-3 Statistical analysis of line imbalance: (a) Exact dependence of G_{LE} on the rotation angle α (solid curves) versus linear approximation by Taylor expansion (dashed curves); (b) Mean value and standard deviation of F_{LE} ($\sigma_\alpha = \pi/18$; $Z_{GL} = Z_{GR} = 1$ kΩ): Theoretical prediction (solid curves) versus numerical results obtained by 1000 repeated-run simulations (dashed curves).

5.1.3 Comparison between line and termination imbalance

In order to clearly put in evidence the role of line and termination imbalance, a quantitative comparison about transfer function F_{LE} has been made. In this comparison, the parameter values are the same as the section 5.1.2(h = 50 mm, r = 0.5 mm, d = 2.5 mm, l = 1 m), which has line imbalance with $\sigma_\alpha = \pi/18$. Then, the result of F_{LE} due to line imbalance is calculated by using the previous model. When considering termination imbalance, a 2% degree of uncertainty with respect to the nominal impedance is assumed and the result of F_{LE} due to termination imbalance is evaluated by repeated-runs for 1000 randomly selected values of δ_R and δ_L. The comparison, which is in both cases of low (0Ω) and high (1000Ω) grounding impedances, is shown in Figure 5-4. In the same figures, the black lines represent the predictions obtained by (5.11) and (5.12) for the mean value (solid curve) and standard deviation (dashed curves) of the transfer function F_{LE} due to line imbalance while the 1000 colorful lines represent the simulations results due to termination imbalance.

Apart from the low-frequency range, where imbalance due to line terminations is undoubtedly prevailing, the comparison shows that in the standing-wave region of the line the two contributions may become comparable depending on the CM impedance of the terminal networks. As a matter of fact, while F_{LE} due to termination imbalance results to be almost unaffected by Z_{GL}, Z_{GR}, the corresponding transfer function due to line imbalance exhibits a considerable sensitivity to these impedances. Indeed, an increase of more than 15 dB can be observed by comparing the black curves in Figure 5-4(a) with those in Figure 5-4(b). Therefore, although line imbalance is usually considered smaller than imbalance due to line terminations, the analysis here proposed shows that such an effect may not-negligibly contribute to the overall CM voltage in the presence of high-valued CM impedances.

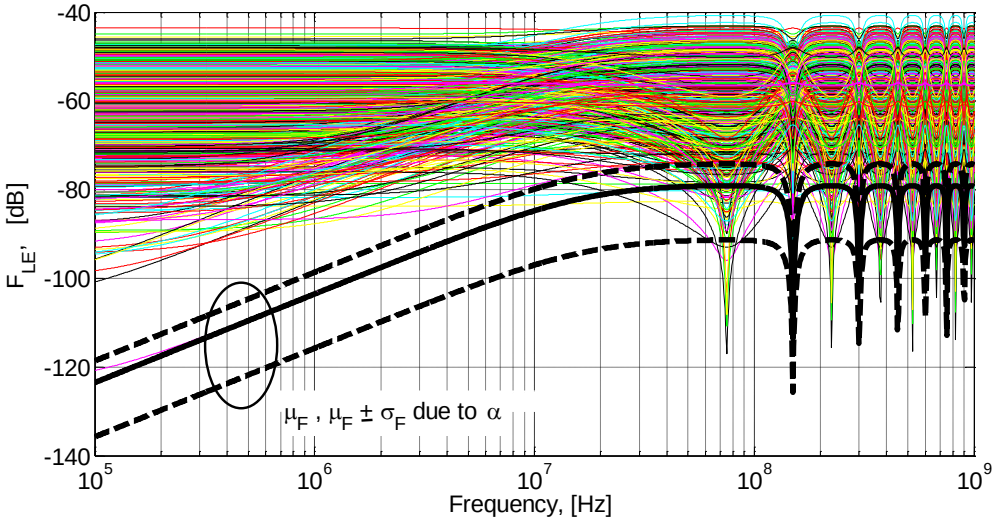

(a)

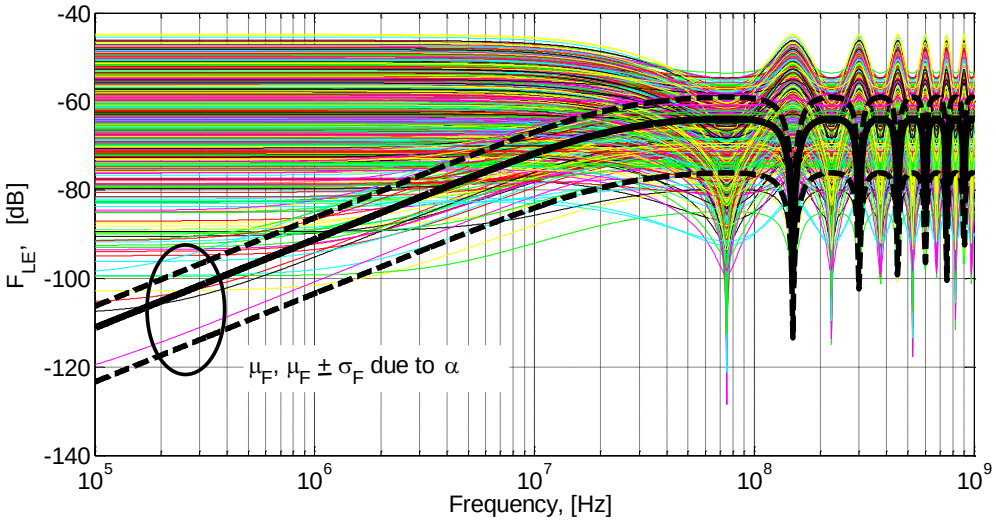

(b)

Figure 5-4 Comparison of line imbalance (statistical estimates of F_{LE}) versus termination imbalance (1000 repeated-run simulations) for two different values of the ground impedances Z_{GL}, Z_{GR}: (a) Z_{GL}, Z_{GR} = 0 Ω; and (b) Z_{GL}, Z_{GR} = 1 kΩ.

5.2 Superposition

In section 2.2, we defined the modal matrices $\mathbf{Z}_{C,m}$, $\mathbf{Z}_{C,m}^{-1}$ and $\mathbf{Z}_{X,m}$ as in (2.16)(2.33) and (2.37), which enables to study the effects due to line and termination imbalance separately, and to subsequently superimpose the two effects (by the superposition principle) to predict the overall modal voltages and currents at line terminals.

5.2.1 Superposition of line and termination imbalances

As long as weak-imbalance assumption is satisfied, effects due to termination and line imbalance can be simultaneously accounted for by superimposing the proposed approximate models in chapter 3 and 4. This leads to the equivalent CM circuit in Figure 5-5, whose sources still involve the DM currents and voltages in Figure 3-2(a) through (3.8), (3.9) and in Figure 4-1(a) though (4.5), (4.6).

Specific examples of results are shown in Figure 5-6, where the overall CM voltage at the left termination is compared with the contributions due to line and terminations imbalance. These plots were obtained for ground impedances equal to $Z_{GL} = Z_{GR} = 1\text{k}\Omega$ (condition leading to maximum contribution due to line imbalance and minimum contribution due to termination imbalance, according to the analysis in section 5.1), and by assuming: $\Delta h = 0.4\ d$, $\Delta Z_L = \Delta Z_R = 0.05\ Z_D/2$. More precisely, the plots in Figure 5-6(a) were evaluated for $\Delta Z_L = \Delta Z_R$, those in Figure 5-6 (b) for $\Delta Z_L = -\Delta Z_R$. Solid-grey curves were obtained by exact solution of MTL equations, whereas dotted-black curves were predicted by the approximate model in Figure 5-5.

Besides proving model accuracy, these results show that–given specific degrees of imbalance–the two contributions may add or subtract each other, depending on the combination of signs of the involved imbalance coefficients. As a rule of thumb, for positive values of ΔZ_ℓ, the two contributions subtract each other if ΔZ_L, ΔZ_R have the same sign [Figure 5-6(a)]. Conversely, if ΔZ_L, ΔZ_R are opposite in sign (and $\Delta Z_\ell > 0$), the two contributions add each other and lead to the largest CM voltages.

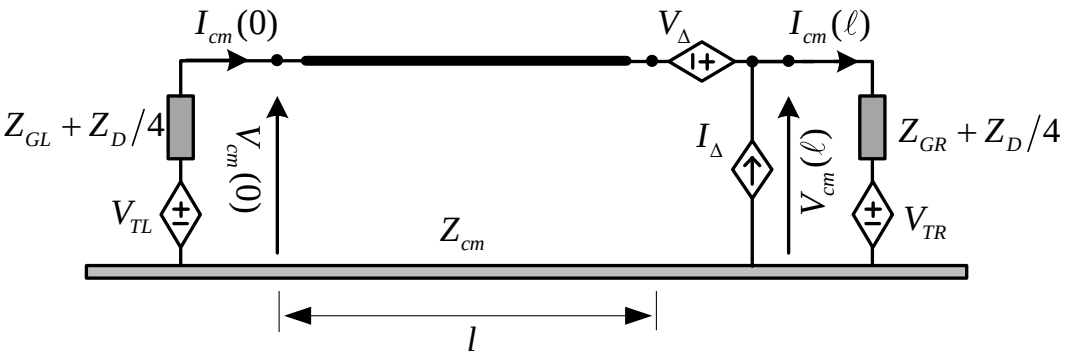

Figure 5-5 Equivalent CM circuit accounting for DM-to-CM conversion due to line and termination imbalance.

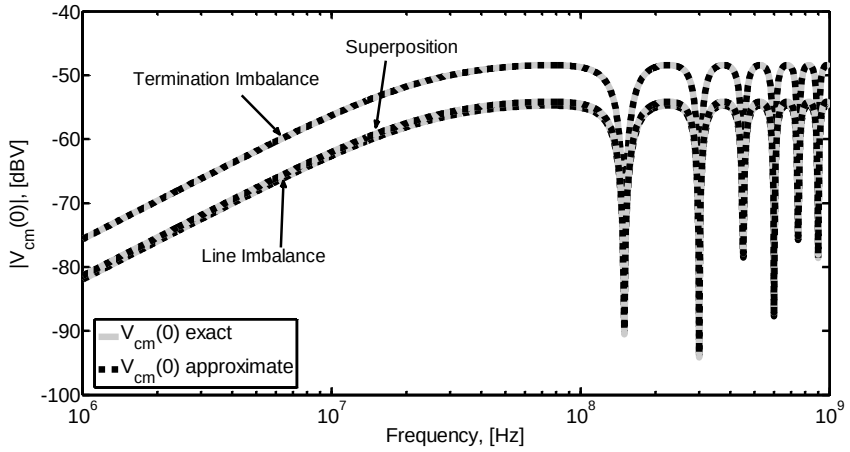

(a)

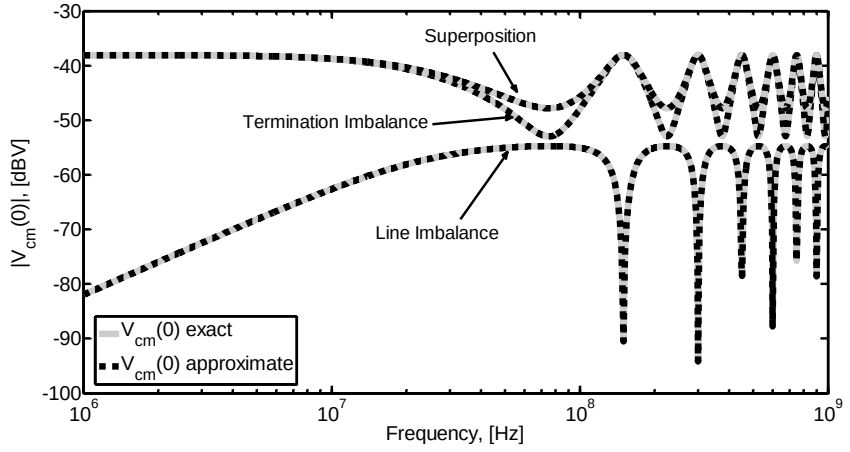

(b)

Figure 5-6 CM voltages obtained by superposition of the contributions due to line and termination imbalance (Z_G = 1 kΩ): (a) $\Delta Z_L = \Delta Z_R$; and (b) $\Delta Z_L = -\Delta Z_R$.

5.2.2 CM-TO-DM conversion

The proposed model in section 5.2.1 can be successfully extended to analyze the opposite mechanism of conversion from CM (excited by the CM source V_{SL}=V_{SR}) to DM. Indeed, as long as the weak imbalance assumption is satisfied, CM voltages and currents at line terminals can be predicted as the first step by the CM equivalent circuit in Figure 3-5(a), and subsequently exploited as source terms, i.e.,

$$V'_{\Delta} = -j\sin(\beta\ell)\Delta Z_{\ell} I_{cm}(0), \tag{5.13}$$

$$I'_{\Delta} = j\sin(\beta\ell)\Delta Z_{\ell}(Z_{cm}Z_{dm})^{-1}V_{cm}(0), \tag{5.14}$$

$$V'_{TL} = -\Delta Z_L I_{cm}(0), \tag{5.15}$$

$$V'_{TR} = -\Delta Z_R I_{cm}(\ell) \tag{5.16}$$

in the equivalent DM circuit in Figure 5-7.

Simulation results can be obtained to prove the accuracy of such an approximate model even for relatively large degrees of imbalance affecting the wiring structure and its terminal loads. The most significant difference with respect to DM-to-CM conversion is concerned with the role played by the ground impedances Z_{GL}, Z_{GR}. Namely, for CM-to-DM conversion small values of Z_{GL}, Z_{GR} lead to maximum DM voltages due to line imbalance, while in the same condition, minimum CM voltages were obtained for DM-to-CM conversion. In particular, in the specific test case Z_{GL} = Z_{GR} = 0 Ω, DM voltages due to CM-to-DM conversion are four times larger (12 dB shift) than the corresponding CM voltages due to DM-to-CM conversion, due to the fact that the terminal impedances of the DM circuit in Figure 5-7 are four times larger than those of the equivalent CM circuit in Figure 5-5. Conversely, no significant differences with respect to DM-to-CM conversion are worth noting as far as (a) imbalance due to terminal loads, and (b) superposition of the two contributions are concerned.

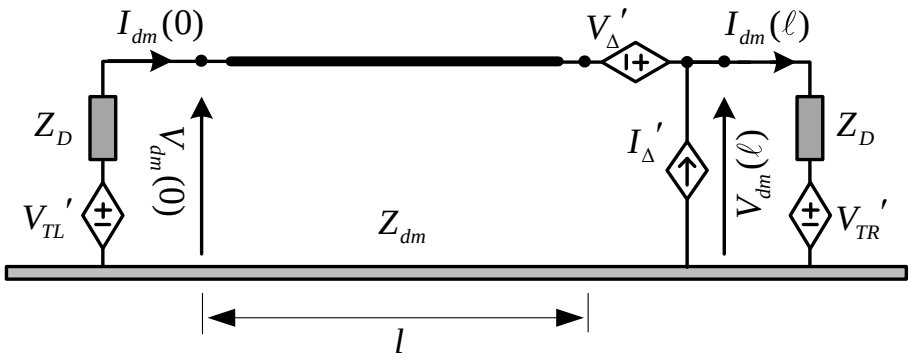

Figure 5-7 DM circuit accounting for CM-to-DM conversion due to line and termination imbalance.

6 MODEL EXTENSION TO INHOMOGENEOUS MEDIA

In the above chapters, the TLs are all set in homogeneous media for sake of brevity, which means that the transmission lines are bare and without any dielectrics around the wires. Hereinafter, the proposed prediction model is extended to the analysis of transmission lines in inhomogeneous media. The derivation focuses on the conversion of the differential mode signal into common mode noise responsible for undesired radiated emissions, and leads to an approximate circuit model for CM-current prediction, in which the effects due to mode conversion are included by distributed voltage and current sources.

6.1 Model extension

6.1.1 Transmission line equations

In the presence of inhomogeneous media, the line p.u.l. inductance and capacitance matrices take the same expressions in (2.10), with the difference that the p.u.l. capacitance matrix cannot be obtained any longer from the p.u.l. inductance matrix by the relationship $\mathbf{C} = v_0^{-2} \cdot \mathbf{L}^{-1}$, but requires numerical evaluation to obtain 1) the p.u.l. capacitance matrix $\mathbf{C}$ with dielectrics and also 2) inductance matrix $\mathbf{L}$ from the free space p.u.l. capacitance matrix, which is got by numerical simulation, by $\mathbf{L} = v_0^{-2} \cdot \mathbf{C}^{-1}$. Conversely, termination imbalance is not influenced by inhomogeneous media. Particularly, in the modal domain defined by the transformation matrices in (2.11) and (2.12), these p.u.l. matrices can still be written as a perturbation of those associated with the corresponding balanced structure as

$$\mathbf{L}_m = \mathbf{T}_V^{-1} \cdot \mathbf{L} \cdot \mathbf{T}_I \cong \mathbf{L}_m^{bal} + \begin{bmatrix} 0 & \Delta l \\ \Delta l & 0 \end{bmatrix}; \quad \mathbf{L}_m^{bal} = \begin{bmatrix} \ell_{CM} & 0 \\ 0 & \ell_{DM} \end{bmatrix} \tag{6.1}$$

$$\mathbf{C}_m = \mathbf{T}_I^{-1} \cdot \mathbf{C} \cdot \mathbf{T}_V \cong \mathbf{C}_m^{bal} + \begin{bmatrix} 0 & \Delta c \\ \Delta c & 0 \end{bmatrix}; \quad \mathbf{C}_m^{bal} = \begin{bmatrix} c_{CM} & 0 \\ 0 & c_{DM} \end{bmatrix} \tag{6.2}$$

where ℓ_{CM}, c_{CM} and ℓ_{DM}, c_{DM} denote the CM and DM p.u.l. inductance and capacitance associated with the balanced structure, whereas inductive and capacitive coefficients $\Delta l = (\ell_1 - \ell_2)/2$ and $\Delta c = (c_1 - c_2)/2$ account for the effects due to line imbalance.

While considering the line imbalance only and the termination is perfectly balanced, the first-order MTL equations of the wiring structure described in section 2 can be written in the modal domain [see (2.3)-(2.4)] as:

$$\frac{d}{dz}\mathbf{V}_m(z) = -j\omega\mathbf{L}_m \cdot \mathbf{I}_m(z), \tag{6.3}$$

$$\frac{d}{dz}\mathbf{I}_m(z) = -j\omega\mathbf{C}_m \cdot \mathbf{V}_m(z), \tag{6.4}$$

where $\mathbf{V}_m = \begin{pmatrix} V_{CM} & V_{DM} \end{pmatrix}^T$, $\mathbf{I}_m = \begin{pmatrix} I_{CM} & I_{DM} \end{pmatrix}^T$ means the modal voltages and modal currents of the MTLs in inhomogeneous media.

Due to the non-null entries Δl, Δc in (6.1),(6.2), the system of equations in (6.3)-(6.4) is coupled and should be solved simultaneously for the unknown CM and DM voltages and currents by enforcing the port-constrains in (2.8)-(2.9).

However, as we proved in chapter 2, as long as the DM and CM lines are weakly coupled, that is as long as geometrical imbalance is weak, the CM, which is not directly excited by the voltage source V_S, can be interpreted as a leakage of the dominant DM, and its back-interaction on DM quantities can be neglected. In analogy to crosstalk prediction [10], [20], the above weak coupling condition can be rephrased in terms of the imbalance coefficients k_ℓ, k_c in as:

$$k_\ell = \frac{\Delta\ell}{\sqrt{\ell_{CM}\ell_{DM}}}, \tag{6.5}$$

$$k_c = \frac{\Delta c}{\sqrt{c_{CM}c_{DM}}} \tag{6.6}$$

$\max\{k_\ell^2, k_c^2\} << 1$, that is, as a rule of thumb, $\max\{k_\ell^2, k_c^2\} < 0.1$.

From the standpoint of line solution, this means neglecting all contributions due to CM quantities in the equations related to the DM. Accordingly, DM-related equations in (6.3), (6.4) can be approximated as:

$$\begin{aligned}\frac{dV_{DM}(z)}{dz} &= -j\omega\left[\Delta\ell I_{DM}(z)+\ell_{DM} I_{DM}(z)\right] \\ &\cong -j\omega\ell_{DM} I_{DM}(z),\end{aligned} \tag{6.7}$$

$$\begin{aligned}\frac{dI_{DM}(z)}{dz} &= -j\omega\left[\Delta c V_{CM}(z)+c_{DM} V_{DM}(z)\right] \\ &\cong -j\omega c_{DM} V_{DM}(z),\end{aligned} \tag{6.8}$$

and solved as the first-step, disregarding the presence of the CM circuit. Indeed, since line terminal sections are perfectly balanced, DM quantities can be readily predicted by solution of the equivalent modal TL in Figure 6-1, where: $\gamma_{DM} = j\omega/v_{DM}$, $v_{DM} = \sqrt{\ell_{DM} c_{DM}}$, $Z_{C,DM} = \sqrt{\ell_{DM}/c_{DM}}$.

Once the DM circuit is solved and DM currents and voltages are known at each line position *z*, they behave as source terms for the CM equations, which can be accordingly re-written in matrix form as：

$$\frac{d}{dz}\begin{pmatrix} V_{CM}(z) \\ I_{CM}(z)\end{pmatrix} + j\omega\begin{bmatrix} 0 & \ell_{CM} \\ c_{CM} & 0\end{bmatrix}\cdot\begin{pmatrix} V_{CM}(z) \\ I_{CM}(z)\end{pmatrix} = \begin{pmatrix} V_{\Delta}(z) \\ I_{\Delta}(z)\end{pmatrix}, \tag{6.9}$$

$$V_{\Delta}(z) = -j\omega\Delta\ell I_{DM}(z), \tag{6.10}$$

$$I_{\Delta}(z) = -j\omega\Delta c V_{DM}(z). \tag{6.11}$$

Equations (6.9)-(6.11) allow the circuit interpretation in Figure 6-2, where an infinitesimal section of CM circuit is represented. According to this representation, DM-to-CM conversion is incorporated into the CM circuit by infinitesimal voltage and current sources, proportional to DM currents and voltages at line position *z* through the inductive and capacitive parameters $\Delta\ell$ and Δc , respectively.

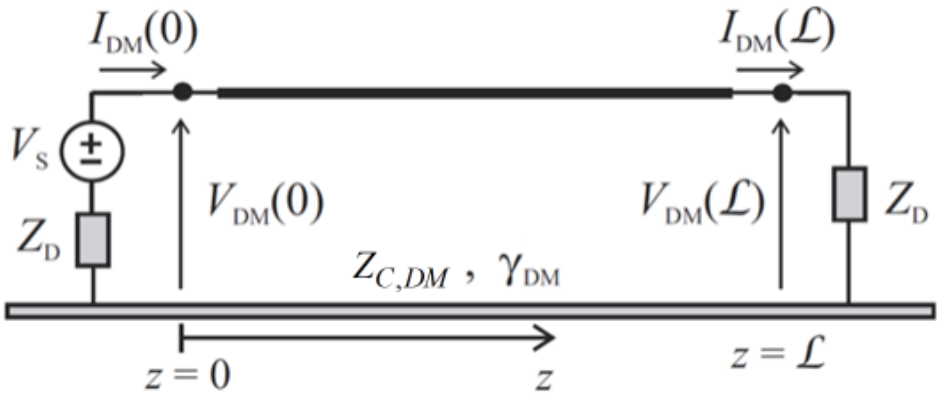

Figure 6-1 Approximate DM equivalent circuit, obtained by neglecting the back-interaction of CM currents/voltages on DM quantities.

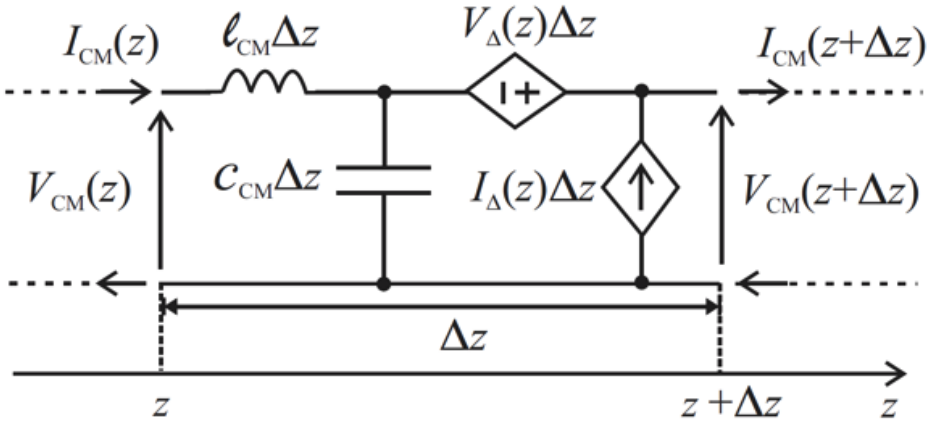

Figure 6-2 Infinitesimal line section of the CM circuit: Effects due to DM-to-CM conversion are modelled by infinitesimal voltage and current sources.

6.1.2 Equivalent CM circuit

In this Section, circuit interpretation and closed-form solution of the CM system of equations in (6.9)-(6.11) is addressed with the twofold objective of evaluating the CM quantities induced at line terminals (key-ingredients for estimating the conversion loss parameters in[11]) and the CM current distribution, from which REs can be predicted.

6.1.2.1 Prediction of CM quantities at line terminals

By recognizing the direct analogy between the phasor form of TL equations in (6.9)–with spatial parameter *z*–and the equations of a lumped-parameter dynamic system–with time parameter *t*–the general solution of the system of equations in (6.9) can be cast as follows [14]:

$$\begin{pmatrix} V_{CM}(z) \\ I_{CM}(z) \end{pmatrix} = \mathbf{\Phi}(z) \cdot \begin{pmatrix} V_{CM}(0) \\ I_{CM}(0) \end{pmatrix} + \int_0^z \mathbf{\Phi}(z-\tau) \cdot \begin{pmatrix} V_{\Delta}(\tau) \\ I_{\Delta}(\tau) \end{pmatrix} d\tau \tag{6.12}$$

where:

$$\mathbf{\Phi}(z) = \begin{bmatrix} \cosh(\gamma_{CM} z) & -\sinh(\gamma_{CM} z) Z_{C,CM} \\ -\sinh(\gamma_{CM} z) Z_{C,CM}^{-1} & \cosh(\gamma_{CM} z) \end{bmatrix}, \tag{6.13}$$

and $\gamma_{CM} = j\omega / v_{CM}$, $v_{CM} = \sqrt{\ell_{CM} c_{CM}}$, $Z_{C,CM} = \sqrt{\ell_{CM} / c_{CM}}$.

Starting from the general solution in (6.12), an equivalent CM circuit at line terminals can be obtained by evaluating (6.13) for $z = \mathcal{L}$. This yields:

$$\begin{pmatrix} V_{CM}(\mathcal{L}) \\ I_{CM}(\mathcal{L}) \end{pmatrix} = \mathbf{\Phi}(\mathcal{L}) \cdot \begin{pmatrix} V_{CM}(0) \\ I_{CM}(0) \end{pmatrix} + \begin{pmatrix} V_{\Delta T} \\ I_{\Delta T} \end{pmatrix}, \tag{6.14}$$

where the source vector

$$\begin{pmatrix} V_{\Delta T} \\ I_{\Delta T} \end{pmatrix} = \int_0^{\mathcal{L}} \mathbf{\Phi}(\mathcal{L}-\tau) \cdot \begin{pmatrix} -j\omega \Delta \ell I_{DM}(\tau) \\ -j\omega \Delta c V_{DM}(\tau) \end{pmatrix} d\tau \tag{6.15}$$

can be interpreted by a pair of lumped voltage and current sources connected at the right termination of the CM circuit as shown in Figure 6-3.

Suitable analytical expressions for these sources can be obtained by expressing $I_{DM}(\tau), V_{DM}(\tau)$ in (6.15) as function of the DM current at the right termination, i.e., $I_{DM}(\mathcal{L})$. After some algebra, $V_{\Delta T}, I_{\Delta T}$ take the closed-form expressions:

$$\frac{V_{\Delta T}}{I_{DM}(\mathcal{L})} = j\omega \left[K_+ (Sh_+ + \alpha_D Ch_+) - K_- (Sh_- + \alpha_D Ch_-) - \alpha_D \left(K_+ - K_- \right) \right], \tag{6.16}$$

$$\frac{I_{\Delta T}}{I_{DM}(\mathcal{L})} = \frac{-j\omega}{Z_{C,CM}} \left[K_+ (Ch_+ + \alpha_D Sh_+) + K_- (Ch_- + \alpha_D Sh_-) - \left(K_+ + K_- \right) \right], \tag{6.17}$$

where $\alpha_D = Z_D / Z_{DM}$ denotes the degree of mismatching of the DM circuit, and

$$Sh_{\pm} = \sinh\left[(\gamma_{DM} \pm \gamma_{CM}) \mathcal{L} \right], \tag{6.18}$$

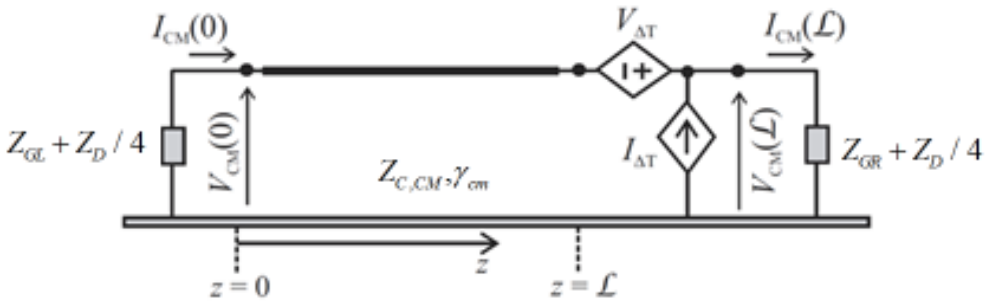

Figure 6-3 Equivalent CM circuit at line terminals: Effects due to DM-to-CM conversion are modelled by two lumped voltage and current sources connected at the right termination.

$$Ch_{\pm} = \cosh\left[(\gamma_{DM} \pm \gamma_{CM})\mathcal{L}\right], \tag{6.19}$$

$$K_{\pm} = \frac{\Delta c Z_{C,CM} Z_{C,DM} \mp \Delta\ell}{2(\gamma_{DM} \pm \gamma_{CM})}. \tag{6.20}$$

6.1.2.2 Prediction of the CM current distribution

In addition to voltages and currents at line terminals, the model in (6.12), (6.13) allows to evaluate the CM current distribution at each line position *z*, as key-ingredient to predict the RE generated by the differential line in the presence of geometrical imbalance.

Indeed, starting from (6.12), the CM current at line position *z* can be written as the sum of two contributions as $I_{CM}(z) = I'_{CM}(z) + I''_{CM}(z)$. The first contribution, i.e.,

$$I'_{CM}(z) = -\sinh(\gamma_{CM} z) Z_{C,CM}^{-1} V_{CM}(0) + \cosh(\gamma_{CM} z) I_{CM}(0), \tag{6.21}$$

can be interpreted as the CM current distribution due to the lumped sources $V_{\Delta T}, I_{\Delta T}$ in (6.16), (6.17), and can be easily evaluated by solution of the equivalent circuit in Figure 6-3. This yields the expression: $V_{\Delta}(z), I_{\Delta}(z)$

$$I'_{CM}(z) = \frac{\left[\beta_L \sinh(\gamma_{CM} z) + \cosh(\gamma_{CM} z)\right](Z_{C,CM}^{-1} V_{\Delta T} - \beta_R I_{\Delta T})}{(\beta_L + \beta_R)\cosh(\gamma_{CM}\mathcal{L}) + (1 + \beta_L \beta_R)\sinh(\gamma_{CM}\mathcal{L})} \tag{6.22}$$

where $\beta_L = (Z_L + Z_D/4)/Z_{C,CM}$, $\beta_R = (Z_R + Z_D/4)/Z_{C,CM}$ denote the degree of matching/ mismatching of the CM circuit.

Conversely, the second contribution, i.e.,

$$I''_{CM}(z)=\int_0^z \mathbf{\Phi}(z-\tau)\cdot\begin{pmatrix}V_\Delta(\tau)\\ I_\Delta(\tau)\end{pmatrix}d\tau \tag{6.23}$$

is due to the infinitesimal voltage and current sources distributed along the CM TL, and cannot be predicted by the model in Figure 6-3, which assures equivalence at line terminals only. Hence, explicit solution of the convolution integral in (6.23) is required, which yields:

$$I''_{CM}(z)=\frac{-j\omega I_{DM}(\mathcal{L})}{Z_{C,CM}}\left[K_+(Ch'_+ +\alpha Sh'_+)+K_-(Ch'_- +\alpha Sh'_-)-\left(K_+ +K_-\right)(Ch_D+\alpha Sh_D)\right] \tag{6.24}$$

where K_+, K_- take the same expressions in (6.20), whereas $Sh'_\pm=\sinh(\gamma_{DM}\mathcal{L}\pm\gamma_{CM}z)$, $Ch'_\pm=\cosh(\gamma_{DM}\mathcal{L}\pm\gamma_{CM}z)$, $Sh_D=\sinh[\gamma_{DM}(\mathcal{L}-z)]$, $Ch_D=\cosh[\gamma_{DM}(\mathcal{L}-z)]$.

6.1.2.3 Validation and comparative analysis

In this Section, exact (rigorous) solution of MTL equations is used as reference to assess the accuracy of the predictions obtained by the approximate model here proposed, which neglects the back-interaction of CM quantities on the DM. To this end, different realizations of the PCB cross-section sketched in Figure 2-2(c) are considered. They are composed of a pair of coplanar micro-strips printed on top of a double-face printed circuit board (PCB) with substrate height h=1.425 mm, substrate relative permittivity ε_r=4.4, and trace thickness t=35μm. The traces are kept at fix distance (i.e., d=0.5 mm), but their width is varied so to test model accuracy for different degrees of imbalance. Particularly, the results shown in the following were obtained for the four test cases in Table 6-1。

Among these, the first cross-section (i.e., PCB 1) was considered as the reference, since not affected by line imbalance, while the other ones were obtained starting from it by symmetrically increasing/decreasing the trace width w_1, w_2. The corresponding modal characteristic impedances, propagation velocities and imbalance coefficients k_ℓ, k_c were evaluated by post-processing according to (2.11), (2.12) the p.u.l. parameters obtained by electrostatic simulation carried out by the FEM-based numerical code Maxwell [21]. The obtained values are listed in Table 6-2, and show that, despite k_ℓ, k_c significantly increase

from one realization to the other, the corresponding DM and CM characteristic impedances and propagation velocities are almost unchanged.

Table 6-1 Trace widths for the PCBs under analysis

	w_1	w_2
PCB 1	0.6 mm	0.6 mm
PCB 2	0.5 mm	0.7 mm
PCB 3	0.4 mm	0.8 mm
PCB 4	0.3 mm	0.9 mm

Table 6-2 Modal Characteristic Parameters for the PCBs in Table 6-1

	PCB 1	PCB 2	PCB 3	PCB 4
$Z_{C,DM}$ [Ω]	125.8	126.8	127.8	131
$Z_{C,CM}$ [Ω]	65.2	65.4	65.6	66.4
v_{DM} [m/s]	$1.85\ 10^8$	$1.85\ 10^8$	$1.83\ 10^8$	$1.82\ 10^8$
v_{CM} [m/s]	$1.69\ 10^8$	$1.69\ 10^8$	$1.68\ 10^8$	$1.66\ 10^8$
k_ℓ	0	0.05	0.11	0.16
k_c	0	-0.06	-0.12	-0.19

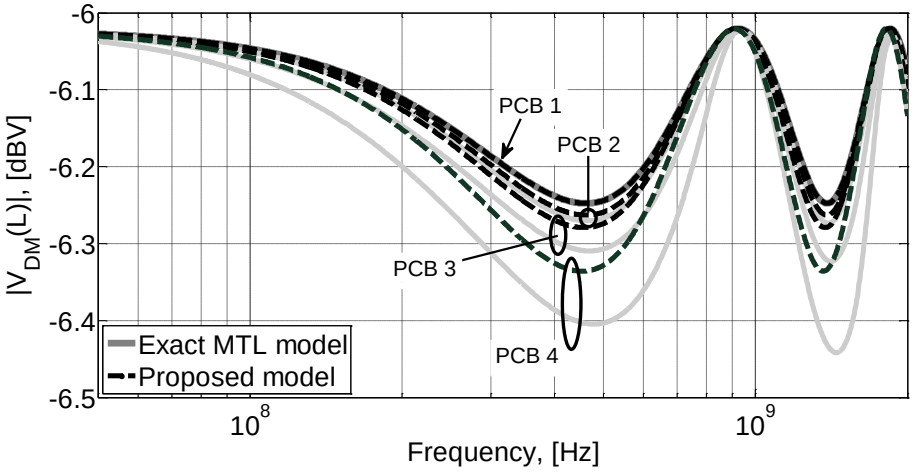

(a)

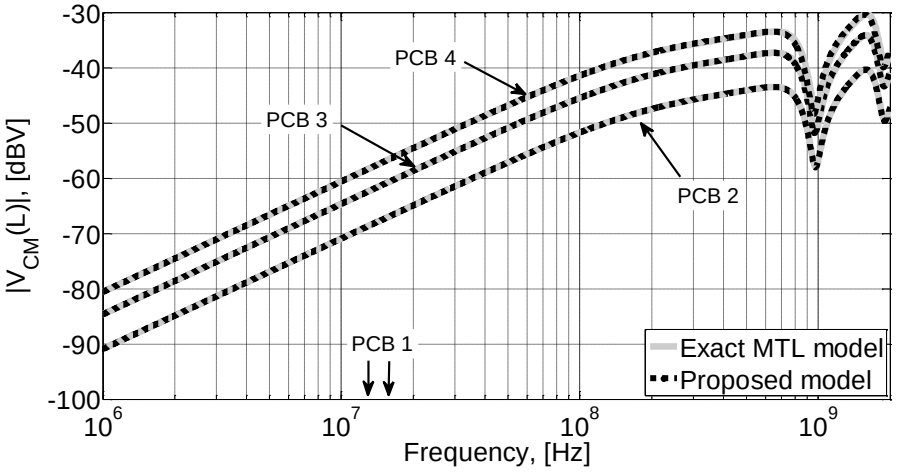

(b)

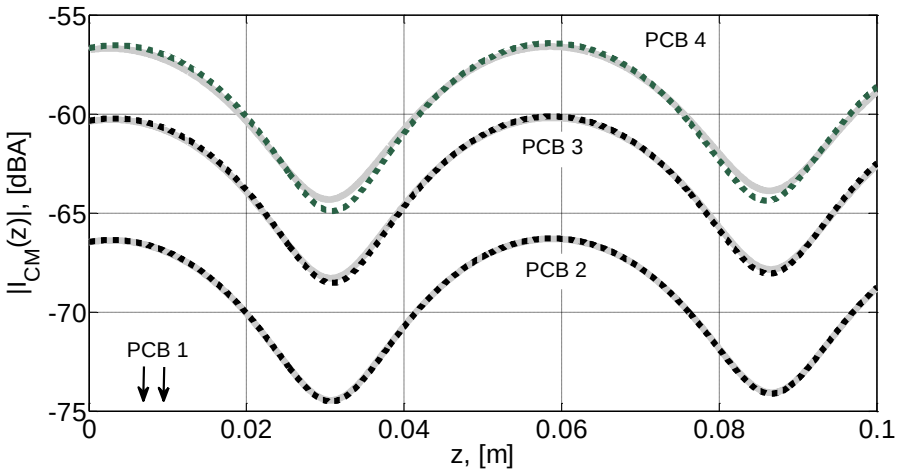

(c)

Figure 6-4 Model validation vs exact solution of MTL equations (ground impedances: Z_{GL} = Z_{GR} = 0Ω): DM (a) and CM (b) voltages at the right termination and CM current distribution (c) at 1.5 GHz.

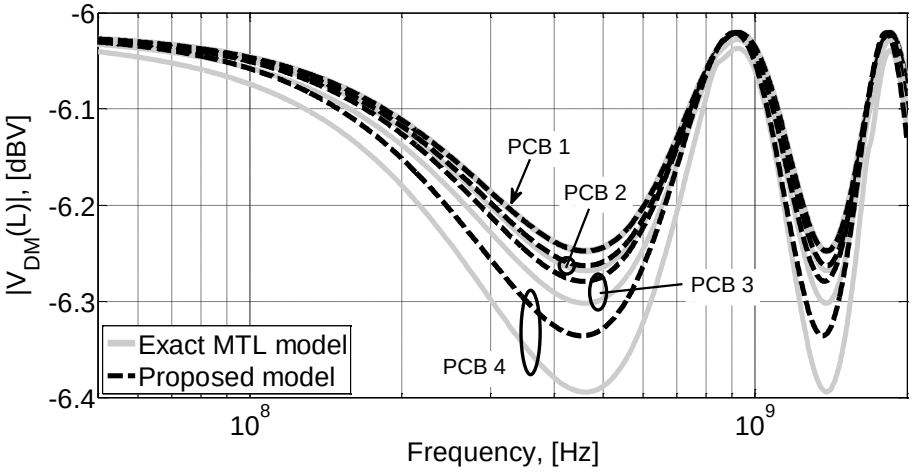

(a)

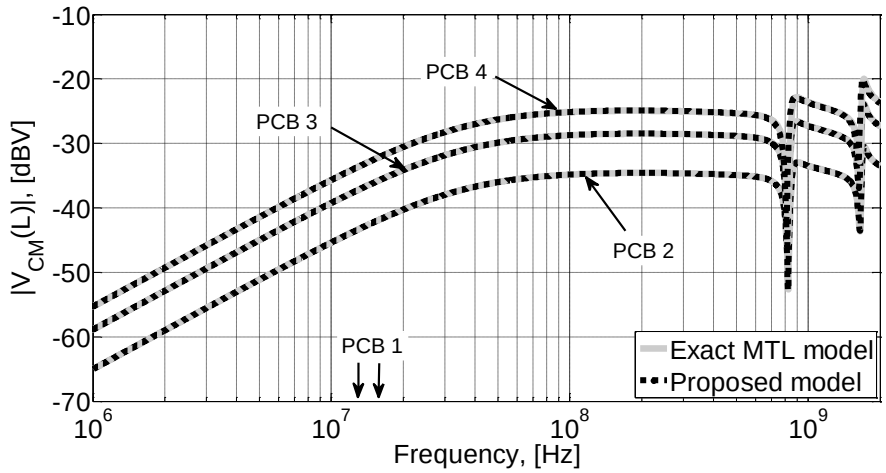

(b)

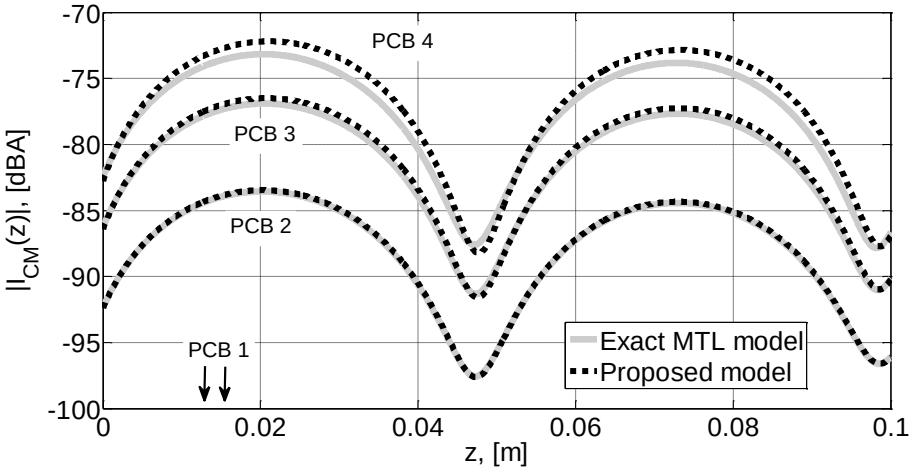

(c)

Figure 6-5 Model validation vs exact solution of MTL equations (ground impedances: Z_{GL} = Z_{GR} = 1 kΩ): DM (a) and CM (b) voltages at the right termination and CM current distribution (c) at 1.5 GHz.

In particular, since the DM characteristic impedance of all PCBs is around 125–130Ω, for numerical simulation the series impedances of each terminal network was set to the value Z_D = 100Ω, which leads to a mismatching coefficient for the DM circuit on the order of $\alpha \approx 0.76-0.8$. Predictions obtained by the approximate model here proposed (dashed curves) are compared versus those obtained by exact solution of MTL equations (solid curves) in Figure 6-4 and Figure 6-5, for two different values of the ground impedances Z_{GL}, Z_{GR}, that is: $Z_{GL} = Z_{GR}$ = 0Ω, and $Z_{GL} = Z_{GR}$ = 1 kΩ, respectively.

Simulations were carried out in the frequency interval from 1 MHz up to 2 GHz with a line length of 10 cm. The plots in (a) and (b) show the comparison in terms of DM (a) and CM (b) voltages at the right termination of the differential line (DM voltages have been plotted in a limited frequency range to improve figure readability). The comparison in terms of CM current distribution along the line length (at 1.5 GHz) is shown in (c). The comparison shows that, as long as the weak-imbalance assumption is satisfied, predictions obtained by the proposed model result to be in satisfactory agreement with those obtained by exact solution of the MTL equations. In particular, even in the worst case here consider of a trace three times wider than the other (test case anyway satisfying the weak-imbalance condition in Sec.6.1.1, i.e., $k_c^2 \cong 0.036 << 1$), the maximum discrepancies are on the order of 0.1 dB for the DM, and of 1 dB for the CM. Conversely, for a degree of imbalance close to or exceeding the validity limit of the proposed model (i.e., $k_c^2 \cong 0.1$), prediction accuracy degrades both for the DM and the CM due to a gradually increasing shift of the resonance frequencies.

6.2 LF model and analogy with crosstalk

For electrically-short TLs, low-frequency (LF) expressions for the induced sources $V_{\Delta T}$, $I_{\Delta T}$ in (6.16),(6.17) can be readily obtained by approximating the terms in (6.18), (6.19) as: $Sh_{\pm} \cong (\gamma_{DM} \pm \gamma_{CM})\mathcal{L}$, $Ch_{\pm} \cong 1$. After some simple algebra, and by recognizing that $\alpha_D Z_{C,DM} I_{DM}(\mathcal{L}) = V_{DM}(\mathcal{L})$, the following expressions are obtained:

$$V_{\Delta T} \cong -j\omega\Delta\ell\mathcal{L} I_{DM}(\mathcal{L}), \tag{6.25}$$

$$I_{\Delta T} \cong -j\omega \Delta c \mathcal{L} V_{DM}(\mathcal{L}). \tag{6.26}$$

These expressions exhibit a strict analogy to those involved in crosstalk analysis, and have the potential to outline the twofold nature of mode conversion. Indeed, in [10], [20],the LF model of the receptor circuit incorporates the interference due to the generator circuit by: (a) a voltage source proportional to the current into the generator circuit and to the total mutual inductance $L_m = \ell_m \mathcal{L}$ (inductive coupling) between the two circuits, and (b) a current source proportional to the voltage across the generator circuit and to the total mutual capacitance $C_m = c_m \mathcal{L}$ (capacitive coupling) between the two circuits. In a similar fashion, the interference due to the DM circuit (i.e., the modal circuit directly driven by the voltage source V_S) is included into the CM circuit by: (a) a voltage source $V_{\Delta T}$ proportional to the current in the DM circuit through the total inductance $\Delta L = \Delta \ell \mathcal{L}$, and (b) a current source $I_{\Delta T}$ proportional to the DM voltage through the total capacitance $\Delta C = \Delta c \mathcal{L}$. Additionally, currents and voltages in the *source* circuit (here, the DM circuit) can be computed by neglecting the presence of the *receptor* circuit (here, the CM circuit).

Likewise for crosstalk, at LF voltages and currents induced into the CM circuit increase with a frequency-slope of +20dB/decade. Additionally, the predominance of one contribution over the other is strictly related to the value of the terminal loads. Indeed, the voltages (and currents) induced across the left (superscript L) and right (superscript R) terminations of the CM circuit can be written as the superposition of inductive and capacitive contributions (first and second terms into brackets, respectively) as:

$$V_{CM}^{L} = -\frac{j\omega}{2}\left(-\frac{\Delta L}{\alpha Z_{C,DM}} + \Delta C Z_{C,CM} \beta_R \right) \frac{\beta_L}{\beta_L + \beta_R} V_S, \tag{6.27}$$

$$V_{CM}^{R} = -\frac{j\omega}{2}\left(\frac{\Delta L}{\alpha Z_{C,DM}} + \Delta C Z_{C,CM} \beta_L \right) \frac{\beta_R}{\beta_L + \beta_R} V_S. \tag{6.28}$$

Since in practically-relevant cases the terminations of the DM circuit are designed to be almost matched to the DM characteristic impedance of the differential line (i.e., $\alpha_D \cong 1$), it can be concluded the prevalence of one contribution over the other is mainly determined

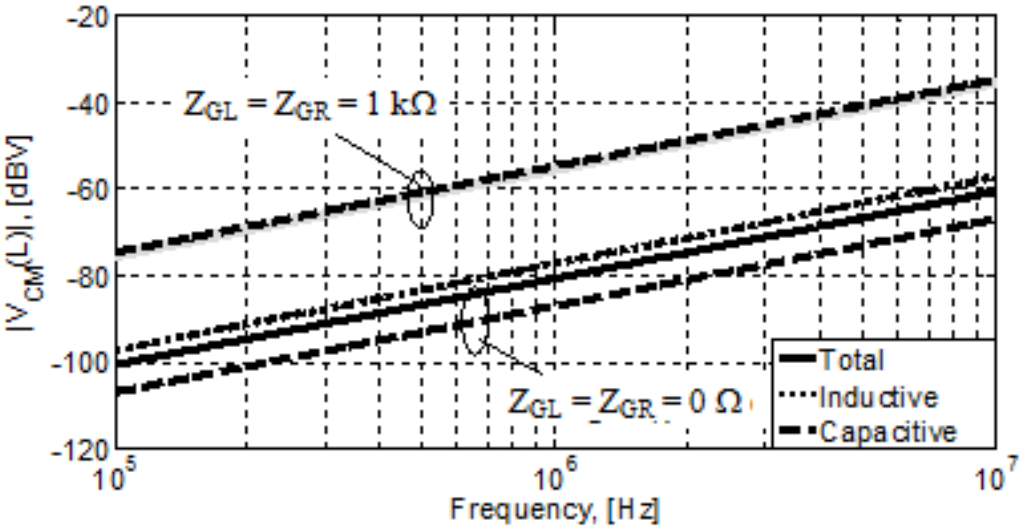

Figure 6-6 LF model: Inductive (dotted) and capacitive (dashed) contributions to the total (solid) CM voltage in (6.28) for two different values of $Z_{GL} = Z_{GR}$ that is: (a) $Z_{GL} = Z_{GR} = 0\Omega$ (lower curves), and (b) $Z_G = Z_{GR} = 1$ kΩ upper curves).

by the value of Z_{GL}, Z_{GR}. Indeed, the capacitive contribution is predominant for large values of Z_{GL}, Z_{GR}. Vice-versa, if these impedances take small values, the inductive contribution is prevailing. Furthermore, starting from the results obtained for crosstalk, one would expect a partial compensation of inductive and capacitive contributions at the right termination (i.e., far from the source), and vice-versa maximum interference at the left termination. The expressions in (6.27), (6.28) apparently clash with this expectation, as the two contributions sum in (6.27) and subtract in (6.28). However, the contradiction is only apparent, since $\Delta\ell$ and Δc are always opposite in sign. Indeed, if the self-inductance of a signal line increases, its self-capacitance decreases, and vice-versa (see Table 6-2). As an explicative example, inductive (dotted curves) and capacitive (dashed curves) contributions to the total (solid curves) CM voltage V_{CM}^R in (6.28) are plotted in Figure 6-6 for the last micro-strip line in Section 6.1.2.3(see PCB 4 in Table 6-1). Simulations were carried out from 100 kHz up to 10 MHz, and were obtained for two different values of ground impedances, that is $Z_{GL} = Z_{GR} = 0\Omega$ and $Z_{GL} = Z_{GR} = 1$ kΩ.

Since in both cases $Z_D = 100\Omega$, the inductive contribution (dotted curve) is the same, whereas the capacitive contribution increases proportionally to $Z_{GL} = Z_{GR}$. Therefore, while for $Z_{GL} = Z_{GR} = 0\ \Omega$ the inductive contribution is fairly larger than the capacitive one (actually, they are anyway comparable in magnitude, as a slight compensation between

them is observed in the total voltage V_{CM}^{R}), for $Z_{GL} = Z_{GR} = 1\ k\Omega$ DM-to-CM conversion can be fully ascribed to the capacitive contribution.

7 SPICE MODELING AND EXPERIMENTAL VALIDATION

In order to have a clear view of this mode conversion and to predict the worst case, two SPICE models, namely in homogeneous and inhomogeneous media, are built based on the previous models. The SPICE models can be used as a tool to predict the potential interference in advance in order to get a better EMC design. And then the experimental validations on PCB are also carried out for assessing the model accuracy.

7.1 SPICE modeling

7.1.1 Differential lines in homogeneous medium

For SPICE implementation, a 1m long DL characterized by the geometrical parameters mentioned in Sub-section 2.2 and imbalance coefficients $\Delta h = d/2$, $\Delta Z_L = \Delta Z_R = 0.05\ Z_D / 2$ is considered. For such a DL, the SPICE schematic representative for DM into CM conversion is shown in Figure 7-1(a). In this model, three (instead of two) two-conductor TLs have been implemented (either by **T** or **T-lossy** parts, [14]), in order to allow separate evaluation of the two contributions to the overall CM voltages. Indeed, the TL in the middle represents the DM circuit (dominant mode), with characteristic impedance Z_{dm}=193 Ω, and, without loss of generality, matched terminations $Z_D = Z_{dm}$. The upper and lowest TLs are CM circuits, with characteristic impedance Z_{cm} = 269 Ω and terminal impedances $Z_{GL(R)} + Z_D / 4 \approx 1$ kΩ. Particularly, the lowest CM circuit is used to predict the contribution due to termination imbalance. Accordingly, this circuit is fed at both terminations by current-controlled voltage sources with constant gain, i.e., $|\Delta Z_L| = |\Delta Z_R| = 4.8$ Ω. Note that the additional voltage-controlled voltage sources (with unitary gains) are included to avoid crossed connections.

Conversely, implementation of the frequency-dependent sources accounting for line imbalance involves the ABM (Analog Behavioral Model) parts **ELAPLACE** and **GLAPLACE**, [14]. These parts are voltage-controlled voltage (**ELAPLACE**) and current (**GLAPLACE**) sources, whose frequency-dependent gains are assigned in terms of Laplace transform. For the specific test case under analysis, the current source I_Δ in (4.6) is implemented by a **GLAPLACE** part with trans-admittance [according to (4.6)]

$$Y_{\Delta}(s) = \frac{I_{\Delta}}{V_{dm}(0)} \cong 14.4 \sinh\left(s T_D\right) \mu\Omega^{-1}, \tag{7.1}$$

where $T_D = \ell / v_0 = 10/3 \text{ns}$ and controlled by the DM voltage at the left termination of the DM TL. Conversely, since ABM current-controlled sources are not available in SPICE, the voltage source V_{Δ} in (4.5) is implemented by an **ELAPLACE** part controlled–instead of by the DM current $I_{dm}(0)$–by the voltage drop across the series impedance Z_D at the left DL end. According to this implementation, and in line with (4.5), the dimensionless gain of the involved **ELAPLACE** part takes the expression:

$$K_{\Delta}(s) = \frac{V_{\Delta}}{Z_D I_{dm}(0)} \cong -4 \cdot 10^{-3} \sinh\left(s T_D\right). \tag{7.2}$$

Based on previous analysis, the SPICE schematic in Figure 7-1(a) can be conveniently exploited to predict worst-case CM voltages at DL terminations due to specific degrees of imbalance affecting the line cross-section and the DL terminal networks.

As an explicative example, let's assume that the imbalance coefficients may randomly vary (uniform distribution) within the confidence intervals: $-d/2 \le \Delta h \le d/2$, and $-0.05\ Z_D/2 \le \Delta Z_L, \Delta Z_R \le 0.05\ Z_D/2$. Predictions for the CM voltages at the left termination obtained by 1000 repeated simulations based on exact solution of MTL equations are plotted (colored curves) in Figure 7-1(b). In spite of the wide spread of results, upper bounds to these curves can be readily obtained by running the SPICE schematic twice, and by summing (for each simulation) the magnitude of the contributions due to line and termination imbalance. In the former simulation, the unitary gains of the voltage-controlled voltage sources have the same sign as in Figure 7-1(a), in the latter, they have opposite signs. The obtained results are plotted in Figure 7-1(b) by dashed- and solid-black curves, respectively, that effectively upper-bound the colored curves in the considered frequency range.

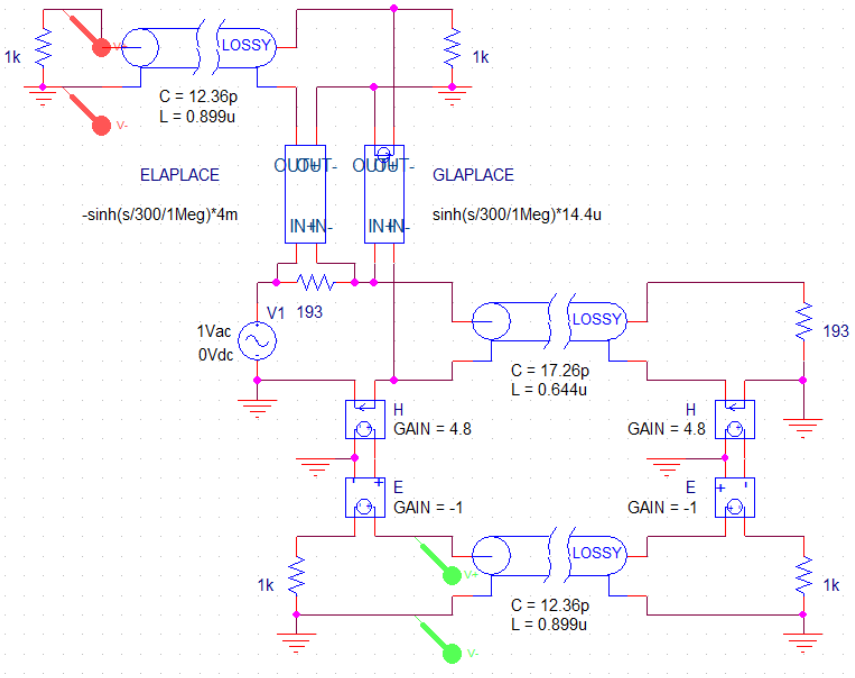

(a)

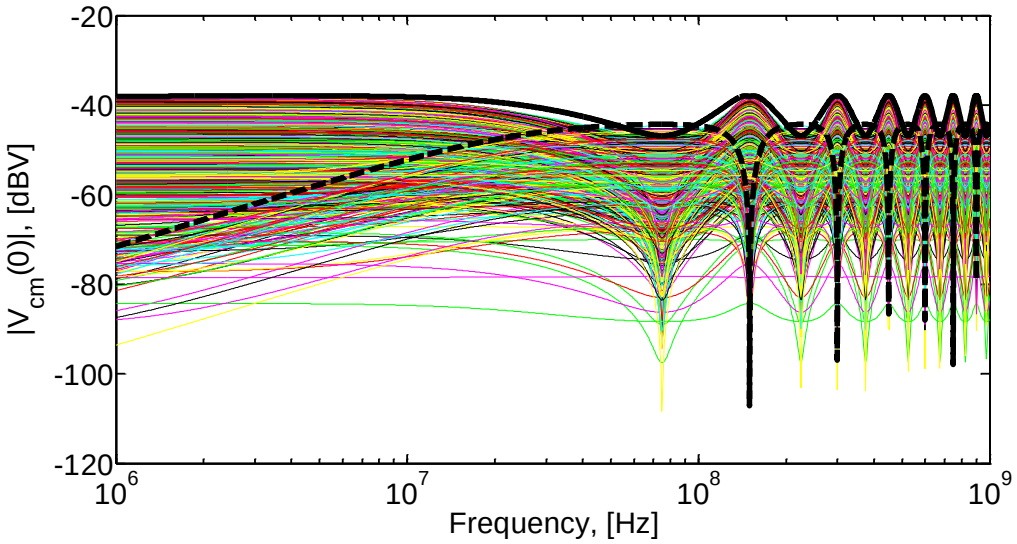

(b)

Figure 7-1 Implementation in SPICE: (a) schematic of the unbalanced DL excited by a DM source. (b) SPICE predictions (black curves) vs 1000 repeated simulations obtained by exact solution of MTL equations (left TL end).

7.1.2 Differential lines in inhomogeneous media

As the above SPICE example for circuit implementation, the 1 m-long DL characterized by the geometrical parameters mentioned in Sub-section 2.2 and imbalance coefficients in the previous sub-section 7.1.1 (i.e., $\Delta h=d/2$, $\Delta Z_L=\Delta Z_R=0.05Z_D/2$) is here re-considered with the

two wires surrounded by a dielectric jacket with thickness t=0.3mm and relative dielectric permittivity. For this wiring structure, numerical evaluation [21] of the modal p.u.l. inductance and capacitance parameters in (2.11)-(2.12) yields the values: $\ell_{cm} = 894.8\,\text{nH/m}$, $c_{cm} = 12.88\,\text{pF/m}$, $\ell_{dm} = 626.6\,\text{nH/m}$, $c_{dm} = 22.33\,\text{pF/m}$, $\Delta l = 2.3\,\text{nH/m}$, $\Delta c = -0.05\,\text{pF/m}$, hence: $Z_{dm} = 167.5\,\Omega$, $Z_{cm} = 263\,\Omega$, $v_{dm} = 2.67 \cdot 10^8\,\text{m/s}$, $v_{cm} = 2.945 \cdot 10^8\,\text{m/s}$.

The obtained SPICE schematic is shown in Figure 7-2(a). Likewise in Figure 7-1(a), separate evaluation of the contributions to the overall CM voltages due to line and termination imbalance is achieved by the use of three two-conductor TLs here implemented by **T-lossy** parts with p.u.l. parameters $\ell_{dm}, c_{dm}, \ell_{cm}, c_{cm}$. The loads at the terminations of the DM circuit (TL in the middle) are matched, that is: $Z_D = Z_{dm} = 167.5\ \Omega$. The CM circuits (upper and lowest TLs) are terminated by CM impedances $Z_{GL(R)} + Z_D / 4 \approx 1\ \text{k}\Omega$.

Conversely, mode conversion due to termination imbalance is not influenced by medium un-homogeneity. Hence, the circuit interpretation in Figure 3-2(b), as well as the analytical expressions in equations (3.8) and (3.9), are still valid. The contribution due to termination imbalance is predicted by the lowest CM circuit, which is here driven by current-controlled voltage sources with gain $|\Delta Z_L| = |\Delta Z_R| = 4.188\ \Omega$.

As regards line imbalance (upper CM circuit), implementation in SPICE of the voltage and current sources $V_{\Delta T}, I_{\Delta T}$ is achieved by the use of two ABM parts (e.g., **ELAPLACE** or **GLAPLACE**,) for each source [instead of only one as in Figure 7-1(b)]. To this end, (6.16) -(6.20)(α =1) are re-written in terms of Laplace transform and as functions of $I_{dm}(0)$ and $V_{dm}(0)$:

$$V_{\Delta T}(s) = z_\Delta(s)\, I_{dm}(0) + \alpha_\Delta(s) V_{dm}(0), \qquad I_{\Delta T}(s) = \beta_\Delta(s)\, I_{dm}(0) + y_\Delta(s) V_{dm}(0), \qquad (7.3)$$

where $z_\Delta(s), y_\Delta(s), \alpha_\Delta(s), \beta_\Delta(s)$ denote the frequency-dependent gains of the involved voltage- and current-controlled voltage and current sources. To ease SPICE implementation, expressions for such gains are further reworked, and cast as function of two numerical coefficients only, i.e.,

$$k_{\substack{\Delta,1\\ \Delta,2}} = \frac{v_{dm} v_{cm}}{v_{cm}^2 - v_{dm}^2} \left(\underset{dm}{v_{cm}} \Delta l + \underset{cm}{v_{dm}} Z_{cm} Z_{dm} \Delta c \right), \tag{7.4}$$

As

$$\begin{aligned} z_\Delta(s) &= -k_{\Delta,1} \sinh(s\ell / v_{dm}) + k_{\Delta,2} \sinh(s\ell / v_{cm}), \\ \alpha_\Delta(s) &= Z_{dm}^{-1} k_{\Delta,1} \left[\cosh(s\ell / v_{dm}) - \cosh(s\ell / v_{cm}) \right], \\ \beta_\Delta(s) &= Z_{cm}^{-1} k_{\Delta,2} \left[\cosh(s\ell / v_{dm}) - \cosh(s\ell / v_{cm}) \right], \\ y_\Delta(s) &= Z_{cm}^{-1} Z_{dm}^{-1} \left[k_{\Delta,1} \sinh(s\ell / v_{cm}) - k_{\Delta,2} \sinh(s\ell / v_{dm}) \right], \end{aligned} \tag{7.5}$$

which can be assigned as gains of the involved ABM parts more easily. Note that, due to the lack of current-controlled ABM sources, the current-controlled sources in (7.3) were implemented as voltage-controlled ABM sources dependent on the voltage drop across the series impedance Z_D. Accordingly, the gains of these sources—i.e., coefficients $z_\Delta(s), \beta_\Delta(s)$—were further divided by $Z_{dm} = 167.5\ \Omega$.

Use of the SPICE schematic in Figure 7-2(a) for worst-case prediction of the CM voltages at DL terminations is here exemplified by assuming imbalance coefficients randomly spread within the confidence intervals: $-d/2 \le \Delta h \le d/2$, and $-0.05\ Z_D/2 \le \Delta Z_L, \Delta Z_R \le 0.05\ Z_D/2$ (as in Section 7.1.1).

Likewise for the homogeneous case, only two runs of the SPICE schematic can suffice to this purpose. However, since the contribution due to line imbalance [see eq.(7.4)] is now depending on an inductive and a capacitive coefficient (Δl, Δc, respectively), which are (a) always opposite in sign and (b) not related each other by straightforward relationships (as in the homogeneous case), the two simulations have to be run in either one of the following two sets of conditions. If Δc is assumed to be positive, one simulation shall be run with $\Delta Z_L > 0$ and $\Delta Z_R > 0$, the other (simulation leading to the flat frequency response at low frequency) with $\Delta Z_L < 0$ and $\Delta Z_R > 0$. Vice-versa, if Δc is assumed to be negative (and, as a consequence, Δl is positive), the one simulation requires $\Delta Z_L < 0$ and $\Delta Z_R < 0$, the other involves $\Delta Z_L > 0$ and $\Delta Z_R < 0$.

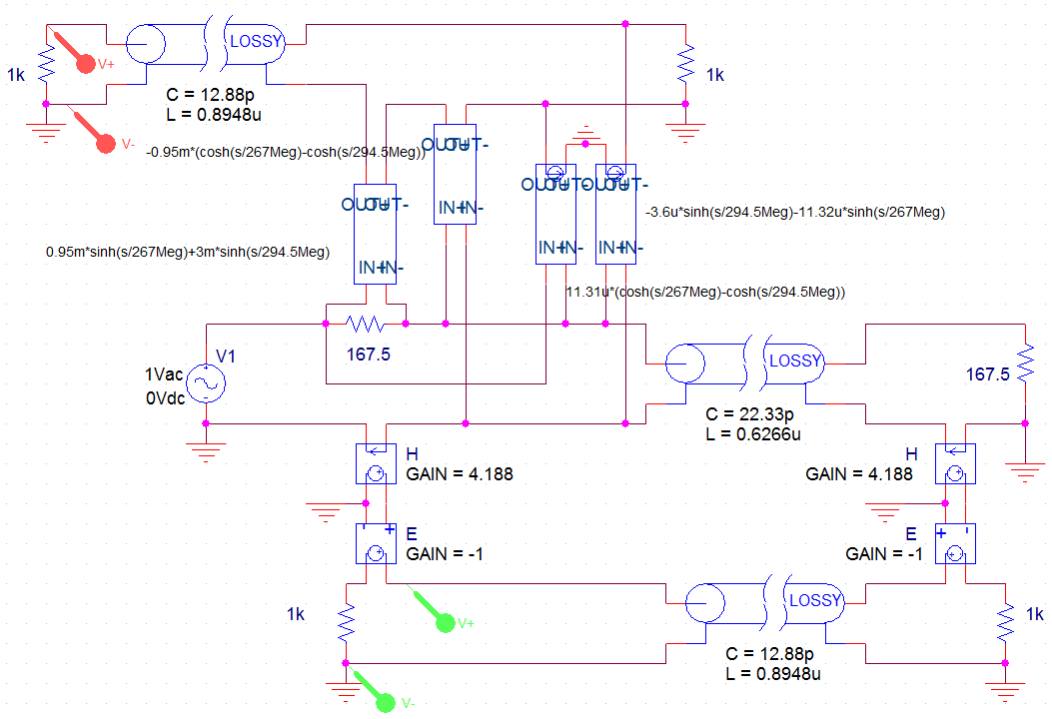

(a)

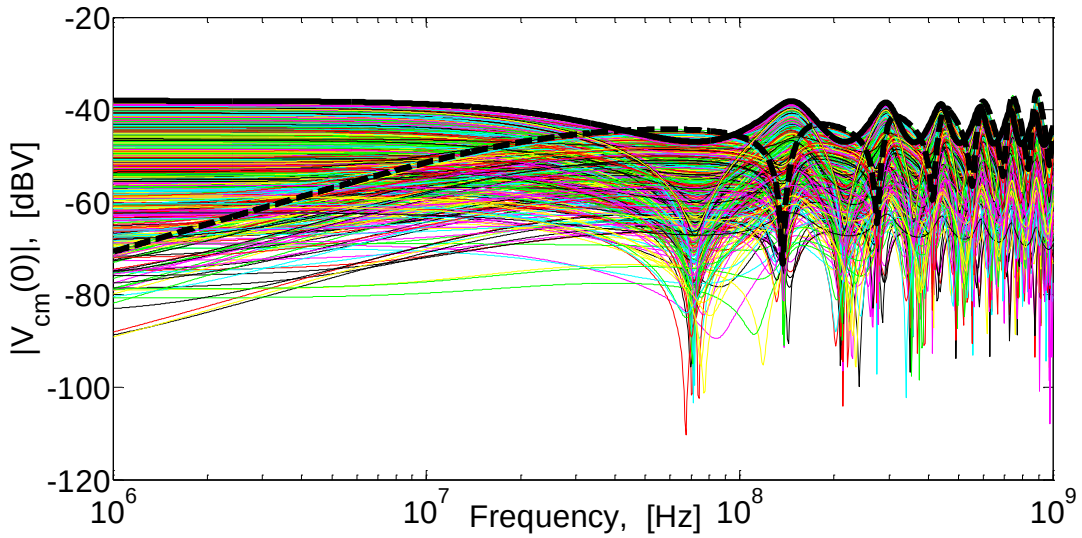

(b)

Figure 7-2 Inhomogeneous medium: (a) SPICE schematic of the unbalanced DL excited by a DM source. (b) SPICE predictions (black curves) vs 1000 repeated simulations obtained by exact solution of MTL equations (left TL end).

Effectiveness of the obtained upper bounds (dashed- and solid-black curves, respectively) is proven in Figure 7-2(b), by comparison versus 1000 repeated simulations based on exact solution of MTL equations (colored curves) with imbalance coefficients randomly selected within the confidence intervals under analysis.

7.2 Experimental validation

In this Section, the model accuracy is further validated by experimental measurement. The prediction line imbalance model in Sec. 6 is validated versus the measurement data obtained by experimental characterization of the pairs of coplanar micro-strips shown in Figure 7-3(a).

In both samples, the two traces are printed on top of a double-face PCB as in Figure 2-2(c). Geometrical and material characteristics of the PCB boards are: substrate height h= 1.6 mm, substrate relative permittivity ε_r = 4.4, trace thickness t = 35μm, trace length = 280 mm. The two traces are kept at distance d = 2 mm. However, they are affected by different degrees of imbalance. Namely, in both pairs one trace has width w_1 = 1 mm, while the other one is made two times [i.e., w_2 = 2 mm in PCB1, Figure 7-3(a)] and three times [i.e., w_2 = 3 mm in PCB2, Figure 7-3 (a)] wider. For these cross-sections, numerical simulations carried out by [21] yield the modal characteristic impedances, propagation velocities, and imbalance coefficients in Table 7-1, and show that, though with different margin, both PCBs satisfy the weak-imbalance condition: Namely: for PCB 1, and for PCB 2.

For the sake of comparison with the predictions obtained by the proposed model, the two PCBs were experimentally characterized at the four output ports in the frequency interval from 100 kHz up to 2 GHz. Measurements were carried out by a two-port Vector Network Analyzer (VNA) Agilent ENA E5071C, by connecting the VNA ports in turn with a pair of SMA (Subminiature version A) ports of the PCB under analysis, while the other two SMA ports were loaded by 50 Ω terminations [see Figure 7-3(b)]. The obtained 4×4 scattering parameter matrices were then converted into chain-parameter notation, and used to evaluate DM and CM quantities at the terminations of each board. This led to the solid curves in Figure 7-4, which represent (as a specific example) the DM (a) and CM (b) currents at the left termination for DM and CM impedances of the terminal networks equal to 100 Ω and 25 Ω, respectively. (These values mimic the impedances adopted in typical setups for Conversion Loss measurement [11][12]). The corresponding predictions obtained by the proposed model are plotted in the same figure by dashed lines. For prediction, the overall line length was set equal to 300 mm, so to account for the presence of the two SMA connectors (10 mm long) soldered at the terminations of each PCB trace.

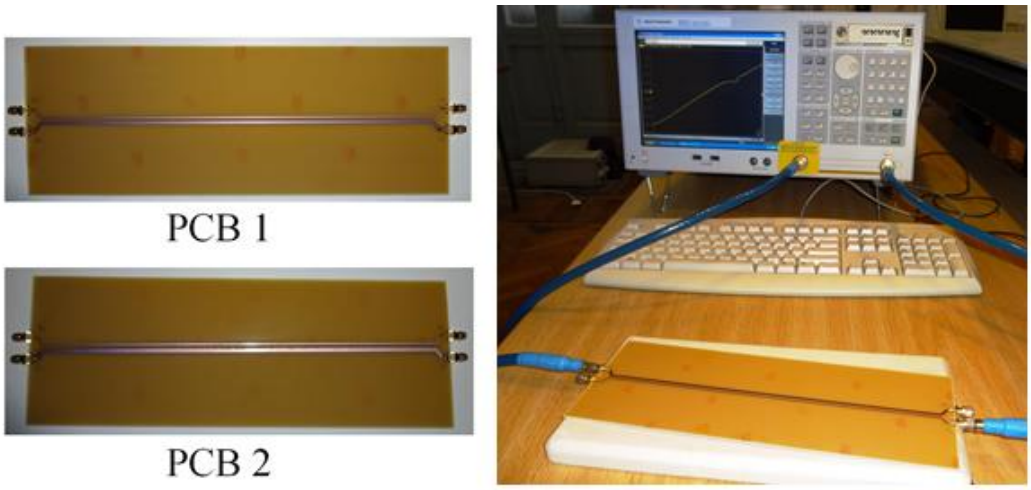

(a) (b)

Figure 7-3 PCB boards (a) and measurement setup (b) for experimental validation of the proposed model.

Table 7-1 Modal Parameters for the PCBs in Figure 7-3(a).

	PCB 1	PCB 2
Z_{DM}	125 Ω	113Ω
Z_{CM}	40 Ω	35.5Ω
v_{DM}	$1.78\ 10^8$ m/s	$1.72\ 10^8$ m/s
v_{CM}	$1.63\ 10^8$ m/s	$1.58\ 10^8$ m/s
k_ℓ	0.14	0.24
k_c	-0.165	-0.28

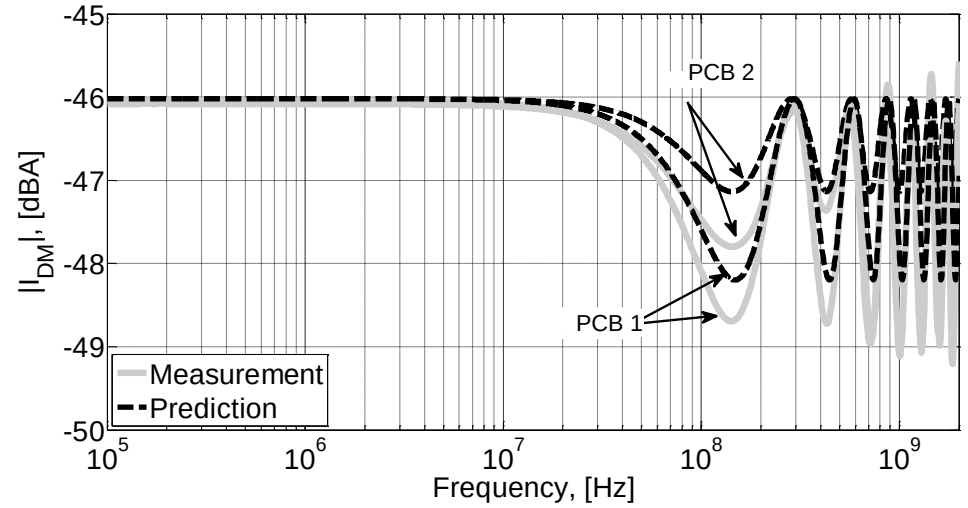

(a)

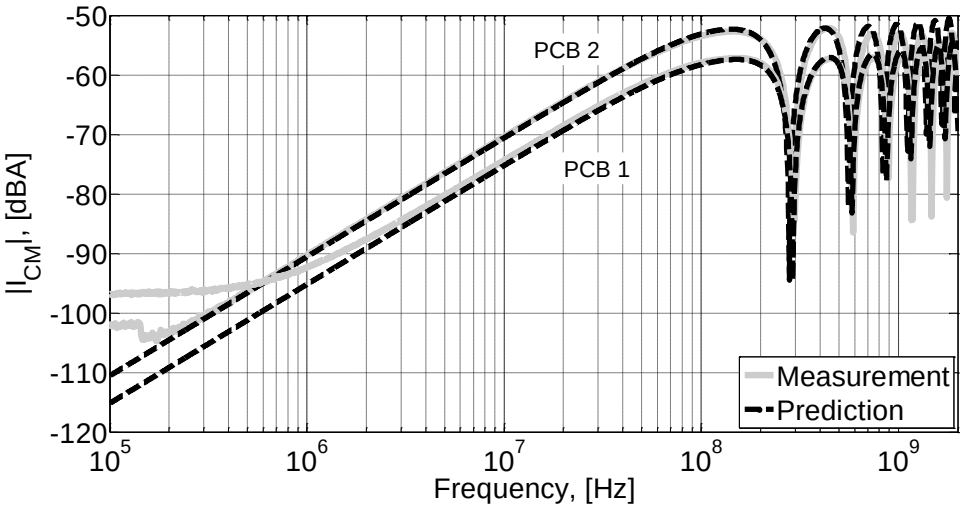

(b)

Figure 7-4 DM (a) and CM (b) currents at the left termination of the PCBs in Figure 7-3(a): Measurement (solid curves) versus prediction (dashed curved) obtained by the proposed model.

Even if the prediction model does not account for losses, that are responsible for the attenuation experienced by the frequency response of the measured quantities above 1 GHz, the comparison shows a good agreement. This is true also for the CM current of PCB 2, which exhibits negligible shifts of the resonance frequencies (null-points), even if the degree of imbalance is very close to the limit of validity of the proposed model.

8 CONCLUSION

In this work, the concept of weak imbalance of TLs and terminations was combined with modal analysis to give a circuit interpretation—in terms of dependent sources—of the modal conversions both in homogeneous and inhomogeneous media. Prediction models has been derived in detail for DM-to-CM conversion, at the basis of REs, and then extended to CM-to-DM conversion, which is responsible for radiated [22] and conducted susceptibility [23]. The accuracy of these models is also validated versus exact MTL solution.

In developing and validating the equivalent models for termination imbalance, the analysis has shown that mode conversion is significantly more efficient in the presence of low-valued CM impedances. Accordingly, the assumption of weak imbalance could require more stringent conditions on the maximum degree of imbalance if the dominant effect has a DM nature (e.g., for RE prediction), since DM-to-CM conversion is not weighed by the CM impedance. Similarly, based on the proposed conversion model in geometrically-unbalanced differential lines, even for large degrees of imbalance and strong mismatching of the DM circuit, the differences between exact and approximate predictions is negligible for whatever values of ground impedance. Additionally, the bigger the ground impedance, the larger are the induced CM voltages.

In addition to the deterministic prediction model, a statistic model is also developed considering the uncertainties and tolerances in the manufacture process. The result shows a significant meaning considering that LCL/TCL measurement setups usually involve low-valued CM impedances (e.g., [11] foresees Z_{GL}, Z_{GR}=0 Ω), and further stresses the need for supplementing the information provided by such measurement-based parameters with a statistical characterization of the possible effects due to this inherently random and un-controlled phenomenon. Also, a model for the upper-bounds to the near- and far-end conversion loss in unbalanced differential lines is introduced. Additionally, the proposed superposition model also achieves good agreement with the exact case where termination and line imbalance both exist. The superposition model shows that the effects of these two imbalances may add or subtract each other, depending on the combination of signs of the involved imbalance coefficients.

The model derivation have been successfully extended to transmission lines in inhomogeneous media by the use of distributed depended sources along the TLs, which take the close-form expressions of a pair of lumped voltage and current sources connected at the right termination of the CM circuit. It was proved that CM and DM characteristic impedances and propagation constants (see Table 6-2) as well as DM predictions do not exhibit significant variations in the presence and absence of imbalance. For electrically-short TLs, the simplified low-frequency (LF) expressions also lead to the strict analogy between crosstalk.

Eventually, SPICE models have been developed, which allow prediction of modal voltages/currents at the terminations of a DL-circuit affected by undesired imbalance due to asymmetries in the line cross-section (line imbalance) and/or in the terminal networks (termination imbalance) in homogeneous and inhomogeneous media, respectively. Model accuracy has been validated versus exact solution of MTL equations, and suitable guidelines have been derived and discussed to enable worst-case prediction of the involved modal quantities by a limited number of simulations. The model accuracy is further validated by experimental measurement, where the prediction model is validated versus the measurement data obtained by experimental characterization of pairs of coplanar micro-strips.

Although derived for a canonical DL structure, the proposed model can be extended to handle more complex wiring harnesses and terminal networks (e.g., terminal networks characterized at the input pins by measurement can be easily included into the model). Additionally, the proposed modeling approach, based on the representation of the unbalanced line as a perturbation of the corresponding balanced structure, can be efficiently exploited to perform sensitivity analysis of undesired modal quantities to the inherently uncertain and uncontrolled parameters at the basis of mode conversion, and also can be further extended to include non-ideal effects in PCB traces, such as losses and dispersion, and additional phenomena of mode conversion, such as crosstalk-coupling with nearby differential lines. Additionally, crosstalk with nearby pairs can be addressed by re-formulating the MTL equations and the weak imbalance assumption for the multi-pair structure under analysis.

9 REFERENCE

[1] http://en.wikipedia.org/wiki/Differential_signaling

[2] D. E. Bockelman and W. R. Eisenstadt, "Combined differential and common-mode scattering parameters: Theory and simulation," *IEEE Trans. Microw. Theory Tech.*, vol. 43, no. 7, pp. 1530–1539, Jul. 1995.

[3] Y. Kami, F. Xiao, K. Murano, "Mode-port-network approach to analyze power-line EMC problems for PLC," *in Proc. 20th Int. Zurich Symp. on Electromagn. Compat*, Zurich, Switzerland, 9–12, 2009.

[4] J. H. Hagmann, S. Dickmann, "Determination of mode conversion on differential lines," *in Proc. EMC Europe 2008*, Hamburg, Germany, 1–5, 2008.

[5] M. Shimazaki, H. Asai, "Evaluation method of balance mismatch using CMRR measurement for printed circuit board," *in Proc. Asia-Pacific EMC Conference (APEMC)*, Tokyo, Japan, 101–104, 2014.

[6] F. Grassi, G. Spadacini, S. A. Pignari, "The concept of weak imbalance and its role in the emissions and immunity of differential lines," *IEEE Trans. Electromagn. Compat.*, Vol. 55, No. 6, 1346–1349, 2013.

[7] M. Miri, M. McLain, "Electromagnetic radiation from unbalanced transmission lines," *Progress In Electromagnetics Research B*, Vol. 43, 129–150, 2012.

[8] F. Grassi, S. A. Pignari, "Bulk current injection in twisted-wire pairs with not perfectly balanced terminations," *IEEE Trans. Electromagn. Compat*, Vol. 55, No. 6, 1293–1301, 2013.

[9] F. Grassi, S. A. Pignari, "Immunity to conducted noise of data transmission along DC power lines involving twisted-wire pairs above ground," *IEEE Trans. Electromagn. Compat*, Vol. 55, No. 1, 195–207, 2013.

[10] C. R. Paul, *Introduction to Electromagnetic Compatibility*, 2nd ed. New York, NY, USA: Wiley, 2006.

[11] *Transmission aspects of unbalance about earth*, ITU-T Recommendation G.117, Geneva, Switzerland, 1989.

[12] I. P. Macfarlane, “A probe for the measurement of electrical unbalance of networks and devices,” *IEEE Trans. Electromagn. Compat.*, vol. 41, no. 1, pp. 3-14, Feb. 1999.

[13] Rohde & Schwarz, *Measuring balanced components with vector network analyzer ZVB*, Application Note 1EZ53, Sep. 2004

[14] C. R. Paul, *Analysis of Multiconductor Transmission Lines*, Wiley-Interscience, New York, 1994.

[15] S. B. Smith, S. S. Agili, V. Balasubramanian, “Theory and measurement of unbalanced differential-mode transmission lines,” *in Proc. DesignCon 2006,* Santa Clara, CA, USA, Feb. 2006.

[16] K. Sejima, Y. Toyota, K. Iokibe, L. R. Koga, T. Watanabe, “Experimental model validation of mode-conversion sources introduced to modal equivalent circuit,” in *Proc. IEEE Int. Symp. EMC*, Pittsburgh, USA, Aug. 2012, pp. 492-497.

[17] A. K. Agrawal, H. J. Price, and S. H. Gurbaxani, “Transient response of multiconductor lines excited by nonuniform electromagnetic field,” *IEEE Trans. Electromagn. Compat.*, vol. 22, no. 2, pp. 119–129, May 1980.

[18] S. Pignari and F. G. Canavero, “Theoretical assessment of bulk current injection versus radiation,” *IEEE Trans. Electromagn. Compat.*, vol. 38, no. 3, pp. 469–477, Aug. 1996.

[19] A. Papoulis, *Probability, Random Variables, and Stochastic Processes*, MacGraw-Hill Int. Editions, Third Edition, 1991

[20] C. R. Paul, “On the superposition of inductive and capacitive coupling in crosstalk prediction models,” *IEEE Trans. Electromagn. Compat*., vol. 24, no. 3, pp. 335–343, Aug. 1982.

[21] Maxwell 3D v.10, Ansoft Corporation, 1984–2004.

[22] C. Su, T. Hubing, “Imbalance difference model for common-mode radiation from printed circuit boards,” *IEEE Trans. on Electromagn. Compat.*, vol. 53, no. 1, pp. 150-156, Feb. 2011.

[23] Y. Kayano, Y. Tsuda, H. Inoue, “Identifying EM radiation from asymmetrical differential-paired lines with equi-distance routing,” in *Proc. IEEE Int. Symp. EMC*, Pittsburgh, USA, Aug. 2012, pp. 311-316.

APPENDIX A

According to this work, the following papers have been published:

[1] F. Grassi, Yuehong Yang, Xinglong Wu, G. Spadacini, and S.A. Pignari. "On mode conversion in geometrically unbalanced differential lines and its analogy with crosstalk." *IEEE Trans. on Electromagn. Compat.* 57.2 (2015): 283-291.

[2] F. Grassi, Xinglong Wu, Yuehong Yang, G. Spadacini, and S.A. Pignari, "Modeling of Imbalance in Differential Lines Targeted to SPICE Simulation" .*Progress In Electromagnetics Research B*, Vol. 62, pp. 225–239, 2015.

[3] Yuehong Yang, Xinglong Wu, F. Grassi. G. Spadacini, and S.A. Pignari, "Upper-Bounds to the Near- and Far-End Conversion Loss in Unbalanced Differential Lines". *Proc. Microwave Conference (APMC),* 393-395 2014 Sendai, Japan. 2014.

[4] Xinglong Wu, Yuehong Yang, Grassi F. Spadacini, G. and Pignari, S.A. "Statistical characterization of line-imbalance in differential lines." *Proc. XXXIth General Assembly of International Union of Radio Science (URSI),* 1 - 4 Beijing, P. R. China, 2014.

APPENDIX B

The abstract of another research works finished by WU, Xinglong in China:

With the wider use of electronic systems, the reliability of electronic device under extreme condition is increasing important. When the microstructures of electronic devices suffer electromagnetic pulses or electrostatic discharges, the instantaneous high electric fields or high currents, which are produced by these pulses or discharges, may cause failure of total system functions due to damage in small areas. With the development of the semiconductor industry, the overall design ideas are turning to the ideas which regard interconnects design as the core. Interconnection systems is a major factor restricting the improvement of semiconductor system performance and reliability. Therefore, it has a great significance to study the failure characteristics of interconnects under pulse wave for improving interconnect and overall system reliability.

This work firstly designs and produces different kinds of Al line structures and silicon dioxide film samples with the Al electrodes on their surface. Then, the substrate film thickness, surface topography, Al thickness, Al width and spacing of prepared samples are tested. After that, the test system for interconnects under nanosecond square wave pulses is designed and built. The wave propagation of this system is analyzed and the waveforms in both matching and mismatching cases are successfully explained. Considering the sample, this work proposes and the injection test procedure for the interconnects under square pulses. And the injection tests are implemented due to the above procedure. The endurance and failure characteristics of both interconnects of different structures and silicon dioxide substrates of different thicknesses under square wave pulses with different pulse widths are studied.

The study shows that: for interconnects which have 5-15μm line widths, at the moment of injection, the rising rate of their resistance is almost proportional to the injection energy. When the difference between the values of instantaneous resistance at the moment of injection and the original resistance rises to the specific multiple of the original resistance value, interconnects will fail. This specific multiple is almost independent on the line width. The energy threshold for interconnect failure under square wave pulse increases with pulse width. Considering the square wave pulse with 100-1000ns pulse width, interconnect

failure model can't be seen as an 'adiabatic' model. The surrounding medium, including the coverage material and its physical limitation to Al lines, has an great influence on interconnect failure. The degree of influence also increases with the pulse width. The pulse tolerance capability of silicon dioxide substrate increases with the film thicknesses. The relationship between them is not linear. For the substrate with the same thickness, the pulse tolerance capability is almost independent on pulse width when pulse width changes from 100ns to 1us.

This work has a significant for understanding the failure law of interconnects under pulse. And it is also useful for the design of on-chip interconnects.

The abstract of another research works finished by YANG, Yuehong in China:

Along with the environment problem and energy crisis, the photovoltaic (PV) power generation techniques plays a more and more important rule in every country, which improves very fast. The inverter is the most important part in the PV system, so its price, efficiency, stability, safety and the robustness is of great concern nowadays. The experimental platform of the three-level T-type PV grid-connected inverter is established first in this work, and then the common-mode (CM) electromagnetic (EMC) issues are discussed follow by.

In order to analysis the CM EMC problem of the T-type inverter, firstly, the experiment platform is designed and established, which satisfies with the design requirements. Based on the selected topology of the PV system and the designed parameters, the CM ground current analysis model is constructed. By applying the simulation tool Psim, the CM voltage and current is simulated with referring to the EMI test and verifying the reasonability of the proposed model. With the analysis of the space-vector pulse width modulation (SVPWM) techniques, the impact factors of the CM EMC issues is discussed furthermore.

Firstly, the design of the main circuit, the modeling and the design of the control strategy of the three-level T-type inverter are proposed, based on which the inverter is established. Secondly, in order to analysis the CM issues of the designed inverter, the parasitic capacitance of the T-type module is calculated based on the numerical calculation and simulation on Maxwell 3D. Thirdly, the analysis model of the CM is proposed. Furthermore, this thesis also analyzes the relationship between the SVPWM technique and the CM EMC problem. Finally, the experiments and EMI tests are conducted.

According to the theoretical and experimental results, it proves that the design of the inverter and the analysis model of the CM EMC problems are right. And the conclusions are made at last.